University of Stavanger

Faculty of Science and Technology

MASTER'S THESIS

Study program: Master in Petroleum Engineering Specialization: Petroleum Production	Spring semester, 2014 Open
Writer: Mamonov Aleksandr	…… (Writer's signature)

Faculty supervisor: Aly Anis Hamouda

Thesis title:

Mechanism of primary and secondary oil flooding for recovery from sandstone by low salinity water

Credits (ECTS): 30

Key words: - Low Salinity Water - Enhanced oil recovery - Sandstone - Mineral dissolution - Clay materials - pH - Pressure drop	Pages: 104 + enclosure: 8 Stavanger, 16.06.2014 Date/year

ACKNOWLEDGEMENTS

I want to thank professor Aly Anis Hamouda for the great supervising, ongoing assistance with problems solving and clever ideas during my research work. I appreciate to be one of his thesis students.

For half year I learned a lot of new material and strengthened my theoretical knowledge by practical experience. I’m very thankful for Rinad Munaev and Evgeny Maevskiy for technical support in my work.

I also want to thank my family for their patience and my girlfriend for her moral support. This work would not be possible without them.

Aleksandr Mamonov

ABSTRACT

Low salinity water flooding (LSW) as an enhanced oil recovery (EOR) method has been discussed by many researchers, but consistent approved mechanism is still not found. The main reason of lack of clear understanding of the process is complexity of the oil/brine/rock interactions. Therefore, theme of this project was chosen to study the mechanism(s) behind the low salinity EOR by flooding different brines through the sandstone cores and analyzing obtained data.

This thesis contains a literature review, experimental and discussion parts. Experiments were made for two different sandstone types (Bentheimer and Berea) and two different core lengths. LSW effects were studied as a primary injection fluid and secondary injection fluid - EOR (after flooding with synthetic sea water – SSW). Oil recovery and pressure drop across the core were detected and for effluent water samples were measured pH, ions concentration and amount of silicon/aluminum.

This work was made with the intention of improving the understanding of processes during flooding with low salinity brine. The idea was to study different sandstone types and define relationship between core length and amount of brine/rock interactions. Results showed that the main reason for improved oil recovery by using LSW brines can be the wettability changing of the rock surface. Possible underlying reason for this process is sandstone minerals dissolution, which was confirmed by increased amount of K^+ in effluent water samples. pH of effluent water samples showed stably higher values than pH of influent LSW, which can be the consequence of minerals dissolution. Possible double layer expansion together with dissolution process could enhance particle detachment and increased pressure drop across the cores.

Based on obtained results, Berea sandstone has higher potential for LSW effects due to higher amount of brine/rock interactions and respectively higher oil recovery. Higher amount of K and Si was found in effluent samples for Berea type in compare with Bentheimer. Oil recovery measurements for long cores also showed higher values than for short cores, which tell us about the dependency of the results on the core length.

TABLE OF CONTENTS

ACKNOWLEDGEMENTS ii
ABSTRACT iii
LIST OF FIGURES vi
LIST OF TABLES ix
NOMENCLATURE x
1 INTRODUCTION 1
2 LITERATURE REVIEW 2
2.1 Sandstone 2
2.2 Clay minerals 3
2.3 Oil recovery 7
2.3.1 Primary oil recovery 8
2.2.2 Secondary oil recovery 8
2.3.3 Tertiary recovery 9
2.3.4 Low salinity water flooding 10
2.4 Parameters governing fluid and rock interactions 11
2.4.1 Porosity 11
2.4.2 Saturation 12
2.4.3 Darcy's Law 12
2.4.4 Wettability 14
2.4.5 Contact angle 15
2.4.6 Surface and interfacial tension 16
2.4.7 Capillary pressure 16
2.5 LSW mechanisms 18
2.5.1 Fine migration or permeability reduction 18
2.5.2 pH effects 19
2.5.3 Multicomponent ion exchange 22
2.5.4 Double layer expansion 23
2.5.5 Wettability alteration 26

2.6 Modeling and numerical simulation of LSW 29
3 EXPERIMENTAL PART 30
3.1 Materials 30
3.1.1 Cores 30
3.1.2 Oil 31
3.1.3 Brines 32
3.2 Core preparation and test procedure 35
3.2.1 Saturation procedure 35
3.2.2 Flooding procedure 41
3.2.3 Analysis 42
4 RESULTS AND DISCUSSION 44
4.1 Core floods overview 44
4.2 Core Al-4 Short Bentheimer, SSW-LSW 46
4.3 Core Al-7 Long Bentheimer, SSW-LSW 52
4.4 Core Al-11 Short Berea, SSW-LSW 55
4.5 Core Al-8 Long Berea, SSW-LSW 59
4.6 Core Al-6 Short Bentheimer, LSW 62
4.7 Core Al-12 Long Bentheimer, LSW 65
4.8 Core Al-10 Short Berea, LSW 69
4.9 Core Al-9 Long Berea, LSW 72
4.10 Simulation part 75
4.11 Analysis of aluminum (Al) and silicon (Si) 83
4.12 Summary of results 88
5 CONCLUSIONS AND PROPOSED MECHANISM 100
REFERENCES 101
APPENDIX 105

LIST OF FIGURES

Figure 1– Sandstone rock (Sandstone picture, geology.com) 2
Figure 2 - Tetrahedral and octahedral coordination for kaolinite structure 3
Figure 3 - Structure of different clay minerals 5
Figure 4 - The main phases of a field development plan (Vladimir Alvarado and Eduardo Manrique, 2010) 7
Figure 5 - Oil-water relative permeability curves (Nnaemeka Ezekwe, 2011) 13
Figure 6 – Illustration of wettability (Ahmed Tarek, 2001) 14
Figure 7 - Water-wet rock and oil-wet rock (Nnaemeka Ezekwe, 2011) 15
Figure 8 - Capillary pressure curve (Ahmed Tarek, 2001) 17
Figure 9 - Proposed mechanism for low salinity EOR effects. Upper: Desorption of basic material. Lower: Desorption of acidic material. The initial pH at reservoir conditions may be in the range of 5 (Tor Austad at al., 2010). 21
Figure 10 - Four of the proposed adsorption mechanisms of organic materials onto clay surface (Ole Martin Valderhaug, 2013) 22
Figure 11 - Illustration of the Double Layer structure near the surface of the negatively charged particle (Ramez A. Nasralla and Hisham A. Nasr-El-Din, 2014). 24
Figure 12 - Wetting contact angles in confined capillaries, (a) Strongly water wet, (b) preferentially water wet, (c) neutral, (d) preferentially oil wet, (e) strongly oil wet (Archer J. S. and Wall C. G, 1986). 26
Figure 13 - Right and left contact angles of crude oil vs. different water salinities at 500 psi and 212°F. Low-salinity water altered the mica surface to be more water-wet (Ramzes A. Nasralla and Hisham A. Nasr-El-Din, 2014). 28
Figure 14 – Measurement of NN-DMDA amount for required concentration 31
Figure 15 – Preparation of brines: filtration setup and brine storage 32
Figure 16 - PAAR densitometer DMA 46 34
Figure 17 – Oven with cores and weighing of core 35
Figure 18 – Vacuum setup 36
Figure 19 - Hassler core holder in disassembled state 37
Figure 20 – Core placement and wrapping procedure 38
Figure 21 – Heating of plastic cover and putting rubber cover 38
Figure 22 – Picture of flooding setup 39
Figure 23 – Scheme of flooding setup 39
Figure 24 – pH measurements 42
Figure 25 - Dionex ICS-3000 chromatograph 42
Figure 26 – Spectrometer Optima 4300 DV ICP-OES 43
Figure 27 – Flooding sequences 45
Figure 28 – Oil recovery and pH for influent and effluent during flooding with SSW – LSW for core Al-4 47
Figure 29 – Ions concentrations for effluent samples taken from the SSW - LSW flooding of core Al-4 48
Figure 30 – Pressure drop across the core Al-4 during SSW-LSW flooding 49

Figure 31 - Oil recovery and pH for influent and effluent during flooding with SSW – LSW for core Al-7 53
Figure 32 - Pressure drop across the core Al-7 during SSW-LSW flooding 53
Figure 33 – Ions concentrations for effluent samples taken from the SSW - LSW flooding of core Al-7 54
Figure 34 - Oil recovery and pH for influent and effluent during flooding with SSW – LSW for core Al-11 56
Figure 35 - Pressure drop across the core Al-11 during SSW-LSW flooding 57
Figure 36 - Ions concentrations for effluent samples taken from the SSW - LSW flooding of core Al-11 58
Figure 37 - Oil recovery and pH for influent and effluent during flooding with SSW – LSW for core Al-8 59
Figure 38 - Ions concentrations for effluent samples taken from the SSW - LSW flooding of core Al-8 60
Figure 39 - Pressure drop across the core Al-8 during SSW-LSW flooding 61
Figure 40 - Oil recovery and pH for influent and effluent during flooding with LSW for core Al-6 62
Figure 41 – Pressure drop across the core Al-6 during LSW flooding 63
Figure 42 – Ions concentrations for effluent samples taken from the LSW flooding of core Al-6 64
Figure 43 - Oil recovery and pH for influent and effluent during flooding with LSW for core Al-12 66
Figure 44 – Pressure drop across the core Al-12 during LSW flooding 67
Figure 45 – Ions concentrations for effluent samples taken from the SSW - LSW flooding of core Al-12 68
Figure 46 - Oil recovery and pH for influent and effluent during flooding with LSW for core Al-10 69
Figure 47 – Ions concentrations for effluent samples taken from the LSW flooding of core Al-10 70
Figure 48 - Pressure drop across the core Al-10 during LSW flooding 71
Figure 49 - Oil recovery and pH for influent and effluent during flooding with LSW for core Al-9 72
Figure 50 – Ions concentrations for effluent samples taken from the LSW flooding of core Al-9 73
Figure 51 - Pressure drop across the core Al-9 during LSW flooding 74
Figure 52 – Example of history matching in Sendra for core Al-12 76
Figure 53 - Simulated relative permeability curves for short Bentheimer core Al-4, SSW flooding 77
Figure 54 - Pore Doublet Model (Adrian C Todd, 2005) 79
Figure 55 - Simulated relative permeability curves for short Berea core Al-11, SSW flooding 80
Figure 56 - Simulated relative permeability curves for short Bentheimer core Al-6, LSW flooding 81

Figure 57 - Simulated relative permeability curves for short Berea core Al-10, LSW flooding 82
Figure 58 - Relationship between element contents and temperatures (Qingjie Gong et al., 2012)..... 83
Figure 59 – Concentration of silicon in effluent samples during SSW-LSW flooding for Long Bentheimer and Berea cores..... 86
Figure 60 – Concentration of silicon in effluent samples during LSW flooding for Long Bentheimer and Berea cores..... 86
Figure 61 – Concentration of silicon in effluent samples during SSW-LSW flooding for Short Bentheimer and Berea cores..... 87
Figure 62 – Concentration of silicon in effluent samples during LSW flooding for Short Bentheimer and Berea cores..... 87
Figure 63 – Oil recovery during SSW-LSW flooding 88
Figure 64 – Oil recovery during LSW flooding..... 89
Figure 65 – Pressure drop across the cores during SSW-LSW experiments 90
Figure 66 – Pressure drop across the cores during SSW-LSW experiments 91
Figure 67 - pH measurements for influent and effluent water samples during SSW-LSW flooding 92
Figure 68 - pH measurements for influent and effluent water samples during LSW flooding 93
Figure 69 – Ion concentrations for K^+ in effluent water during SSW-LSW flooding 94
Figure 70 – Ion concentrations for K^+ in effluent water during LSW flooding 94
Figure 71 – Ion concentrations for calcium in effluent water during SSW-LSW flooding..... 96
Figure 72 – Ion concentrations for calcium in effluent water during LSW flooding..... 96
Figure 73 – Ion concentrations for HCO_3^- in effluent water during SSW- LSW flooding..... 97
Figure 74 – Ion concentrations for Mg^{2+} in effluent water during SSW- LSW flooding 98
Figure 75 – Ion concentrations for Na^+ in effluent water during SSW- LSW flooding..... 98
Figure 76 – Ion concentrations for SO_4^{2-} in effluent water during SSW- LSW flooding..... 99
Figure 77 – Ion concentrations for Cl^- in effluent water during SSW- LSW flooding..... 99

LIST OF TABLES

Table 1 – Properties of different sandstone cores 30
Table 2 - Physical properties of N-Decane (Ole Martin Valderhaug, 2013) 31
Table 3 – Composition of brines 33
Table 4 - Viscosity for the different brines and oil 34
Table 5 - Density for the different brines and oil 34
Table 6 – Absolute permeability calculations 40
Table 7 – Core parameters and flooding sequence 45
Table 8 - Dependence of Si concentration in the effluent water on time 84
Table 9 - Solid analysis of the Bentheimer sandstone (Ole Martin Valderhaug, 2013)..... 105
Table 10 - Mineral analysis of Bentheimer sandstone (Ole Martin Valderhaug, 2013) 105
Table 11 - Concentration of Potassium ion for all SSW-LSW and LSW experiments 106
Table 12 - Concentration of Calcium ion for all SSW-LSW and LSW experiments 107
Table 13 - Concentration of Magnesium ion for all SSW-LSW and LSW experiments 108
Table 14 - Concentration of Sodium ion for all SSW-LSW and LSW experiments 109
Table 15 - Concentration of Sulfate ion for all SSW-LSW and LSW experiments..... 110
Table 16 - Concentration of Chloride ion for all SSW-LSW and LSW experiments.....111
Table 17 - Concentration of Carbonate ion for all SSW-LSW and LSW experiments 112

NOMENCLATURE

A: Cross sectional area
AQ: Aquifer water
D: Diameter
EOR: Enhanced Oil Recovery
HPLC: High-performance liquid chromatography
I: ionic strength
ICP: Inductively coupled plasma
IFT: Interfacial Tension
IOR: Improved oil recovery
k: Absolute permeability
L: Length
LSW: Low Salinity Water
m: Mass
OOIP : Original oil in place
P: Pressure
p_c: Capillary pressure
p_d: Displacement pressure
p_{nw}: Pressure in the non-wetting phase
p_w: Pressure in the wetting phase
PV: Pore volume
Q: Flow rate
r: Radius
S_{gas}: Gas saturation
S_i: Fluid saturation
S_{oil}: Oil saturation
S_{water}: Water saturation
SSW: Synthetic Sea Water
T: Temperature
TDS: Total dissolved solids
V: Volume
φ: Porosity
μ: Dynamic viscosity
Δ: Difference
θ: Contact angle
σ: Interfacial tension
ρ: Density

Subscripts:
o: oil
orw: oil residual water
prod: produced oil
ro: relative oil
rw: relative water
w: water
wc: water critical
wi: water initial

1 INTRODUCTION

For many years water flooding is the proven method in petroleum industry for stimulating oil production. It is simple and economical technique to maintain reservoir pressure, which is commonly using as a secondary recovery method.

In recent years, there is a passionate discussion about using of low salinity water flooding (LSW) as a secondary or tertiary recovery mode after conventional high salinity flooding. Several researchers showed that implementation of LSW can increase amount of produced oil from both laboratory and field experiments.

Originally idea about LSW implementation came from Tang, G.Q. and Morrow, N.R. (1999). They studied possibility of crude oil/brine/rock interactions to change wettability and identified conditions (presence of potentially mobile fines - clay, initial water saturation and crude oil) for increase in oil recovery with decrease in salinity for Berea sandstone (Tang, G.Q. and Morrow, N.R., 1999). Afterwards several other mechanisms were proposed such as wettability alteration, multicomponent ion exchange, increase in pH, mineral dissolution and expansion of electrical double layer.

Positive results obtained from low salinity water injection are contrasted by other results where the LSW did not show any oil increment. For this reason there is still no approved mechanism according to which low salinity can be used as enhanced oil recovery (EOR) method in industry.

According to statistical information more than 50% of oil was found in sandstone reservoirs, containing clay mineral, which is indicative as the favorable condition for LSW (Cuong T.Q. Dang et al., 2013). Proposed low salinity mechanisms for sandstone are not clear, contain many contradictions and may act together or separately. Many unanswered questions are inhibiting LSW propagation. Hence, full understanding of oil/brine/rock interaction during low salinity flooding can become breakthrough for petroleum industry.

2 LITERATURE REVIEW

2.1 Sandstone

The majority of petroleum reserves in the world are found in ancient sandstones which have porosity and permeability (Robert J. Weimer and Tillman, R.W., 1982). *Sandstones* are clastic sedimentary rocks composed of mainly sand size particles or grains set in a matrix of silt or clay and more or less firmly united by a cementing material (commonly silica, iron oxide, or calcium carbonate). The sand particles usually consist of quartz, and the term "sandstone", when used without qualification, indicates a rock containing about 85-90% quartz (Halliburton, 2011).

Sandstone reservoirs are generally created by the accumulation of large amounts of clastic sediments which is characteristic of depositional environments such as river channels, deltas, beaches, lakes and submarine fans. Diagenetic changes may include precipitation of clay minerals in the pore space, occlusion of pores by mineral cements, or even creation of additional pores by dissolution of some sediments (Halliburton, 2011).

Figure 1– Sandstone rock (Sandstone picture, geology.com)

2.2 Clay minerals

Clays are the product of slow transformations of high temperature rocks into reactive, fine grained material (Bruce B. Velde and Alain Meunier, 2008). Basically it is sedimentary rock composed of <2 µm particles. The main chemical components of the clay is SiO_2 (30-70%), Al_2O_3 (10-40 %) and H_2O (5-10 %). Certain amounts of Fe_2O_3 (FeO), TiO_2, CaO, MgO, K_2O, Na_2O, CO_2, MnO, SO_3, P_2O_5 also can be presented in composition.

Clay minerals are composed of a combination of two types of layer structures which are coordinations of oxygen anions with various cations. Two types of sheets are known following the number of anions coordinated with the captions, one of six-fold coordinations (tetrahedral) and the other of eight-fold coordination (octahedral coordination) (Bruce B. Velde and Alain Meunier, 2008).

These layers are linked to each other into planar layers by sharing oxygen ions between Si^{4+} or Al^{3+} ions of the adjacent tetrahedral or octahedral. The space between the oxygen octahedral and tetrahedral are mostly taken by the Si^{4+} and Al^{3+} ions, but to ensure charge balance other cations such as potassium, calcium, magnesium and iron are necessary in the clay structure (Ole Martin Valderhaug, 2013). Kaolinite structure as an example of tetrahedral and octahedral coordination is showed on Figure 2 below.

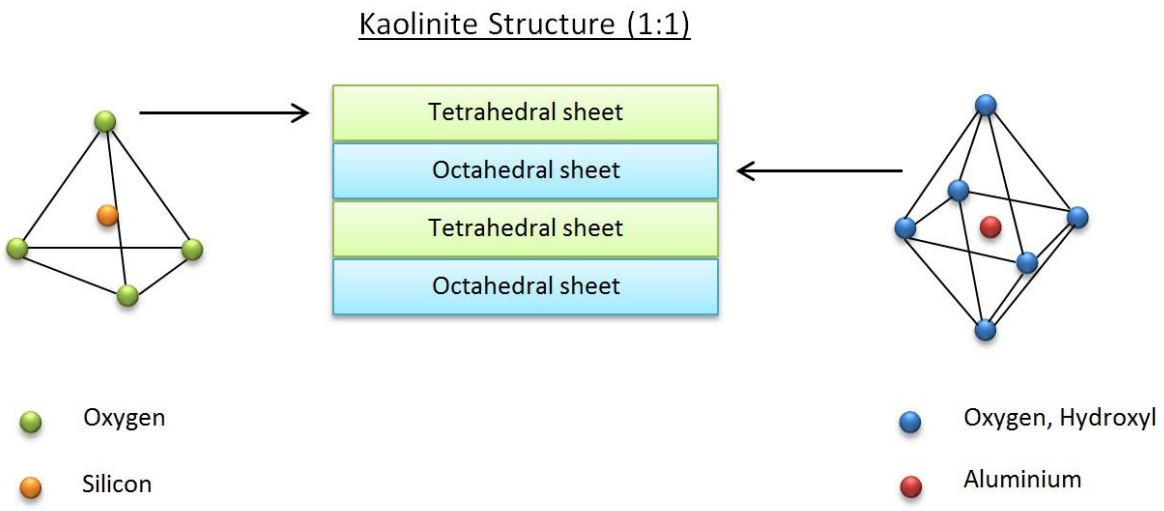

Figure 2 - Tetrahedral and octahedral coordination for kaolinite structure

Different types of clay minerals with different structure can be presented in sandstone.

Kaolinite is one of the main clay minerals with chemical composition: $Al_2Si_2O_5(OH)_4$. This mineral has a 1:1 structure connected by O-H-O bonds, with one silica tetrahedral layer with an aluminum-hydroxyl layer coordinated to it. (Figure 3) (Bruce B. Velde and Alain Meunier, 2008).

Illite is very similar in chemistry and structure to muscovite, but occurs as much smaller crystals. There is considerable variation in composition due to ion substitution, but a general formula is: $KAl_3Si_3O_{10}(OH)_2$. This mineral has 2:1 structure consisting of repeating tetrahedral – octahedral – tetrahedral layers connected by O-K-O bonds (Figure 3).

Chlorite has a general formula: $(Mg,Fe)_3(Si,Al)_4O_{10}(OH)_2 \cdot (Mg,Fe)_3(OH)_6$. There is much variation in Fe:Mg ratio and substitution of other metals, forming a multitude of sub-varieties. Chlorite has a 2:1:1 sandwich structure, consisting of negatively charged tetrahedral – octahedral – tetrahedral layers. Chlorite's interlayer space consist of an additional octahedral layer that is positively charged and comprised of cations and hydroxyl ions, $(Mg^{2+}, Fe^{3+})(OH)_6$, commonly described as the brucite - like layer. Chlorite´s structure will then have the following build up; T – O – T – Brucite – T – O – T. (Ole Martin Valderhaug, 2013) (Figure 3).

Smectite has extremely variable composition, as well as a complicated formula, including K, Na, Ca, Fe, Mg, and more. It is a group of species including montmorillonite, bentonite, saponite, and more. Smectite has the same structure as illite, but less binding by K+. The interlayer also contains water and cations from the last aqueous medium smedrite was in contact with (Dagny Håmsø, 2011) (Figure 3).

There are also *mixed-layer* clays which consist of layers of kaolin, chlorite, or illite alternating with smectite layers. The layering may be random or ordered, with all gradations in between.

Schematic structure of different clay minerals is shown on Figure 3 below.

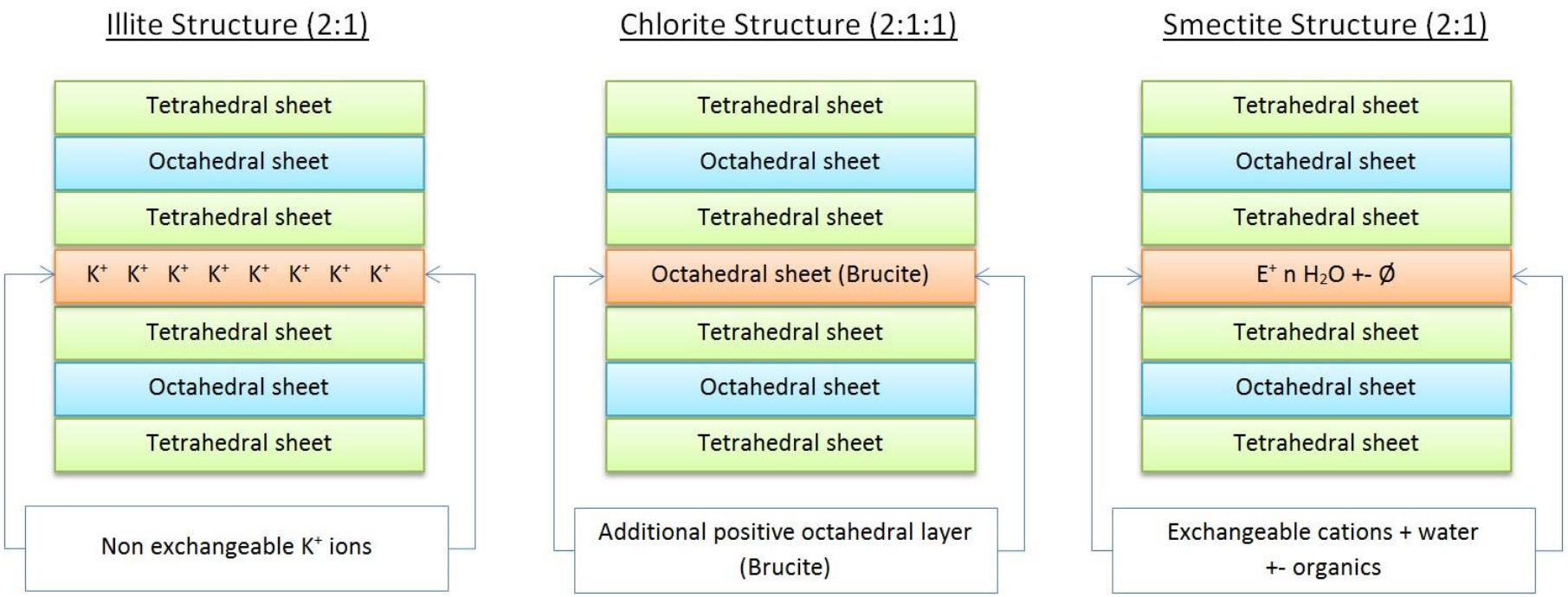

Figure 3 - Structure of different clay minerals

Clay minerals has unbalanced negative charges on the edges of the unit cells, this is a characteristic that separates them from the other silicates (Ole Martin Valderhaug, 2013). Clays become charged as a result of amorphous substitution. The substitution of Si^{4+} by Al^{3+} in the tetrahedral layers or of Al^{3+} by Mg^{2+}, Zn^{2+} or Fe^{2+} in the octahedral layers leads to a net negative charge (Terence Cosgrove, 2010).

Cations in the solution are attracted and held by weak quasi-bonding forces, including electrostatic and van der Waals forces, and depending on the conditions they are exchanged and not held permanently. Various cations have different relative strengths and replacing power. Weakly adsorbed cations may easily be exchanged, and therefore the relative replacing power of a particular cationic species depends on its strength of binding (Ole Martin Valderhaug, 2013).

The quantity of cations per unite weight of clay is reported as the cation exchange capacity (CEC) and it is expressed in milliequivalents per 100 g of dry clay. The CEC of montmorillonite is within the range of 80 – 150 meq/100g. Illite and chlorite is about 10 – 40 meq/100g and for kaolinite 3- 10 meq/100g (Dagny Håmsø, 2011).

It is believed that the relative replacing power of cations in room temperature is as follows (Ole Martin Valderhaug, 2013):

$$Li^{+}<Na^{+}<K^{+}<Mg^{2+}<Ca^{2+}<Sr^{2+}<Ba^{2+}<H^{+}<Al^{3+}$$

It means that in certain conditions and equal concentrations ability of H^{+} to displace K^{+} will be stronger than for K^{+} to displace H^{+}. These ions have different solubility-to-temperature relationships and with increasing temperature the replacing power may be different (Dagny Håmsø, 2011).

2.3 Oil recovery

Reservoir development planning refers to strategies that begin with the exploration and appraisal well phase and end with the abandonment phase of a particular field to establish the course of action during the productive life of the asset. (Vladimir Alvarado and Eduardo Manrique, 2010). Recovery of hydrocarbons from a reservoir may make exclusive use of the inherent energy of the system (*primary recovery*); energy may be added to the system in the form of injected fluids (*secondary recovery*); some of the residual hydrocarbon trapped during conventional recovery processes may be mobilized (*tertiary or enhanced oil recovery*) (Archer J.S. and Wall C.G., 1986). Reservoir development cycle is shown below on Figure 4. The main aim of performing different techniques for producing oil at different stages is maximizing oil recovery.

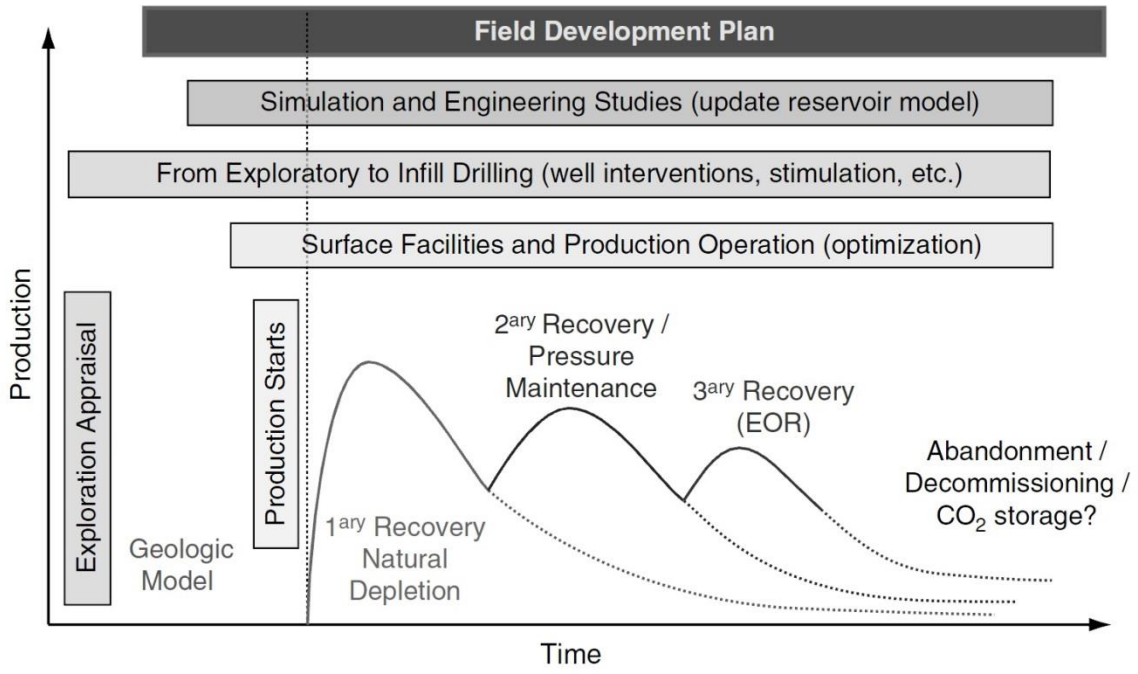

Figure 4 - The main phases of a field development plan (Vladimir Alvarado and Eduardo Manrique, 2010)

2.3.1 Primary oil recovery

Primary oil recovery describes the production of hydrocarbons under the natural driving mechanisms present in the reservoir without supplementary help from injected fluids such as gas or water. In most cases, the natural driving mechanism is a relatively inefficient process and results in a low overall oil recovery (Ahmed Tarek, 2001).

Possible sources of replacement for produced fluids are (Archer J.S. and Wall C.G., 1986):

- expansion of undersaturated oil above the bubble-point;
- the release of gas from solution in the oil at and below the bubble-point;
- invasion of the original oil-bearing reservoir by gas from a free gas cap;
- invasion of the original oil-bearing reservoir by water from an adjacent or underlying aquifer.

All replacement processes involve a reduction in pressure in the original oil zone, although pressure drops may be small if gas caps are large, and aquifers large and permeable, and pressures may stabilize at constant or declining reservoir offtake rates under favorable circumstances (Archer J.S. and Wall C.G., 1986).

The lack of sufficient natural drive in most reservoirs has led to the practice of supplementing the natural reservoir energy by introducing some form of artificial drive, the most basic method being the injection of gas or water (Ahmed Tarek, 2001).

2.2.2 Secondary oil recovery

Secondary recovery refers to techniques, such as gas or water injection, whose purpose is mainly to raise or maintain reservoir pressure (Larry W. Lake, 2010). Usually, the selected secondary recovery process follows the primary recovery but it can also be conducted concurrently with the primary recovery. Waterflooding is perhaps the most common method of secondary recovery (Ahmed Tarek, 2001).

Before waterflooding will be implemented for reservoir set of parameters should be considered: rock properties, well locations, reservoir depth and geometry, fluid saturation and properties, primary reservoir driving mechanism.

2.3.3 Tertiary recovery

Tertiary (enhanced) oil recovery is that additional recovery over and above what could be recovered by primary and secondary recovery methods. Various methods of enhanced oil recovery (EOR) are essentially designed to recover oil, commonly described as residual oil, left in the reservoir after both primary and secondary recovery methods have been exploited to their respective economic limits (Ahmed Tarek, 2001).

EOR processes involve the injection of a fluid or fluids of some type into reservoir. The injected fluids and injection processes supplement the natural energy present in reservoir to displace oil to a producing well. In addition, the injected fluids interact with the reservoir rock/oil system to create conditions favorable for oil recovery (Don W. Green and G. Paul Willhite, 1998).

EOR processes can be classified into five categories (Don W. Green and G. Paul Willhite, 1998):

- mobility-control;
- miscible;
- thermal;
- other processes, such as microbial EOR.

Choice of one or other EOR method depends on many factors such as rock and oil properties, availability and price. Worldwide investigations in EOR area aimed to find cheap and effective technology. In this thesis we will focus on one of these methods: Low salinity water flooding, which can be useful with right understanding of process.

2.3.4 Low salinity water flooding

Unlike traditional water flooding low salinity technique refers to tertiary oil recovery. Many researchers showed positive results of LSW to improve oil recovery in secondary and tertiary modes. Low salinity flooding has become an attractive enhanced oil recovery method as it shows more advantages than conventional chemical EOR methods in terms of chemical costs, environmental impact, and field process implementation (Cuong T.Q. Dang et al., 2013). Because of the complexity of the core-oil-brine-rock interactions, the mechanism(s) of low-salinity enhanced oil recovery is still being discussed and none of the suggested mechanisms has, thus far, been accepted as the main process (Aly Anis Hamouda and Ole Martin Valderhaug, 2014).

There are several physical/chemical factors which may be real reason of successful implementation of LSW in some cases. The general agreement among researchers is that injecting low-salinity brine creates a wetting state more favorable for oil recovery (Ramez A. Nasralla and Hisham A. Nasr-El-Din, 2014). In case of sandstone the presence of clay minerals is considered to be a favorable condition for the high efficiency of process. This recovery concept is quite attractive as 50% of the world's conventional petroleum reservoirs are found in sandstones that commonly contain clay minerals. LSW can also be considered for secondary recovery, or combined with other EOR approaches such as CO; miscible flooding, polymer, and surfactant-polymer for a higher oil recovery factor in tertiary mode. (Cuong T.Q. Dang et al., 2013).

2.4 Parameters governing fluid and rock interactions

There are several parameters governing fluid and rock interactions which can affect oil recovery. Knowledge of the physical properties of the rock and the existing interaction between the hydrocarbon system and the formation is essential in understanding and evaluating the performance of a given reservoir (Ahmed Tarek, 2001).

2.4.1 Porosity

Porosity is the ratio of void space in a rock to the total volume of rock, and reflects the fluid storage capacity of the reservoir (Halliburton, 2011). Mathematical determination of this parameter represents relationship:

$$Porosity\ (\varphi) = \frac{pore\ volume}{bulk\ volume} \quad (1)$$

As the sediments were deposited and the rocks were being formed during past geological times, some void spaces that developed became isolated from the other void spaces by excessive cementation. Thus, many of the void spaces are interconnected while some of the pore spaces are completely isolated. This leads to two distinct types of porosity, namely (Ahmed Tarek, 2001):

• Absolute porosity (ratio of the total pore space in the rock with respect to the bulk volume)

• Effective porosity (percentage of interconnected pore space with respect to the bulk volume).

Porosity can approach, in very well sorted uncompacted sand, a theoretical maximum of 47.6%. In sandstone, this value is typically much lower due to cementation and compaction and lying in the range of 10-35% (Halliburton, 2011).

2.4.2 Saturation

Saturation is defined as that fraction, or percent, of the pore volume occupied by a particular fluid (oil, gas, or water). This property is expressed mathematically by the following relationship (Ahmed Tarek, 2001):

$$Fluid\ saturation\ (S_i) = \frac{total\ volume\ of\ the\ fluid}{pore\ volume} \quad (2)$$

Total saturation of each individual phase will be 100% (or 1):

$$S_{oil} + S_{gas} + S_{water} = 1 \quad (3)$$

For any reservoir, there is a certain value of water saturation at which all of the contained water will be trapped by capillary pressure and/or by adsorption of water on the surface of rock grains (surface tension). This is referred to as *irreducible water saturation* (Halliburton, 2011).

2.4.3 Darcy's Law

In 1856, Henry Darcy demonstrated through a series of experiments that the flow velocity of a homogenous fluid through a porous medium under laminar (non-turbulent) conditions is proportional to the potential gradient (Nnaemeka Ezekwe, 2011). Equation for Darcy's Law:

$$Q = \frac{k}{\mu} \cdot \frac{\Delta P}{L} \cdot A, \quad (4)$$

where: Q - flow rate, cm^3/sec

k – permeability, Darcy

μ – dynamic viscosity, centipoise

ΔP - pressure different across sample, atm

L - length of sample, cm

A - cross sectional area of sample, cm^2

For the units described above, k (permeability coefficient) has been arbitrarily assigned a unit called Darcy in honor of the man responsible for the development of the theory of flow through porous media (Ahmed Tarek, 2001). The *permeability* of a rock is the description of the ease with which fluid can pass through the pore structure (Adrian C Todd, 2005).

If the porous medium is completely saturated (100% saturated) with a single fluid, the permeability measured is the absolute permeability. *Absolute permeability* is an intrinsic property of the porous medium, and the magnitude of absolute permeability is independent of the type of fluid in the pore spaces. When the pore spaces in the porous medium are occupied by more than one fluid, the permeability measured is the *effective permeability* of the porous medium to that particular fluid. For instance, the effective permeability of a porous medium to oil is the permeability to oil when other fluids, including oil, occupy the pore spaces (Nnaemeka Ezekwe, 2011).

Relative permeability is defined as the ratio of effective permeability to absolute permeability of a porous medium. Relative permeability data can be presented graphically in plots called relative permeability curves. A typical relative permeability curve for an oil-water system is shown in Figure 5 (Nnaemeka Ezekwe, 2011)

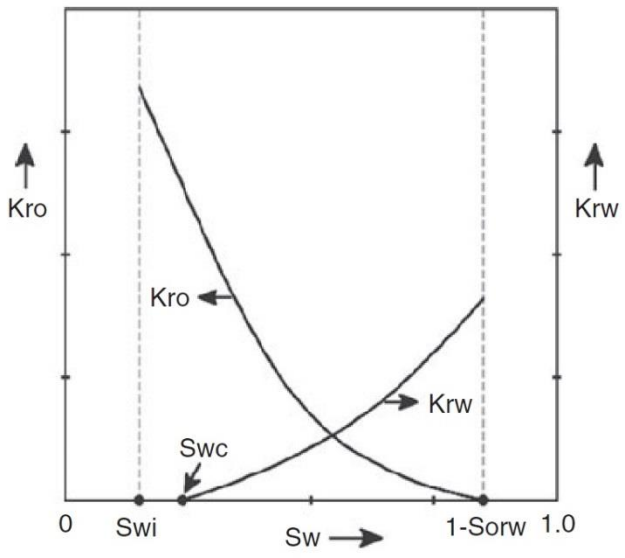

Figure 5 - Oil-water relative permeability curves (Nnaemeka Ezekwe, 2011)

In Figure 5, the range of water saturation is from the initial water saturation, S_{wi} to water saturation at residual oil saturation, $1 - S_{orw}$. Oil relative permeability, k_{ro}, is highest at S_{wi} and declines to zero at $1 - S_{orw}$. Water relative permeability, k_{rw}, increases from zero at S_{wi} to its highest value at $1 - S_{orw}$. Figure 5 shows the location of critical water saturation, S_{wc}. Critical water saturation is the level of water saturation at which water starts to flow in the reservoir (Nnaemeka Ezekwe, 2011).

2.4.4 Wettability

Wettability is defined as the tendency of one fluid to spread on or adhere to a solid surface in the presence of other immiscible fluids. The concept of wettability is illustrated in Figure 6. Small drops of three liquids— mercury, oil, and water—are placed on a clean glass plate. The three droplets are then observed from one side as illustrated in Figure 6. It is noted that the mercury retains a spherical shape, the oil droplet develops an approximately hemispherical shape, but the water tends to spread over the glass surface. The tendency of a liquid to spread over the surface of a solid is an indication of the *wetting* characteristics of the liquid for the solid (Ahmed Tarek, 2001).

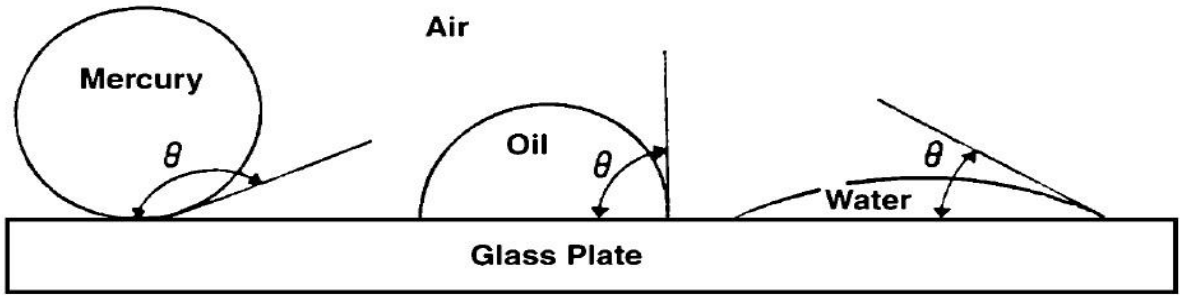

Figure 6 – Illustration of wettability (Ahmed Tarek, 2001)

The surface of a water-wet rock, preferentially maintains contact with water, while the surface of an oil-wet rock will preferentially maintain contact with oil in an oil-water system. The most common method of determining rock wettability is by measurement of the *contact angle*, between the rock surface and the fluid system. (Nnaemeka Ezekwe, 2011).

The composition of the reservoir oil affects the wettability of the rock. The wetting state of reservoir rock is affected by the presence of polar compounds such as asphaltenes, film forming components, and high molecular weight paraffins. Other factors that may affect rock wettability include the type of minerals present in the rock, the reservoir rock type (quartz, silica, calcite, etc.), and salinity of the connate water (Nnaemeka Ezekwe, 2011).

The wettability of reservoir rocks to the fluids is important in that the distribution of the fluids in the porous media is a function of wettability. Because of the attractive forces, the wetting phase tends to occupy the smaller pores of the rock and the non-wetting phase occupies the more open channels (Ahmed Tarek, 2001).

2.4.5 Contact angle

Spreading tendency can be expressed more conveniently by measuring the angle of contact at the liquid-solid surface (Ahmed Tarek, 2001). For an oil-water system in contact with a solid surface, the contact angle, θ is the angle between the fluid-solid interface measured through the water phase. The rock surface is considered to be water-wet when $\theta < 90°$ and oil-wet when $\theta > 90°$ (Figure 7). When $\theta \approx 90°$, the rock surface is considered to be intermediate- or neutral-wet (Nnaemeka Ezekwe, 2011).

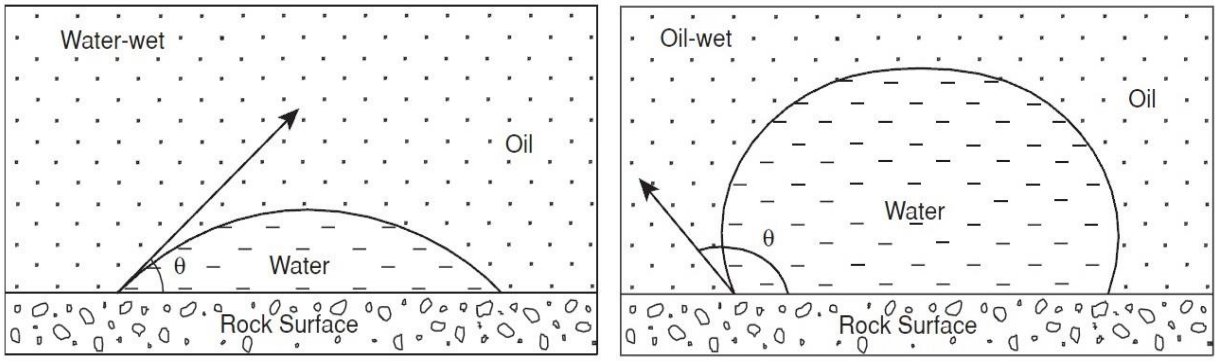

Figure 7 - Water-wet rock and oil-wet rock (Nnaemeka Ezekwe, 2011)

2.4.6 Surface and interfacial tension

Term *surface tension* is used to describe the forces acting on the interface of liquid and gas. When the interface is between two liquids, the acting forces are called *interfacial tension* (Ahmed Tarek, 2001).

Whenever immiscible phase coexist in a porous medium as in essentially all processes of interest, surface energy related to the fluid interfaces influences the saturations, distributions, and displacement of the phases (Don W. Green and G. Paul Willhite, 1998). This means that when two or more immiscible phases come into contact, interfacial energy is created. This translates in turn into a tension or stress on the surface of the interface, just like a membrane or a balloon. As a result, work is required to deform the fluid–fluid interfaces. When the immiscible phases are located in the pores of a rock, the interfaces curve, and a pressure difference across the interfaces develops—namely, the *capillary pressure* (Vladimir Alvarado and Eduardo Manrique, 2010). The surface or interfacial tension has the units of force per unit of length, e.g., dynes/cm, and is usually denoted by the symbol σ.

2.4.7 Capillary pressure

The capillary forces in a petroleum reservoir are the result of the combined effect of the surface and interfacial tensions of the rock and fluids, the pore size and geometry, and the wetting characteristics of the system (Ahmed Tarek, 2001).

Capillary pressure, p_c is commonly defined as the difference in the pressure of the non-wetting phase and the pressure of the wetting phase. This is represented as (Nnaemeka Ezekwe, 2011):

$$p_c = p_{nw} - p_w \quad (5)$$

where p_{nw} - pressure in the non-wetting phase,

p_w - pressure in the wetting phase.

For example, the capillary pressure for a water-wet rock in an oil/water system:

$$p_c = p_o - p_w \quad (6)$$

The phenomenon of capillarity in reservoirs can be discussed in terms of capillary pressure as measured in capillary tubes. For a capillary tube, capillary pressure is determined as (Nnaemeka Ezekwe, 2011):

$$p_c = \frac{2 \cdot \sigma \cdot cos\theta}{r}, \quad (7)$$

where σ - the interfacial tension between the two immiscible phases, dynes/cm,

θ - contact angle, degrees,

r - radius of the capillary tube, cm.

The interfacial phenomena for a single capillary tube also exist when bundles of interconnected capillaries of varying sizes exist in a porous medium. The capillary pressure that exists within a porous medium between two immiscible phases is a function of the interfacial tensions and the average size of the capillaries which, in turn, controls the curvature of the interface. In addition, the curvature is also a function of the saturation distribution of the fluids involved (Figure 8) (Ahmed Tarek, 2001).

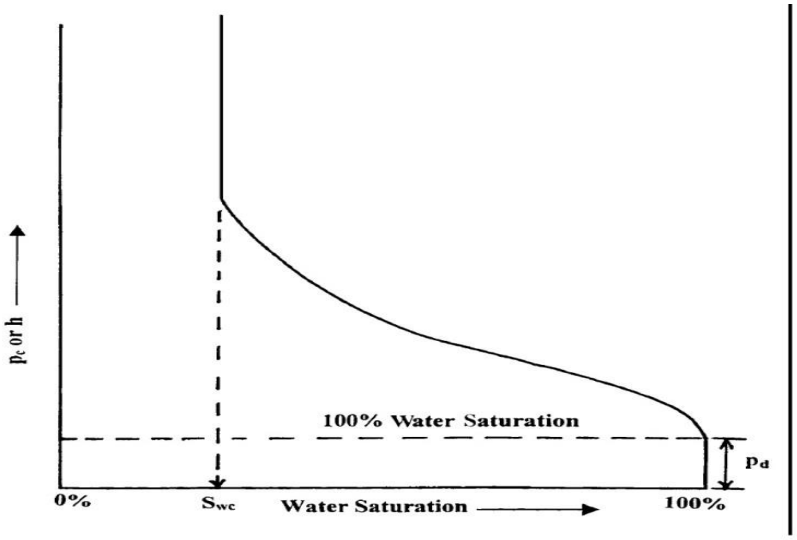

Figure 8 - Capillary pressure curve (Ahmed Tarek, 2001)

Two important phenomena can be observed in Figure 8. First, there is a finite capillary pressure at 100% water saturation that is necessary to force the non-wetting phase into a capillary filled with the wetting phase. This minimum capillary pressure is known as the displacement pressure, p_d (Ahmed Tarek, 2001).

2.5 LSW mechanisms

Numerous core-flooding experiments have shown that Low-Salinity Water Flooding (LSW) could improve oil recovery in sandstone reservoirs (Ahmad Aladasani et al., 2012). Several mechanisms were proposed to explain how the oil recovery could be improved by LSW. However, some of the proposed mechanisms could be only a result of low-salinity waterflooding, rather than the cause of IOR. Some others could contribute to the increase of oil recovery, but may not be the primary mechanism (Ramez A. Nasralla and Hisham A. Nasr-El-Din, 2014).

The debate about the primary mechanism of IOR by low-salinity water creates some uncertainties about the success and the optimum conditions of the application of low-salinity waterflooding on the field scale. (Ramez A. Nasralla and Hisham A. Nasr-El-Din, 2014). The main proposed mechanisms will be presented below.

2.5.1 Fine migration or permeability reduction

In principle, clay tends to hydrate and swell when contacting with fresh water—that is, water containing salts in amounts insufficient to prevent swelling and hydration of the clay. A less-saline solution affects the dispersion of clay and silt in the formation. The clay and silt, upon dispersion, become mobile and follow the paths taken by the greatest proportion of the flowing water. These paths are the domains of high permeability, and the mobile clay and silt become lodged in the smaller pore spaces of these domains and reduce the flow of water through these pore spaces. The permeability of the domains where clay and silt lodge is accordingly reduced, and the water is forced to take other flow paths (Sheng James J., 2011).

Reduction in permeability in the more permeable domains improves the *mobility ratio* of waterflood. Premature breakthrough is thus reduced, and the efficiency of the waterflood is improved. Poorly cemented clay particles, such as kaolinite and illite, can become detached during aqueous flow, especially when flowing brines become fresher (Sheng James J., 2011).

The first explanation for LSW effects was from "migration of fines" by Tang and Morrow in 1999. They observed that fines (mainly kaolinite clay fragments) were released from the rock surface and an increase of spontaneous imbibition recovery with a decrease in salinity for different sandstone cores. During experiments the oil recovery factor increased significantly in the case of Berea sandstone core with more clay content. However, oil recovery is independent of brine salinity when cores were fired and acidized to stabilize fines and saturated with refined mineral oil rather than crude oil. From their results, they suggested that the mobilization of fines resulted in exposure of underlying rock surfaces, which increased the water wetness of the system (Cuong T.Q. Dang et al., 2013).

However, numerous researchers from industry reported that LSW has higher recovery without any observations of fines migration during their experiments and pilot tests. Based on these observations, people questioned about the link between fines migration and the additional oil recovery and it is not the direct cause for the benefits of LSW (Cuong T.Q. Dang et al., 2013).

2.5.2 pH effects

pH is a measure of the acidity or basicity of an aqueous solution. Solutions with a pH less than 7 are said to be acidic and solutions with a pH greater than 7 are basic or alkaline. Pure water has a pH very close to 7 (Wikipedia, pH).

An increase of pH is usually observed during LSW. McGuire et al. (2005) suggested that the EOR mechanisms of LSW appear similar to those of alkaline flooding by generation of in-situ surfactants, changes in wettability, and reduction in the interfacial tension. They also proposed the saponification mechanism of elevated pH and removal of harmful multivalent cations due to low salinity injection by the following chemical reactions (Cuong T.Q. Dang et al., 2013):

$$\begin{cases} (RCOO)_3C_3H_5 + 3NaOH \rightarrow 3(RCOONa) + C_3H_5(OH)_3 \\ fat + alkali \rightarrow soap + glycerol \end{cases} \quad (8)$$

$$\begin{cases} 2(RCOONa) + Ca(HCO_3)_2 \rightarrow (RCOO)_2Ca + 2(NaHCO_3) \\ soap + \text{"hardness"} \rightarrow insolublesoap\ curd \end{cases} \quad (9)$$

Lager, A. (2007) suggested another explanation for the pH increase. This might be explained by dissolution of the small amount of cementing material, carbonate, and cation exchange between the mineral surface and brine.

$$CaCO_3 \leftrightarrow Ca^{2+} + CO_3^{2-} CaCO - Cation\ exchange \quad (10)$$

$$CO_3^{2-} + H_2O \leftrightarrow HCO_3^- + OH^- - Carbonate\ dissolution \quad (11)$$

Nevertheless, the acid number of crude oil should be larger than 0.2 rug KOH/g in order to generate in-situ surfactant; but most of crude oil samples that were used had an acid number of less than 0.05 mg KOH/g. Additionally, the increase and final value of pH after LSW is quite small; therefore, it is difficult to conclude that additional oil recovery is due mainly to in-situ surfactant generation (Cuong T.Q. Dang et al., 2013).

Desorption by pH increase

Since there is lack of evidence on the effects of in-situ surfactant, Austad et al. (2010) proposed a hypothesis of desorption by pH increase (Cuong T.Q. Dang et al., 2013).

In this hypothesis the clay acts as a cation exchanger with a relatively large surface area. Initially, both basic and acidic organic materials are adsorbed onto the clay together with inorganic cations, especially Ca^{2+} from the formation water. A chemical equilibrium is then established at actual reservoir conditions regarding pH, temperature, pressure etc. Remember that the initial pH of the reservoir formation water may be even below 5 due to dissolved CO_2 and H_2S (Tor Austad et al., 2010).

When the low saline water is injected into the reservoir with an ion concentration much lower than that in the initial formation brine, the equilibrium associated with the brine-rock interaction is disturbed, and a net desorption of cations, especially Ca^{2+}, occurs. To compensate for the loss of cations, protons H^+ from the water close to the clay surface adsorb onto the clay, a substitution of Ca^{2+} by H^+ is taking place. This creates a local increase in pH close to the clay surface as illustrated by the following equation using Ca^{2+} as an example (Tor Austad et al., 2010):

$$Clay - Ca^{2+} + H_2O = Clay - H + Ca^{2+} + OH^- \quad (12)$$

The local increase in pH close to the clay surface causes reactions between adsorbed basic and acidic material ordinary acid-base proton transfer reaction, as shown by Equations 13 and 14:

$$Clay - NHR_3^+ + OH^- = Clay + R_3N + H_2O \quad (13)$$

$$Clay - RCOOH + OH^- = Clay + RCOO^- + H_2O \quad (14)$$

Suggested mechanism is schematically illustrated in Figure 9.

The source of OH^- mainly comes from injected water: however, the concentration of OH^- in the reservoir conditions is relative small and it can be easily precipitated by combining with the other divalent ions such as Mg^{2+} instead of exchanging with clay surfaces. It is also difficult to use this hypothesis for explaining the strong dependence of the incremental oil recovery on the divalent ion concentrations such as Ca^{2+} and Mg^{2+} in the injected brine (Cuong T.Q. Dang et al., 2013).

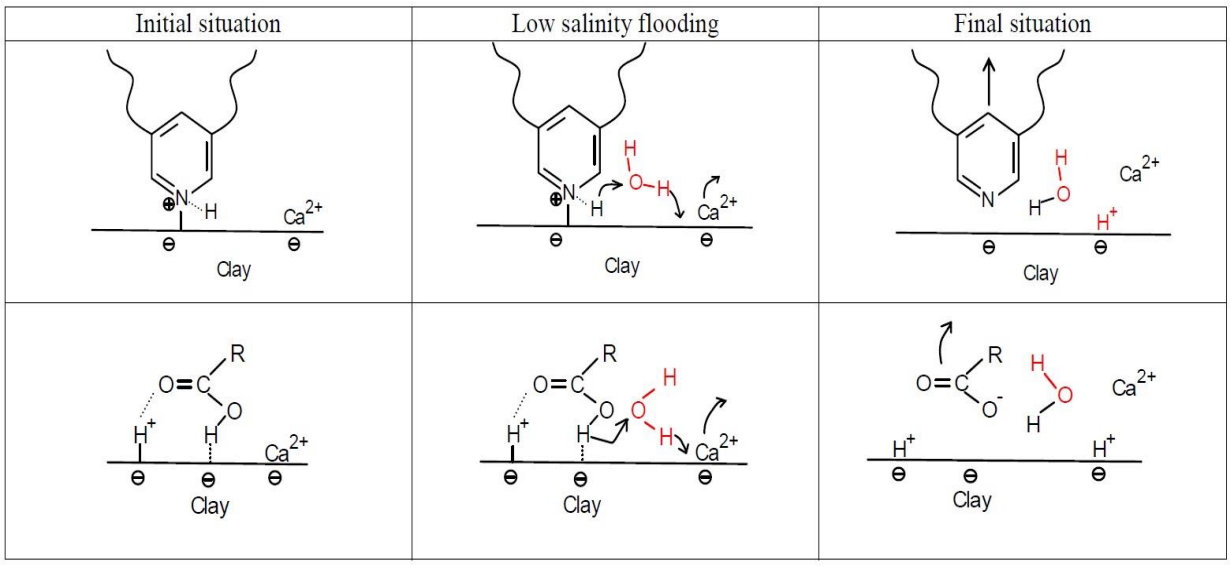

Figure 9 - Proposed mechanism for low salinity EOR effects. Upper: Desorption of basic material. Lower: Desorption of acidic material. The initial pH at reservoir conditions may be in the range of 5 (Tor Austad at al., 2010)

2.5.3 Multicomponent ion exchange

Owing to the different affinities of ions on rock surfaces, the result of multicomponent ion exchange (MIE) is to have multivalents or divalents such as Ca^{2+} and Mg^{2+} strongly adsorbed on rock surfaces until the rock is fully saturated. Multivalent cations at clay surfaces are bonded to polar compounds present in the oil phase (resin and asphaltene) forming organo-metallic complexes and promoting oil-wetness on rock surfaces (Sheng James J., 2011).

Relating to the cations exchange in reservoir conditions Lager, A. (2007) proposed idea about Multicomponent Ionic Exchange (MIE) as the basis for geochromatography. MIE involves the competition of all the ions in pore fluids for the mineral exchange sites (Cuong T.Q. Dang et al., 2013). In his coreflooding experiments concentration of Mg^{2+} decreased in the effluent. Based on this result, Lager, A. (2007) found that cation exchange, ligand bonding, cation bridging and water bridging, have strong effects during LSW (Figure 10).

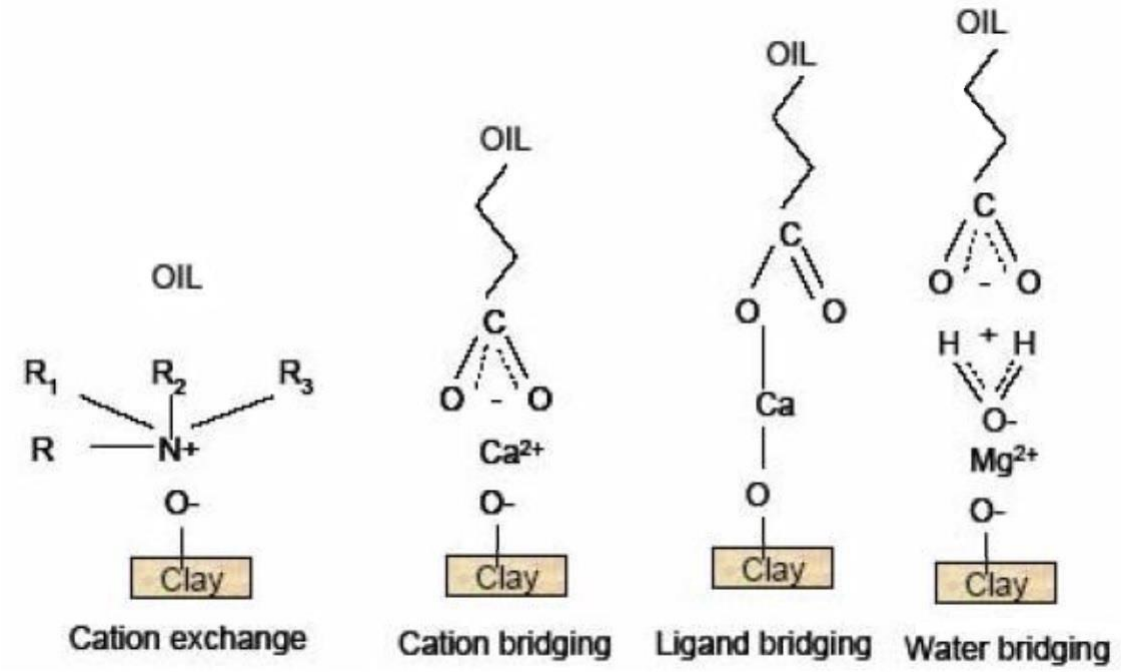

Figure 10 - Four of the proposed adsorption mechanisms of organic materials onto clay surface (Ole Martin Valderhaug, 2013)

During the injection of low-salinity brine, MIE will take place, removing organic polar compounds and organo-metallic complexes from the surface and replacing them with uncomplexed cations (Lager et al., 2006). In theory, desorption of polar compounds from the clay surface should lead to a more water-wet surface, resulting in an increase in oil recovery (Sheng James J., 2011).

Expansion of the electrical double layer due to low salinity flooding enables desorption of polar compounds from the surface. However, Lager did not consider precipitation of $Mg(OH)_2$ which could explain the decrease of the cation Mg^{2+} concentration in the effluent. Additionally, there are no chemical reasons why the strongly hydrated Mg ion should have a superior reactivity toward the active sites on the clay surface compared to Ca^{2+}. Also, Ca^{2+} is typically expected to be stronger adsorbed on the clay mineral instead of desorption during the course of LSW as the explanations from Appelo and Postma (2005) (Cuong T.Q. Dang et al., 2013).

2.5.4 Double layer expansion

Double layer (DL) or an electrical double layer (EDL) is a thin surface layer of spatially separated opposite electrical charges, which is formed at the interface of two phases (Figure 11). Since the spatial separation of charges is always accompanied by the appearance of electric potential difference, EDL can be considered as a kind of micro-capacitor whose distance between the electrodes is determined by the molecular size. Formation of the double layer has a significant effect on the rate of electrode processes, the stability of disperse systems, wettability, friction, and other properties of interfaces.

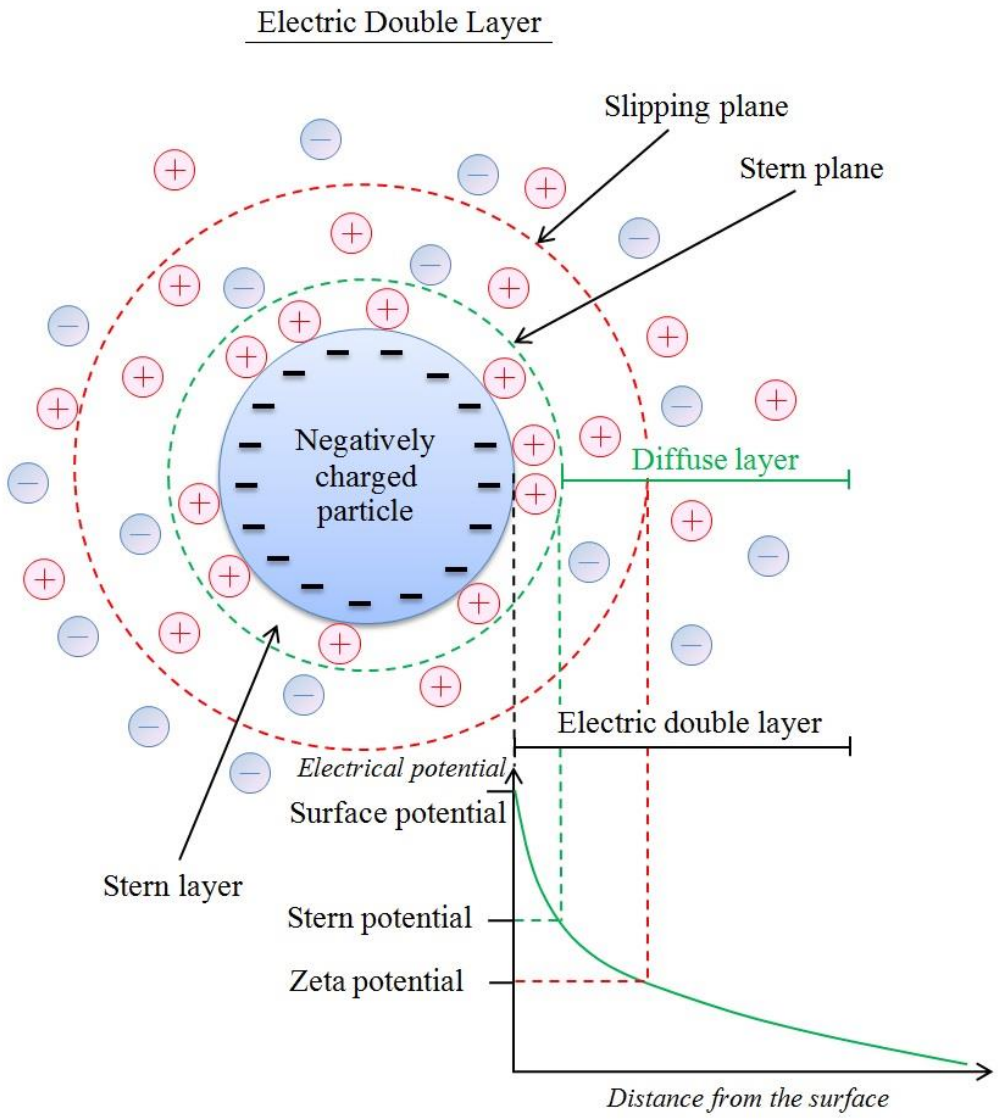

Figure 11 - Illustration of the Double Layer structure near the surface of the negatively charged particle (Ramez A. Nasralla and Hisham A. Nasr-El-Din, 2014)

Zeta potential

Double layer thickness is a function of the electric charges at the oil/brine and rock/brine interfaces, which can be estimated by measuring the zeta-potential (ζ-potential) (Ramez A. Nasralla and Hisham A. Nasr-El-Din, 2014). The zeta potential at the slipping plane is thought to be a good approximation of the (Stern) potential on the Stern layer (Ligthelm, D.J., et al., 2009). The Stern layer is defined as the space between the colloid wall and a distance equal to the ion radius, being free of electrical charge (Shaw, D.J., 1966; Mysels, K.J., 1967) (Figure 11).

The zeta potential of sandstone or clay is significantly affected by the ionic strength of water. Lowering the brine salinity changes the surface charges of sandstone to strongly negative. Furthermore, the surface charge of solids is affected by the cation type. Ca^{2+} and Mg^{2+} result in weak negative charges of Berea sandstone; whereas Na^{+} ions make the charges strongly negative (Ramez A. Nasralla and Hisham A. Nasr-El-Din, 2014).

Double layer expansion

Expansion of electrical double layer is one of possible mechanisms of improved oil recovery by low salinity water flooding. Ligthelm, D.J., et al. (2009) discussed the double layer effect, which is the expansion of the ionic electrical double layer between the clay and oil interfaces and increases in the absolute level of the zeta potential. This is turn yields increased electrostatic repulsion between the clay particle and the oil, leading to desorption of oil components from the surface and increase in water wetness (Cuong T.Q. Dang et al., 2013).

There are several results supporting this theory. Ligthelm, D.J., et al. (2009) performed flooding experiments with brine containing sodium, calcium and magnesium. After oil production had stopped the brine composition was changed to a content of only sodium chloride, with the same ionic strength, and a small increase in oil recovery was observed. These results were explained by cation exchange between brine and divalent cations attached to the rock surface. Then brine was changed to LSW with 100 times lower salinity and significant increase in recovery were observed. These results were explained by double layer expansion mechanism and contribution of ion exchange believed to be small.

Ramez A. Nasralla and Hisham A. Nasr-El-Din (2014) also investigated double layer expansion as a primary oil recovery mechanism. The authors studied the effect of brine salinity on the contact angle measurements with two types of sandstone rocks and three different brines. Ramez A. Nasralla and Hisham A. Nasr-El-Din (2014) showed that low salinity water alters the mica surface to strongly water wet and attributed the wettability alteration to the repulsive forces caused by low salinity water, which results in a thick and stable water film.

During experimental work was performed zeta potential measurements, contact angle tests, core flood experiments. Results showed that the double layer expansion, which is a function of brine salinity and pH, could be the primary oil recovery mechanism. Different brines with different pH were studied and results showed that reducing the pH of low salinity brine changed the electric charges at both oil/brine and rock/brine interfaces from highly negative to closer to zero, which decreases the repulsive forces and reduces the expansion of double layer caused by low salinity water. As a result, the rock becomes more oil wet and oil recovery is suppressed when compared to low salinity water flooding at the original pH of the brines (Ramez A. Nasralla and Hisham A. Nasr-El-Din, 2014). Furthermore oil recovery increasing was observed in secondary injection mode and not in tertiary mode. Authors explained it by trapping of oil clusters after high salinity water injection and not strong enough repulsive forces caused by low salinity water to sweep the residual oil.

2.5.5 Wettability alteration

The contact angle θ is influenced by the tendency of one of the fluids in the immiscible pair to spread on the pore wall surface in preference to the other. The qualitative recognition of preferred spread is called a *wettability preference*, and the fluid which spreads more is said to be the wetting phase fluid (Figure 12) (Archer J.S. and Wall C.G., 1986).

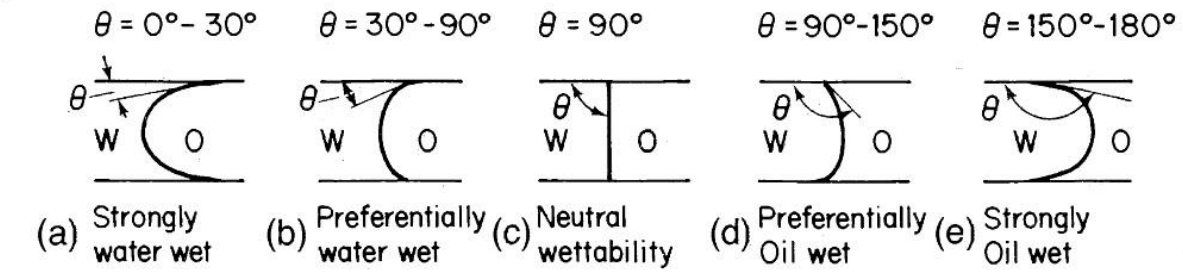

Figure 12 - Wetting contact angles in confined capillaries, (a) Strongly water wet, (b) preferentially water wet, (c) neutral, (d) preferentially oil wet, (e) strongly oil wet (Archer J. S. and Wall C. G, 1986)

The degree of wettability exhibited depends both on the chemical compositions of the fluid pair particularly the asphaltine content of the oil, and o the nature of the pore wall. Pure quartz sandstone o calcite surfaces are likely to be wetted preferentially by water. The presence of certain authigenic clays, particularly chamosite, may promote oil wet character. The capillary pressure forces that influence allowable saturation change in pores of a given size are thus directly influenced by wetting character (Archer J.S. and Wall C.G., 1986).

In despite of plenty of mechanisms and theories regarding LSW the general agreement among researchers is that injecting low salinity brine creates a wetting state more favorable for oil recovery (Ramez A. Nasralla and Hisham A. Nasr-El-Din, 2014). Wettability alteration during low salinity water injection was studied by several authors.

Buckley, J.S. and Yu Liu (1997) studied wettability alteration, caused by crude oil and reservoir rock interactions. They considered different aging time, temperature and fluid composition. Results showed that the rates of both adsorption and desorption of polar crude oil components, as well as the solubility of water in the oil, may all increase with increasing temperature. Also desorption of crude oil components depends on brine composition (Buckley, J.S. and Yu Liu, 1997).

Berg, S. et al. (2010) provided direct experimental evidence of detachment of crude oil from clay minerals. They found that wettability modification of clay surfaces is the microscopic mechanism tor low salinity flooding and emulsification, IFT reduction, fines migration and selective plugging of water-bearing pores via clay swelling are most relevant reasons for higher oil recovery.

Ramez A. Nasralla and Hisham A. Nasr-El-Din (2014) studied wettability alteration of mica by measuring contact angle for crude oil on mica surface (Figure 13). On Figure 13 you can see that NaCI solution altered the rock surface to be more water-wet. Therefore, injection of a monovalent cation is more preferable for oil-recovery improvement. Sea water and the 5000 mg/L $CaCl_2$ solution produced weak charges at the oil/brine and rock/ brine interfaces, which caused weak repulsive forces between the oil and rock surfaces and resulted in a stable water film and a less- water-wet system, as shown by the contact-angle results. The 10% AQ and 5000 mg/L NaCI

solution increased the magnitude of the negative charges. An increase in the magnitude of the negative charge at oil/brine and rock/brine interfaces resulted in higher repulsive forces between oil and rock, which expanded the double layer and produced a more-water-wet system (Ramez A. Nasralla and Hisham A. Nasr-El-Din, 2014).

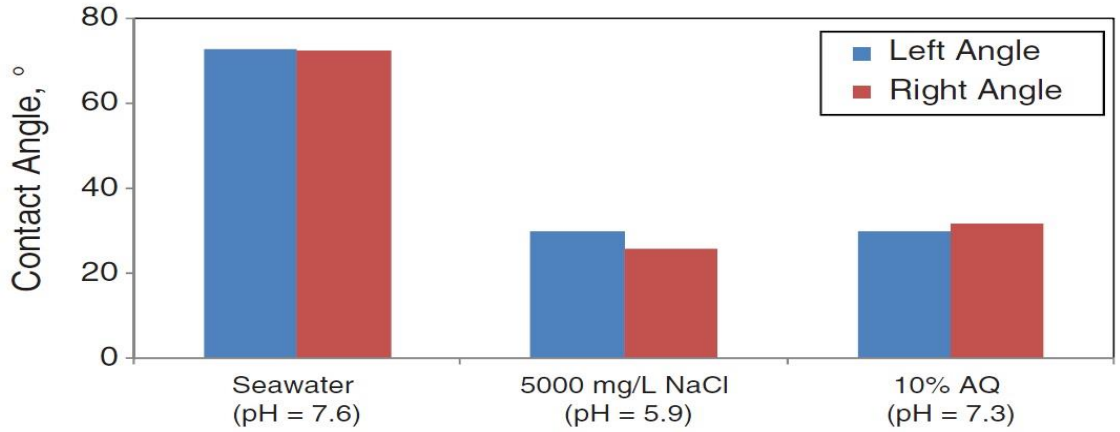

Figure 13 - Right and left contact angles of crude oil vs. different water salinities at 500 psi and 212°F. Low-salinity water altered the mica surface to be more water-wet (Ramzes A. Nasralla and Hisham A. Nasr-El-Din, 2014)

Among the proposed hypotheses, wettability alteration towards increased water wetness during the course of LSW is the widely suggested case of increased oil recovery. It has been experimentally found that the low salinity brine has a significant effect on the shape and the end points of the relative permeability curves, resulting in a lower water relative permeability and higher oil relative permeability (Cuong T.Q. Dang et al., 2013).

2.6 Modeling and numerical simulation of LSW

There are only few modeling works regarding LSW in compare with experimental studies. One of the first modeling works were presented by Gary R. Jerauld et al. (2008). The model represents low-salinity flooding using salinity-dependent oil/water relative permeability functions resulting from wettability change. This is similar to other EOR modeling and conventional fractional-flow theory can be adapted to describe the process for secondary and tertiary low-salinity waterflooding. This simple analysis shows that while some degree of connate-water banking occurs, it need not hinder the process (Gary R. Jerauld et al., 2008).

In their model, salt was modeled as an additional single-lumped component in the aqueous phase; relative permeability and capillary pressure are made a function of salinity, and include the effect of connate water, hysteresis between imbibitions and secondary drainage water relative permeability, and dispersion phenomena. However, this model used a simple linear salinity dependence on residual oil saturation, which is not appropriate for real cases (Cuong T.Q. Dang et al., 2013).

Some of works for LSW simulation were made based on PHREEQC geochemical code. Basically this model gave only an approximation of the pH variation as the mechanism of LSW. Then Cuong T.Q. Dang et al. (2013) introduced a comprehensive ion exchange model with geochemical processes including intra-aqueous and mineral reactions (Cuong T.Q. Dang et al., 2013).

They got excellent agreements between the model and the experiments in terms of effluent ion concentrations, effluent pH, and oil recovery. In addition, the model was also proved to be highly comparable with the ion-exchange model of the geochemistry software PHREEQC for both low salinity and high salinity (Cuong T.Q. Dang et al., 2013).

3 EXPERIMENTAL PART

In this chapter will be described materials, apparatus and experimental procedure. The main part of work is flooding of sandstone cores with different brines. Before flooding the cores were saturated with oil, and then aged for a minimum of 2 weeks.

Flooding was performed at the certain temperature and confining pressure. Oil recovery and pressure drop across the core were detected. For effluent water samples were measured pH, ions concentration and the amount of silicon and aluminum.

3.1 Materials

3.1.1 Cores

Two different types of sandstone were used for experiments – Bentheimer and Berea Sandstone. Properties of all cores are listed below in Table 1. Mineral analysis is given in Appendix, Table 9 and Table 10.

Table 1 – Properties of different sandstone cores

Core Number	Core type	Diameter, cm	PV, mL	Length, cm	Porosity	Permeability, Darcy	S_{wi}, %
Al-1	Short Bentheimer	3,77	12,9	5,07	0,23	1,05	18,3
Al-2	Short Bentheimer	3,77	12,7	4,91	0,23	1,05	21,5
Al-3	Short Bentheimer	3,77	13,1	5,08	0,23	1,05	19,7
Al-4	Short Bentheimer	3,77	12,2	5,03	0,22	1,05	20,7
Al-5	Short Bentheimer	3,77	13,3	5,03	0,24	1,05	20,5
Al-6	Short Bentheimer	3,77	12,1	5,09	0,22	1,05	22,1
Al-7	Long Bentheimer	3,77	22,0	9	0,22	1,05	25,5
Al-8	Long Berea	3,78	22,4	9	0,21	0,8	32,5
Al-9	Long Berea	3,78	20,9	9	0,21	0,8	32,5
Al-10	Short Berea	3,78	11,7	4,96	0,21	0,8	31,4
Al-11	Short Berea	3,78	11,6	5,03	0,21	0,8	31,0
Al-12	Long Bentheimer	3,77	22,4	8,95	0,22	1,05	21,4

3.1.2 Oil

For experiments crude oil was substituted by normal-Decane (*n*-C_{10}), supplied by Chiron AS in high-performance liquid chromatography (HPLC) grade (purity > 99%). Crude oil contains different chemical components and this complicates the interpretation of experiments. Using synthetic oil (N-Decane) will give us more clear and comparable results.

Physical properties of the oil at the room temperature (20°C) and flooding temperature (70°C) obtained from the simulation program PVTsim (20.1) are given in Table 2.

Table 2 - Physical properties of N-Decane (Ole Martin Valderhaug, 2013)

N-Decane / Temperature	Room temperature, 20°C	70°C
Viscosity (cP)	0,920	0,4812
Density (g/ml)	0,730	0,7525

For changing wettability of cores we need to add polar components. For this we used oil-soluble additive N,N-Dimethyldodecylamine (*NN*-DMDA), supplied by Fulka (purity > 99%). Structural formula:

$$CH_3(CH_2)_{11}N(CH_3)_2 \text{ - } \textit{N,N-Dimethyldodecylamine} \quad (15)$$

Figure 14 – Measurement of NN-DMDA amount for required concentration

NN-DMDA concentration of 0,01 mol/L were used. It is assumed that the small concentration of NN-DMDA does not have any significant influence on the properties of the oil; however, it adsorbs on the silicate mineral surface (Aly Anis Hamouda and Ole Martin Valderhaug, 2014).

3.1.3 Brines

For experiments were used two types of brine: *Synthetic Sea Water* (SSW) and *Low Salinity Water* (LSW). LSW is 25 times diluted SSW. Table 3 gives the composition of brines. During preparation of brines different types of chemical reagents were dissolved in distillate water and mixed using magnetic steerer for minimum 3 hours. Then brines were filtrated through a 0.22 μm Millipore filter for removing undissolved particles. All liquids were stored in cleaned glass bottles.

Figure 15 – Preparation of brines: filtration setup and brine storage

Table 3 – Composition of brines

Ion Name	SSW (mole/L)	LSW (mole/L)
HCO3-	0.002	0.00008
Cl-	0.525	0.021
SO42-	0.0240	0.00096
Mg2+	0.045	0.0018
Ca2+	0.013	0.00052
Na+	0.450	0.018
K+	0.010	0.0004
TDS (g/L)	33.39	1.3356
Ionic Strength (mol/L)	0.657	0.0263

The ionic strength of the solution is defined as (Burgot J.-L., 2012)

$$I_c = {}^1/_2 \sum_i c_i \cdot z_i \quad (16)$$

This means that the concentration C_i of each ion i is multiplied by the square of its charge z_i, with all the terms for the various ions in solution summed. I_c is expressed in mol/L, thus explaining the c subscript (Burgot J.-L., 2012).

Dynamic viscosities were calculated using method described by Fabuss et.al., (1969). Accuracy is reported to be 0.4%, range is within 20<T<150 (^{o}C), which is more than sufficient for this case (Ole Martin Valderhaug, 2013). Results are given below in Table 4. Equations for viscosity calculation (Fabuss et.al., 1969):

$$\log\left(\frac{\mu_{sw}}{\mu_w}\right) = 0{,}04281 \cdot I + 0{,}001231 \cdot I^2 + 0{,}000131 \cdot I^3 + (\log(10^3 \cdot \mu_w) \cdot (-0{,}03724 \cdot I + 0{,}018591 \cdot I^2 - 0{,}00271 \cdot I^3) \quad (17)$$

$$\mu_w = (4{,}2844 \cdot 10^{-5}) + \frac{1}{(0{,}157 \cdot (T + 64{,}993)^2 - 91{,}296)} \quad (18)$$

where, μ_w - pure water viscosity, cP

μ_{sw} – viscosity of brine, cP

I – ionic strength, mole/L

T – temperature, ℃

Table 4 - Viscosity for the different brines and oil

Temperature	Room temperature, 23°C	50°C	70°C
Oil (cP)	0,920	0,5802	0,4812
SSW (cP)	0,9971	0,5901	0,4382
LSW (cP)	0,9347	0,5484	0,4052

Density of SSW was calculated using Calculator (Water Density Calculator, 2011), which was made by University of Michigan. Calculated values were checked by PAAR densitometer DMA 46 at room temperature and they correspond with the values given by calculator.

Table 5 - Density for the different brines and oil

Temperature	Room temperature, 23°C	50°C	70°C
SSW g/cm^3	1,024	1,012	1,002
LSW 1:25 g/cm^3	0,999	0,989	0,979

Figure 16 - PAAR densitometer DMA 46

3.2 Core preparation and test procedure

3.2.1 Saturation procedure

For simulation of reservoir conditions all cores before flooding were saturated by SSW for creating initial water saturation (S_{wi}) and aged. The aging procedure aimed to create oil-wet condition for sandstone.

Firstly, all samples were stored in oven with temperature 100℃ for several days. Every day weight of each sample was measured by Mettler Toledo PM4600 DeltaRange Balance. Core was considered dry if its weight did not change within two measurements. Oven and weighing of core are shown on Figure 17.

Figure 17 – Oven with cores and weighing of core

Then geometrical parameters of cores (diameter and length) were measured and used for core volume calculations.

$$V_{dry} = \frac{\pi \cdot D^2}{4} \cdot l, \quad (19)$$

where, D – diameter of core, cm

l – core length, cm

After measurements samples were saturated by sea water using Vacuum Setup (Figure 18).

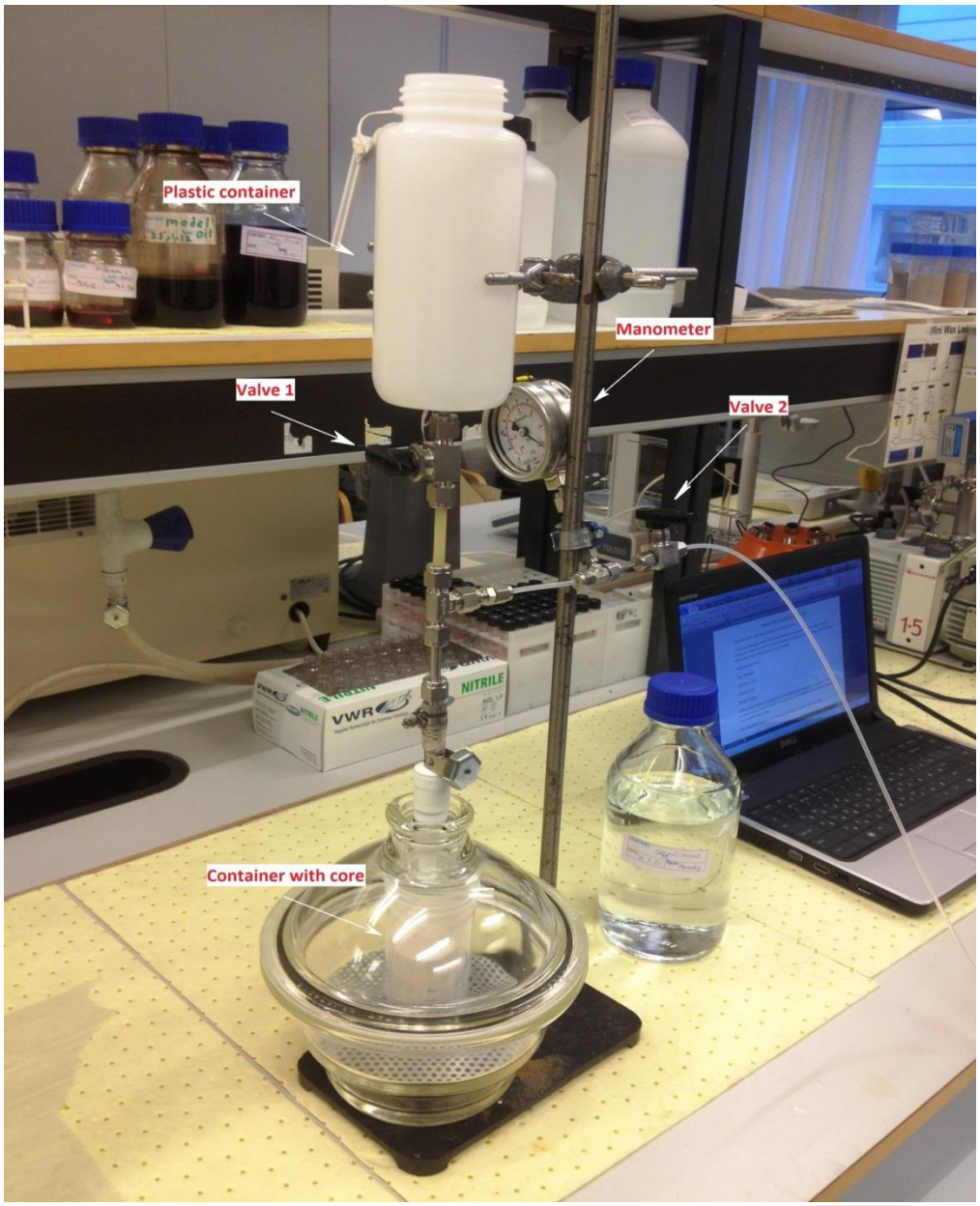

Figure 18 – Vacuum setup

Vacuum setup creates vacuum in glass airtight bowl by using pump and thereby removing air from pore space. Then synthetic sea water from upper plastic container goes to the top of the core by slowly opening Valve 1. Core is fully saturated when manometer shows atmospheric pressure and all water came to the container with core.

After this weight of cores was measured again and used for pore volume (PV) and porosity calculations.

$$PV = \frac{m_{wet} - m_{dry}}{\rho_{SSW}};\ \varphi = \frac{PV}{V_{dry}}, \quad (20), (21)$$

where, PV – pore volume, ml

m_{wet} – weight of core after saturation, g

m_{dry} – weight of core after drying, g

ρ_{SSW} – density of SSW, g/cm^3

φ – porosity

V_{dry} – volume of core, ml

Then flooding procedure with synthetic oil was performed. For this we used Hassler core holder (Figure 19).

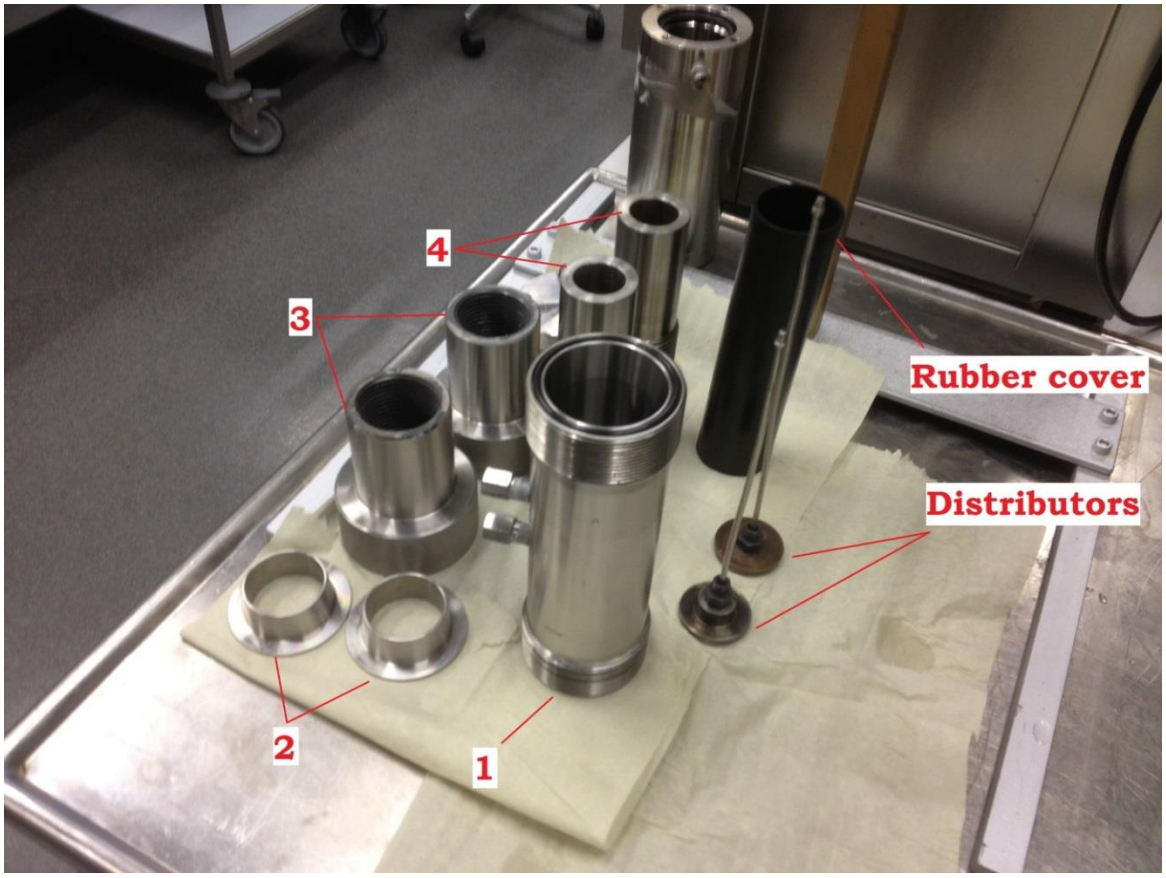

Figure 19 - Hassler core holder in disassembled state

First of all, cores were placed on distributors and wrapped in Teflon paper to exclude any possible evaporation of fluids (Figure 20).

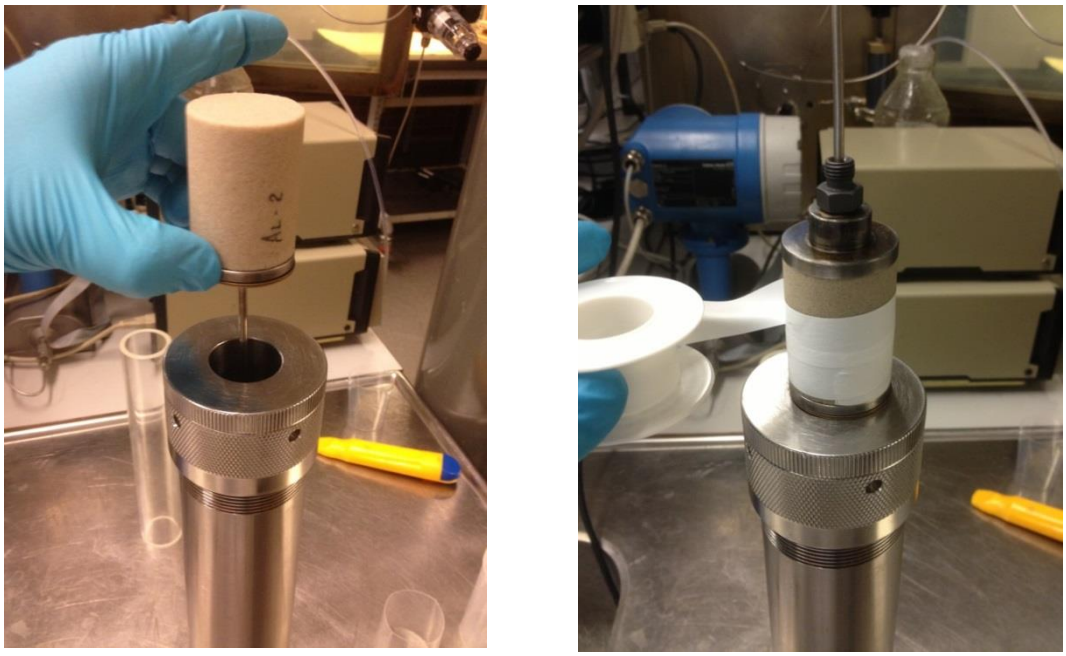

Figure 20 – Core placement and wrapping procedure

Then samples were put inside the plastic cover and heated to establish tight fit (Figure 21). This procedure aimed to prevent contact between core and rubber cover, which will be installed over the core.

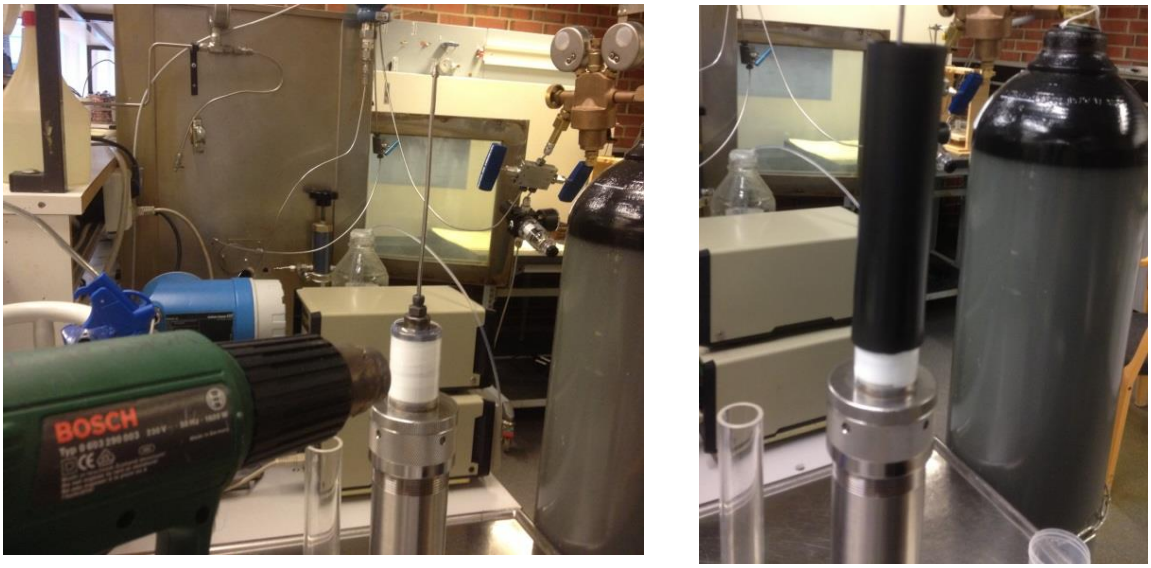

Figure 21 – Heating of plastic cover and putting rubber cover

The core was then put in Hassler core holder and in the oven (flooding setup). Setup for flooding consists of core holder and cylinder with flooding liquid connected to each other, to pumps and manometers. Liquid is produced to test tube. Picture and scheme of flooding setup are shown below on Figure 22 and Figure 23.

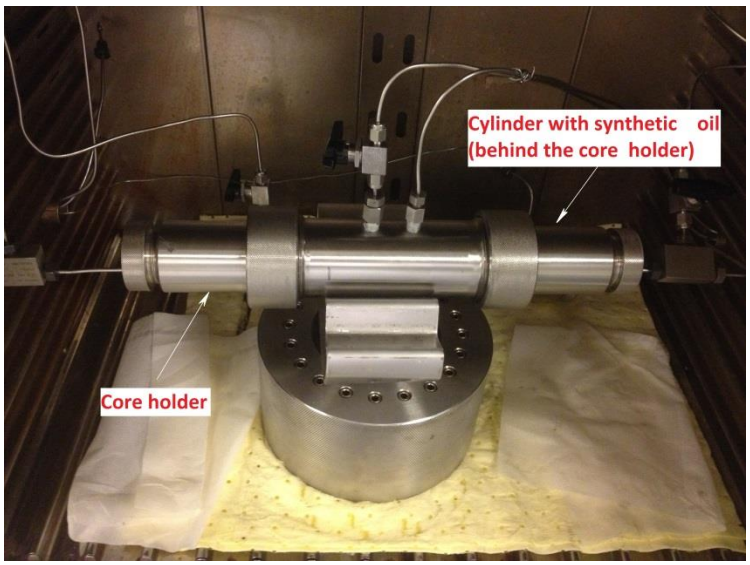

Figure 22 – Picture of flooding setup

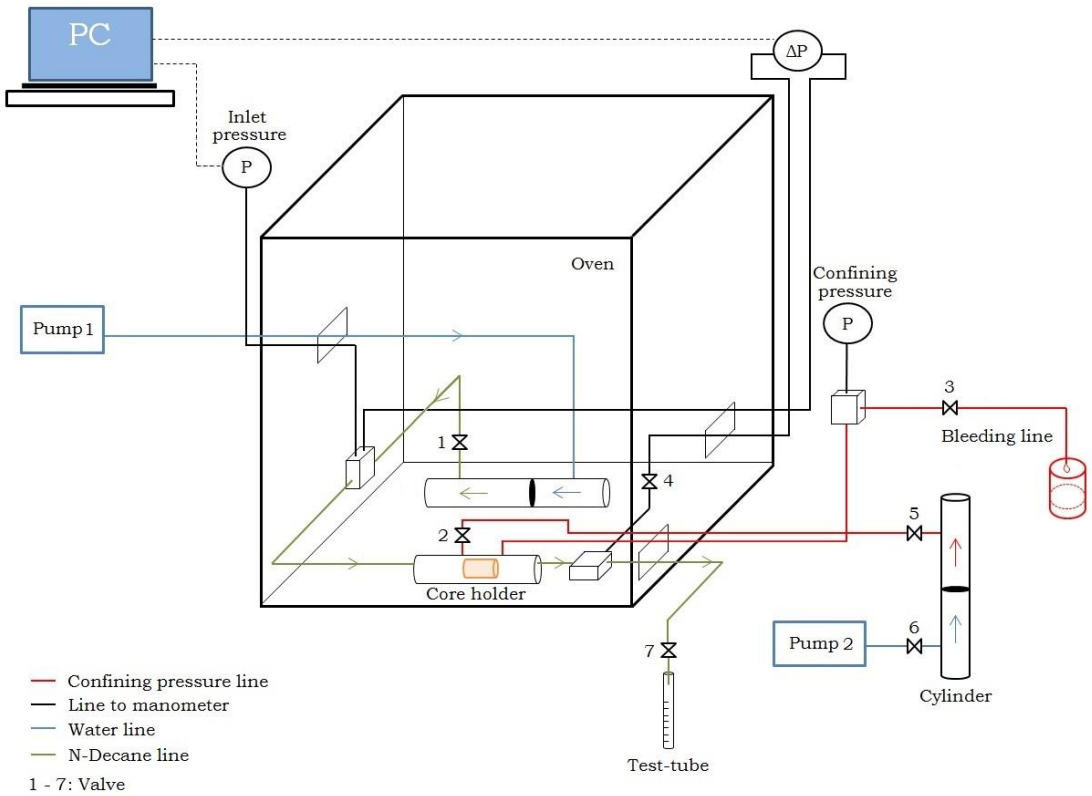

Figure 23 – Scheme of flooding setup

Absolute permeability measurements

Before establishing initial water saturation all cores were flooded with SSW for measuring absolute permeability. SSW was injected with three different rates at the room temperature. Injection rate was kept until stabilizing pressure difference and then switched to the next one.

Absolute permeability was calculated using Darcy's law by averaging results from 3 different flow rates. Measurements were made for two short (≈5cm) and two long (≈9cm) cores both Bentheimer and Berea sandstone. Bentheimer cores were drilled from the same piece of rock and have approximately the same properties. Therefore results for Bentheimer were averaged and used for other samples as well. The same applies for Berea cores. Absolute permeability calculations are presented below.

Table 6 – Absolute permeability calculations

Core Number	Core type	Measured absolute permeability, Darcy	Average permeability, Darcy
Al-1	Short Bentheimer	0,95	1,05
Al-7	Long Bentheimer	1,15	
Al-10	Short Berea	0,75	0,8
Al-8	Long Berea	0,85	

When permeability was measured, SSW in cylinder was replaced by synthetic oil (N-Decane) and flooded through the cores. For simulating reservoir conditions the confining pressure 25 bar was applied by pumping Tellus oil in the space around rubber cover.

Flooding temperature was 50℃ and a flow rate about 10 PV/Day with periodic increasing for reaching maximal possible water out from the core. Amount of drained liquid was detected in test tube. Then for aging the samples were kept in cells filled with synthetic oil minimum for two weeks at 50°C.

Due to previous experience this time is enough for changing wettability of cores from water-wet to more oil-wet. Keeping samples longer than 2 weeks didn't show any deviations in results (Aly Anis Hamouda and Ole Martin Valderhaug, 2014).

3.2.2 Flooding procedure

After two weeks of aging the cores were flooded by different brines. Flooding preparation procedure is similar with preparation for saturation. For each experiment cylinder was filled with different brine.

Flooding was performed at 70℃, confining pressure 25 bars. Outlet line was equipped with backpressure valve which provided outlet pressure 10 bars by compressed nitrogen.

Each core was flooded for at least 4 PV on the low flow rate 4PV/day, and then 4 PV at the high flow rate 16PV/day. Higher velocity applied for oil mobilization and aimed to reach maximum production.

Amount of oil out was recorded continuously by checking the test-tube and then recovery was calculated. Oil recovery as a fraction of original oil in place (OOIP) is defined in the equation (22) below.

$$Recovery = \frac{V_{prod}}{OOIP};\ OOIP = (1 - S_{wi}) \cdot PV, \quad (22)$$

where, V_{prod} – amount of produced oil, ml

$OOIP$ – initial oil in place, ml

S_{wi} – initial water saturation, fraction.

Pressure difference across the core was measured by manometer and transferred to Labview program. During flooding the effluent was collected in test-tube and 3-5 ml water samples were continuously taken. pH was measured for each sample using Mettler Toledo pH meter (Figure 24).

Figure 24 – pH measurements

3.2.3 Analysis

For better understanding LSW mechanism several analyses were performed. The amount of anions and cations in the effluent was measured by Dionex ICS-3000 chromatograph (Figure 25). All water samples were firstly diluted by distillate water (1 to 200 for SSW and 1 to 50 for LSW) and filtrated with 0.2 µm filter for removing possible solid particles. Obtained data in the form of peaks for each ion were manually interpreted using Chromeleon 7 software. For reducing measurement error, area of each peak was corrected. Samples of SSW with known concentration were used as a reference for further interpretation.

Figure 25 - Dionex ICS-3000 chromatograph

Analysis of the amount of Si and Al in the effluent water samples was made by spectrometer PerkinElmer Inc. - Optima 4300 DV ICP-OES (Figure 26). This setup uses inductively coupled plasma mass spectrometry for detecting metals and several non-metals at concentrations as low as one part in 10^{12} (part per trillion). Before running analysis all samples were diluted by 5% HNO_3.

Figure 26 – Spectrometer Optima 4300 DV ICP-OES

4 RESULTS AND DISCUSSION

After performing flooding experiments and analysis all obtained data were interpreted for studying low salinity effects for our rock. We used two different sandstone types with different length and our work may be divided into two parts. The first part is a comparison between Bentheimer and Berea sandstone and second part is comparison between short (≈5cm) and long (≈9cm) cores. Moreover, a comparison between SSW and LSW (1/25) as primary injection fluid was made.

4.1 Core floods overview

For the main study following cores were used:

- 4 Berea and 4 Bentheimer;
- 2 short and 2 long cores for each sandstone type;
- 2 flooding sequences: SSW (followed by LSW) and LSW as a primary injection fluid.

For all cores we have comparable parameters such as diameter, length, initial water saturation, porosity and absolute permeability. These parameters you can see in Table 7 below. So the difference in data between flooding experiments are expected to be dependent mainly on three parameters: *rock type*, *lengths of core (short or long)* and *flooding sequence*. All possible combinations of these three parameters were studied (Figure 27).

Table 7 – Core parameters and flooding sequence

Core	Flooding sequence	Diameter, cm	Length, cm	S_{wi}	Porosity	Permeability, Darcy
Al-4 Short Bentheimer	SSW => LSW	3,77	5,03	20,7	0,22	1,05
Al-7 Long Bentheimer	SSW => LSW	3,77	9	25,5	0,22	1,05
Al-6 Short Bentheimer	LSW	3,77	5,09	22,1	0,22	1,05
Al-12 Long Bentheimer	LSW	3,77	8,95	21,4	0,22	1,05
Al-11 Short Berea	SSW => LSW	3,78	5,03	31,0	0,21	0,8
Al-8 Long Berea	SSW => LSW	3,78	9	32,5	0,21	0,8
Al-10 Short Berea	LSW	3,78	4,96	31,4	0,21	0,8
Al-9 Long Berea	LSW	3,78	9	32,5	0,21	0,8
Al-5 Short Bentheimer	SSW	3,77	5,03	20,5	0,24	1,05

From 12 aged cores 3 were spoiled during flooding due to technical problems. Core **Al-5** was flooded only with SSW as a primary injection fluid and was used as the basis for comparing all other experiments.

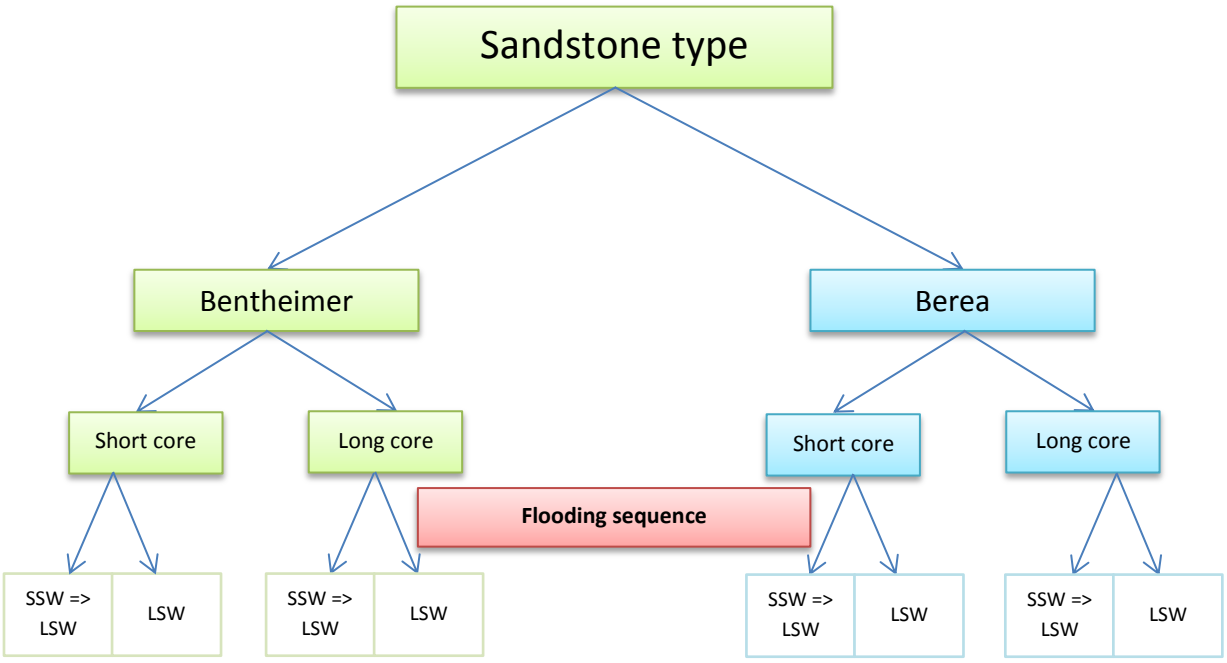

Figure 27 – Flooding sequences

4.2 Core Al-4 Short Bentheimer, SSW-LSW

After aging procedure the Core **Al-4** (Short Bentheimer, 5,03 cm) was flooded with SSW and then with LSW. First 4 pore volumes were flooded by SSW with the injection rate of 4 PV/Day (0,035 ml/min). Then injection rate was increased to 16 PV/Day (0,14 ml/min) and another 4 PV were flooded. This is done in order to mobilize oil that was capillary trapped during the flooding on low flow rate (4 PV/Day). It was assumed that after flooding with increased flow rate (16 PV/Day) only the residual oil is left in pores.

After flooding first 8 pore volumes with SSW, injection fluid was replaced by LSW. Flooding scenario was the same: 4 pore volumes with injection rate 4PV/Day then increasing rate to 16 PV/Day and flooding 4 pore volumes more. Changing injection fluid was performed by shutting down inlet valve and replacing SSW in cylinder by LSW. The main objective of using LSW after SSW flooding is to check possible EOR effect for LSW as a secondary injection fluid.

Flooding results are presented as oil recovery curve and pH measurements plotted versus injected pore volumes of brine (Figure 28). Blue curve represents the oil recovery (in percent from OOIP) which is plotted on the y-axis to the left. For easier data comparison pH measurements were plotted on the y-axis to the right. pH of influent brine is assumed to be constant and presented by green lines and pH of effluent samples presented by red squares. Flooding sequence is showed by vertical black solid lines which divide different injection brines and different injection rates (hereinafter for all graphs).

From the figure below we can see that recovery increases linearly and after early water breakthrough (0,3-0,4 PV) very small additional amount of oil (≈0,1 ml) was produced. Increasing injection rate did not show any increasing in oil recovery. This may be because 4 times increased injection rate is not enough to overcome capillary forces which trap oil. Larger increase of injection rate could show some increase in recovery, but for our experiments we used maximum rate of 16 PV/Day like the most acceptable injection rate from previous experience.

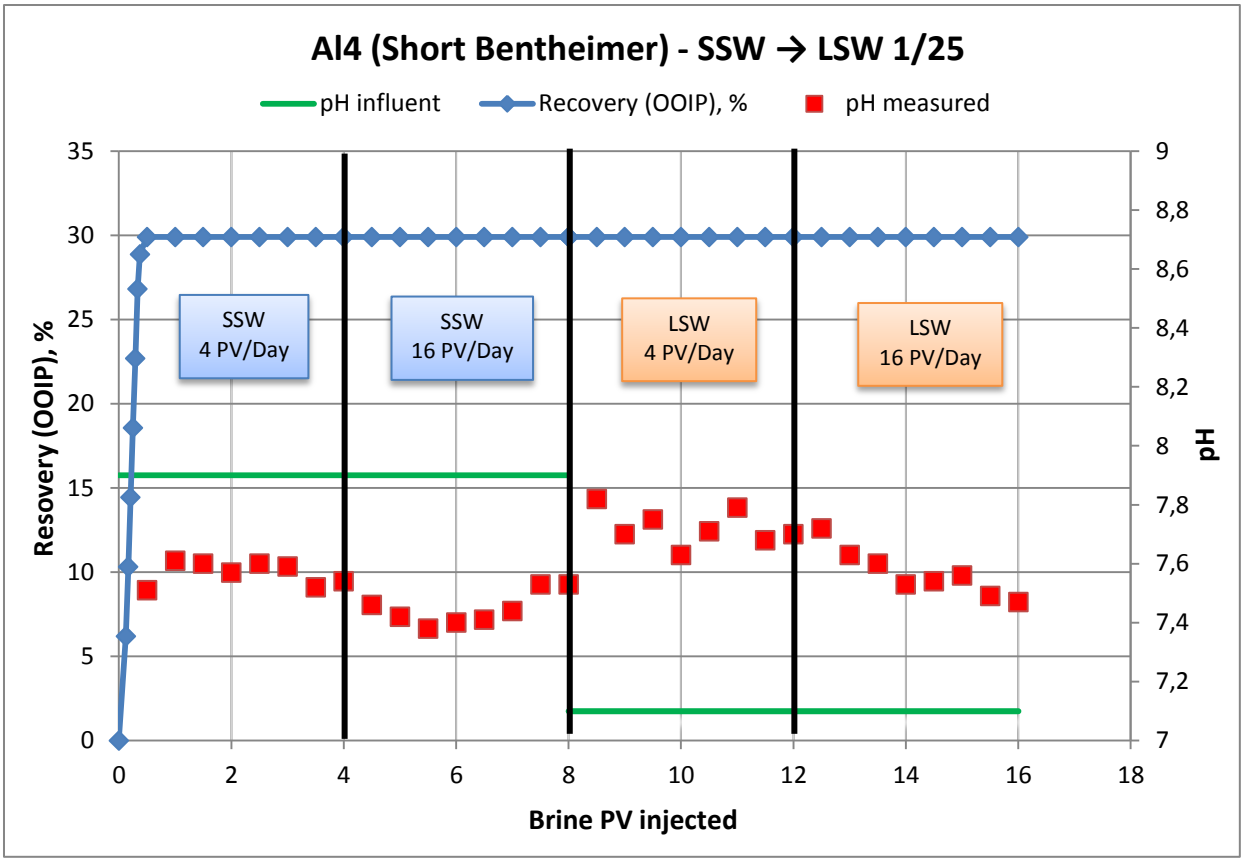

Figure 28 – Oil recovery and pH for influent and effluent during flooding with SSW – LSW for core Al-4

After switching to LSW no additional oil was observed and total recovery from sample is 29,9 %. For explaining this phenomena let's try to analyze other data obtained from experiment.

As we can see from Figure 28 for the first 8 pore volumes of flooding with SSW, pH of effluent is lower than pH of influent. It was observed by several researchers that pH of injection SSW is slightly decreased after flooding (Aly Anis Hamouda and Ole Martin Valderhaug, 2014, RezaeiDoust, A., 2011). Difference between effluent and influent measurements is about 0,3 which is relatively small. Reduction in pH can be due to hydration of magnesium ions at high temperature (70℃) (Aly Anis Hamouda and Ole Martin Valderhaug, 2014).

At the first 4 pore volumes we can see that pH values keep more or less on the same level about 7,6. After switching injection rate to 16 PV/Day we can observe slight decrease in pH. Variation of pH level can be due to rock/brine interactions. As

you will see from the following discussion, we suppose in our work that there exist some rock/brine interactions during flooding with LSW, but most probably SSW also interact with the core.

On Figure 29 you can see ion chromatography results plotted against injected pore volumes of brine. Ion concentration is presented as a relative to known ion concentration of influent LSW. This means that value 1 on the left logarithmic y-axis corresponds to the ion concentration in LSW. Since LSW is 25 times diluted SSW, the value 25 on the left logarithmic y-axis corresponds to the ion concentration in SSW. Values which are higher or lower than 25 for SSW flooding and 1 for LSW flooding represent difference between ion concentration in influent and effluent brines.

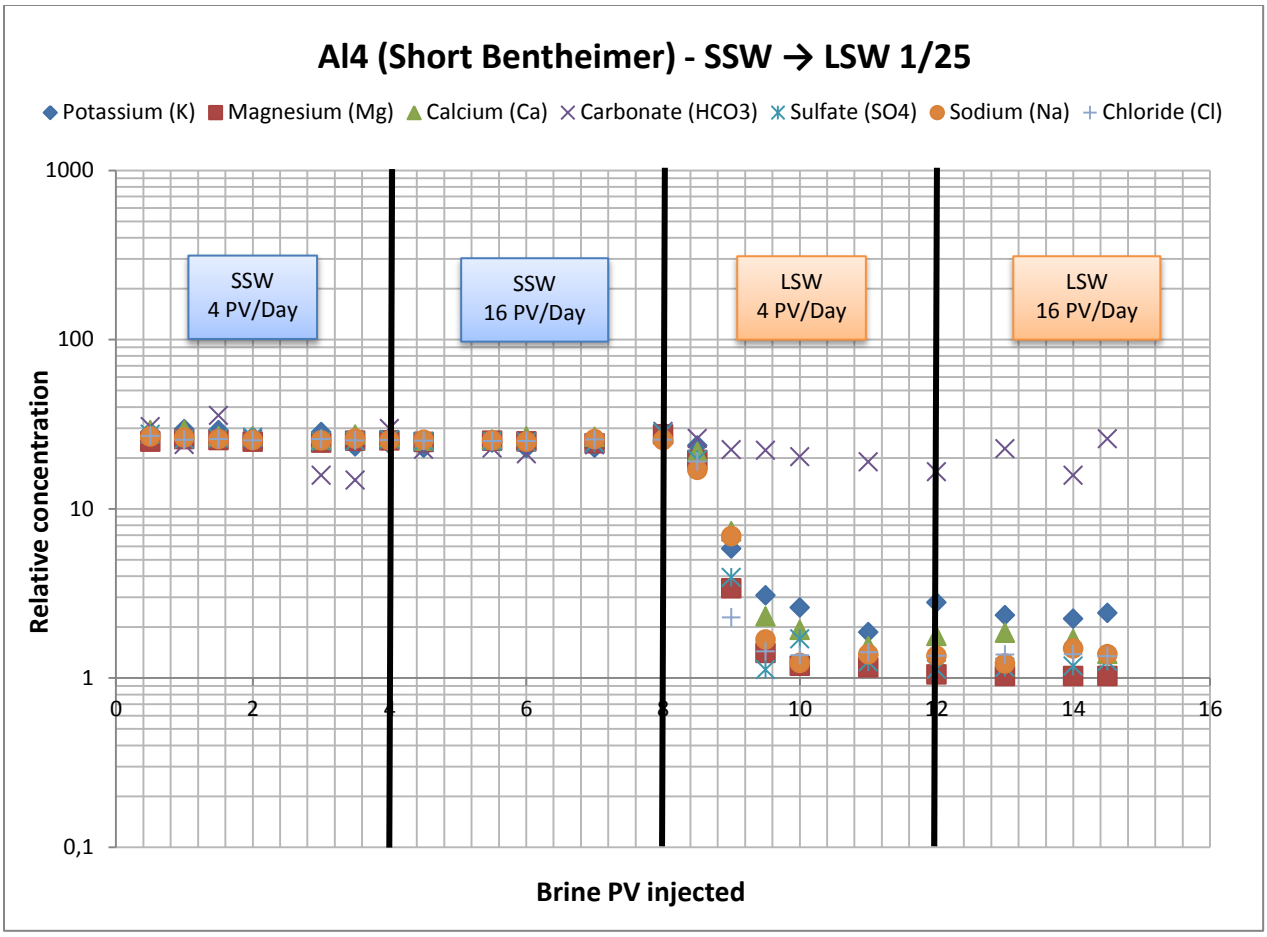

Figure 29 – Ions concentrations for effluent samples taken from the SSW - LSW flooding of core Al-4

We cannot see any significant changes on ion analysis during SSW flooding. For bicarbonate ions we can see some deviations from the SSW level. This can be explained by the complexity of bicarbonate system which depends on pH and interactions with air.

During flooding experiment pressure drop across the core was continuously measured and results are shown on Figure 30. On the Figure 30 pressure drop in µbar is plotted against injected pore volume of brine. Deviations on the graph from the average value are due to low sensitivity of gauge. In the beginning of the flooding we can see peak of pressure drop. This is most probably due to the fact that we have two phases in the core. Before water breakthrough we have the increasing pressure drop because the movement of water through the core is restricted by other phase – synthetic oil. Actual height of the peak is also influenced by the fine migration. Fine migration is possible because of presence of clay material in cores. Ramez A. Nasralla and Hisham A. Nasr-El-Din (2014) observed the same phenomenon during flooding of sandstone cores.

During SSW flooding at 4PV/Day rate we can see that pressure drop is stabilizing after the peak in the beginning. Small peaks can also be explained by fine migrations. After increasing rate to 16PV/Day we can see slow increase of pressure drop and stabilizing after 5th PV with small peaks.

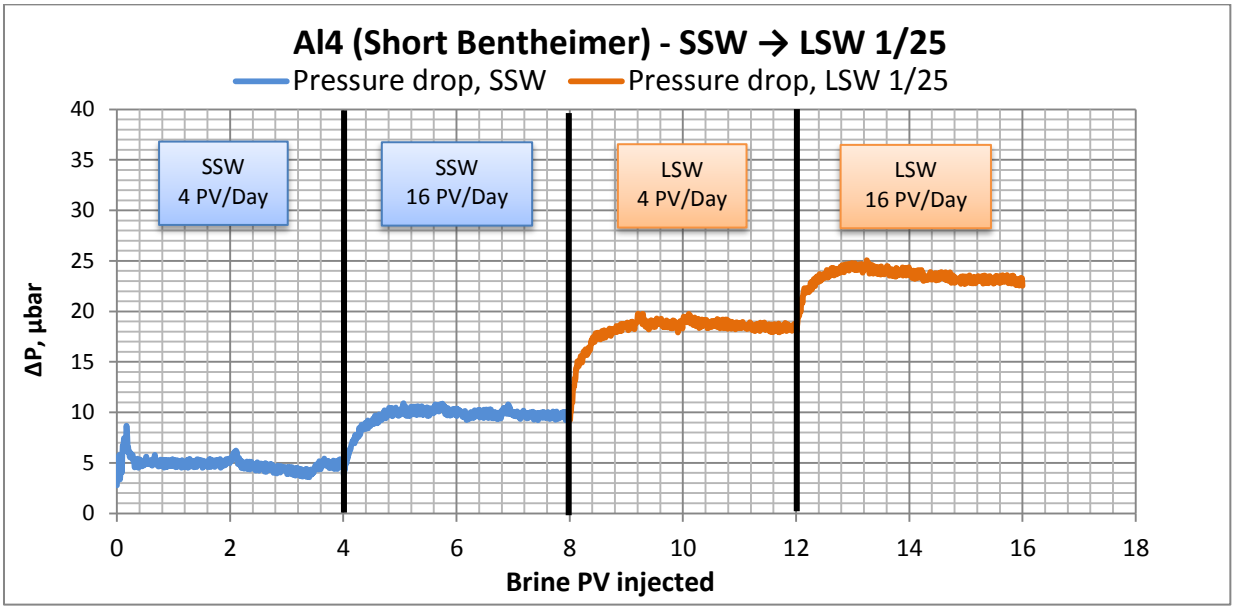

Figure 30 – Pressure drop across the core Al-4 during SSW-LSW flooding

After switching injection fluid to LSW we can see following changes:

1) pH of the effluent samples is higher than for initial pH for LSW;

2) Ions concentration is decreasing and within 4 PV stabilizes on certain level;

3) Pressure drop curve is higher in compare with SSW flooding.

pH increase due to LSW flooding was observed by several researchers (Cuong T.Q. Dang et al., 2013, Tor Austad et al., 2010, Aly Anis Hamouda and Ole Martin Valderhaug, 2014). Possible mechanisms for pH increasing were discussed in theoretical part. Based on results which we get, an increase in pH can be due to combination of three different mechanisms.

First of all high pH values may be related to dissolution of cementing material. As a result the shortage of H^+ will lead to increase in pH. The dissolution reaction is slow and depends on the amount of carbonate material present in the rock (Cuong T.Q. Dang et al., 2013):

$$CaCO_3 + H^+ \leftrightarrow HCO_3^- + Ca^{2+} - Carbonate\ dissolution \quad (23)$$

Results of ion analysis support this theory. After SSW-LSW mixing zone (approximately 8^{th} to 10^{th} PV) ions concentration level is stabilizing. Ca^{2+} ion concentration is stabilizing on value 1,7-1,8, which is almost twice higher than LSW level. Moreover bicarbonate HCO_3^- level is keeping high during all flooding procedure. As was mentioned before bicarbonate system depends on pH and interactions with air. Notwithstanding the deviations that we get because of the bicarbonate ions representing very complex system, the average amount of HCO_3^- for the LSW flooding is definitely higher than in injection fluid. So it can be taken as an indicator that we have carbonate dissolution.

Other possible source of higher amount of Ca^{2+} ion can be desorption of initially adsorbed cations onto the clay as was proposed by Tor Austad et al. (2010). In this mechanism calcium ions adsorb onto the clay surface from the formation water. Then after LSW flooding proton H^+ will be exchanged with cation Ca^{2+} which will lead to increase in pH local to the clay surface. The mechanism is described by the following reaction (Tor Austad et al., 2010):

$$Clay - Ca^{2+} + H_2O = Clay - H^+ + Ca^{2+} + OH^- \quad (24)$$

From chromatography analysis we can see that potassium ion concentration after stabilization reaches level 2,2 – 2,3 which is more than two times higher than for initial LSW. This can be a primary reason of pH increase during LSW flooding. Possible mechanism was suggested by Aly Anis Hamouda and Ole Martin Valderhaug (2014). The increase of the potassium ion concentration with the flooding rate may be explained by the increase of fresh fluid in contact with the mineral surface, which increases the ion exchange between Na^+ and K^+ ions. The ion exchange may be described by the following reaction for the potassium-containing minerals (such as in the core material) represented by K-feldspar (orthoclase) (Aly Anis Hamouda and Ole Martin Valderhaug, 2014).

$$KAlSi_3O_8(s)(orthoclase) + Na^+ = K^+ + NaAlSi_3O_8(s)(albite) \quad (25)$$

The increase of pH may be explained by mineral dissolution, which increases [K+]. The reaction may be described as follow (Aly Anis Hamouda and Ole Martin Valderhaug, 2014):

$$4KAlSi_3O_8(s)(orthoclase) + 22H_2O = AlSi_3O_{10}(s)(kaolinite) + 8H_4SiO_4(aq) + 4K^+ + 4OH^- \quad (26)$$

Produced OH^- increases the alkalinity of the effluent solution. The above equation may explain the increase of the pH and also K^+ concentration (Aly Anis Hamouda and Ole Martin Valderhaug, 2014).

After 3rd PV with SSW flooding and 11th PV with LSW flooding pH level has trend to decrease. This can be explained by lower amount of clay/cementing material for rock/brine interaction. Trend for pressure drop also confirms it by decreasing during last two pore volumes for each salinity.

During LSW flooding pressure drop measurements showed higher values than with SSW (Figure 30). Possible reason of higher pressure drop can be migration of fines due to interactions between LSW and clays (clay dissolution). The dissolution of

clays itself does not lead to increase of pressure, but during this process clay lose its integrity. As a result we have fine migration and some particles block pore throats and the pressure drop across the core increases.

From Figure 28 we can see that during LSW flooding between 8 and 12 PV the average value of pH keeps on the same level (7,71) with some deviations. Then after switching to 16 PV/Day the pH slightly decreases to 7,47. This can be due to the fact that the amount of clays is small and after continuous flooding the large part of them already dissoluted and we observe less interaction. Confirmation for this we can find on the pressure drop graph where at the last pore volumes it is decreasing.

Analysis of data indicates that possibly we observed some rock/brine interactions which are much more pronounced during LSW flooding than with SSW. This interactions lead to mineral dissolution and fine migration which can increase sweep efficiency. The fact that we don't observe here any oil recovery increment after switching to LSW may be due to low amount of material for dissolution.

4.3 Core Al-7 Long Bentheimer, SSW-LSW

Core **Al-7** (Long Bentheimer, 9 cm) was flooded with SSW and followed by LSW. Sandstone type and flooding scenario were similar with previous sample and the main purpose of experiment was studying different core length. On Figure 31 is presented oil recovery curve and pH measurement versus injected pore volumes of brine.

Oil recovery measurements for long core Al-7 showed higher total oil recovery (about 33%) in compare with short core (about 30%). Increase in recovery may be associated with higher amount of brine/rock interactions due to greater core length. For confirming this assumption let's look at other data. Figure 32 shows pressure drop curves for this experiment.

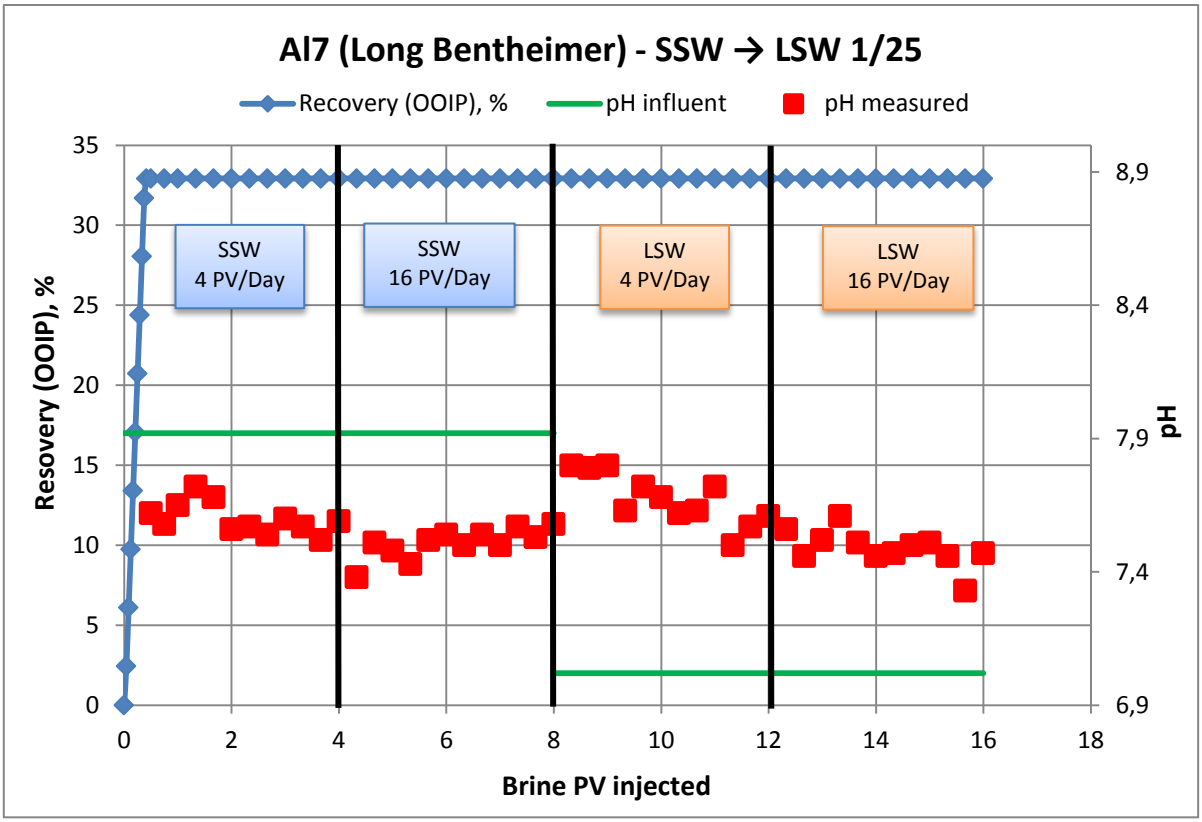

Figure 31 - Oil recovery and pH for influent and effluent during flooding with SSW – LSW for core Al-7

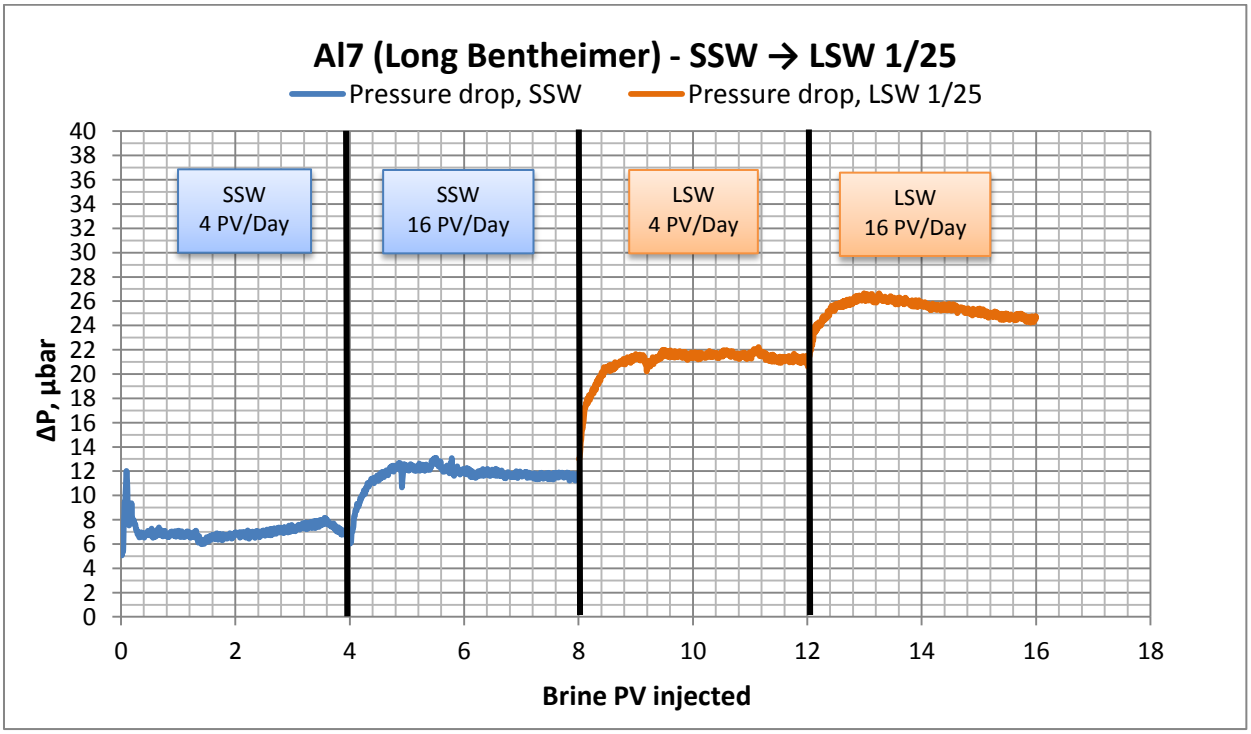

Figure 32 - Pressure drop across the core Al-7 during SSW-LSW flooding

Pressure drop peak in the beginning for long core **Al-7** (12 mbar) is higher than for previous short core Al-4 (8-9 mbar). This indicates that we have higher amount of interactions which can lead to fines detachment and migration. In the end of 1st PV pressure is stabilizing on value 6,8 - 6,9 mbar and then slightly increasing between 2nd and 4th PV. Pressure increasing may be due to blocking of pore throats. After switching injection rate to 16 PV/Day pressure drop is continuously increasing and stabilizing like in previous case, but the value of stabilization level is higher (1 – 1,5 mbar higher for long core). Higher pressure drop is reasonable for longer core.

pH level for SSW flooding follows similar trend with short core, but mean values are slightly higher (7,4 for short core versus 7,5 – 7,6 for long core). This can also be an indication of higher amount of clay and cementing material dissolution.

On Figure 33 is presented ion chromatography analysis for this experiment. The SSW part of analysis (until 8th PV) is almost stable and keeps on SSW level 25.

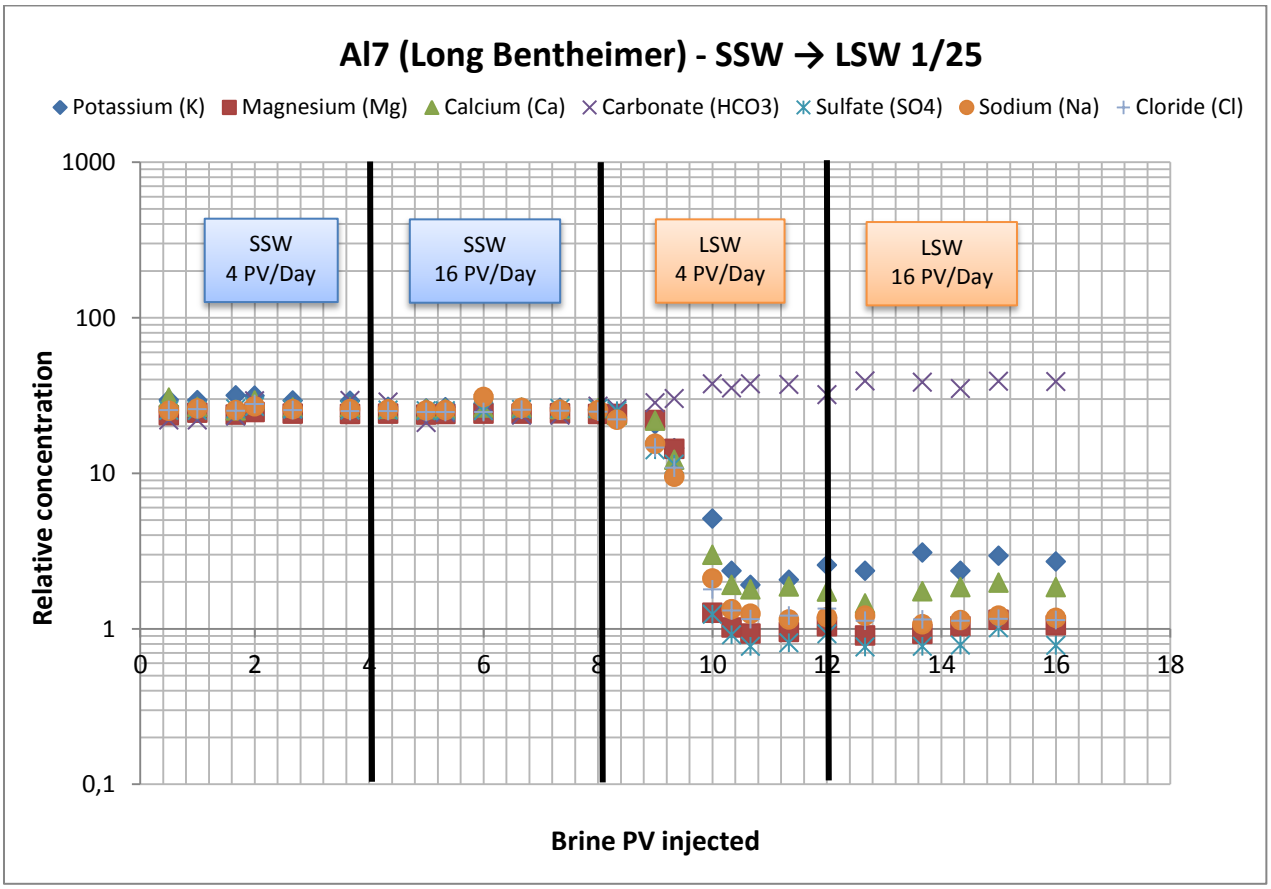

Figure 33 – Ions concentrations for effluent samples taken from the SSW - LSW flooding of core Al-7

After switching injection fluid to LSW as in previous case we have following changes: higher pH for effluent samples, stabilization of ions concentration after mixing zone with expectable excess for K^+ and Ca^{2+} and increasing pressure drop across the core.

Figure 33 shows that ions concentration is decreasing after switching to LSW and then stabilizing after 10^{th} PV. Mixing zone is slightly wider than for short core and concentration decreasing rate is slower. This is reasonable for long core because of bigger pore volume. Each effluent water sample that was taken during the flooding has approximately 4ml volume (which is minimum recommended amount for pH measurement). So as the result we have more water samples for long core and respectively first samples for long core have more SSW in composition.

As for short core we have increased concentration of potassium and calcium in compare with initial LSW concentration, but excess level for long core (2,3 – 2,5) is higher than for short (2,2 – 2,3). This can also be explained by higher amount of rock/brine interactions and respectively clay/cementing material dissolution. This statement may be confirmed by higher pressure drop (21-22 for long and 19-20 for short core at the rate 4 PV/Day for LSW), caused by pore plugging and slightly higher pH values (7,7 for long and 7,6 for short core at the rate 4 PV/Day for LSW) with the same trend to decrease.

4.4 Core Al-11 Short Berea, SSW-LSW

We studied different core length by flooding the same brine through the same sandstone type (Bentheimer). Now we will study another sandstone type (Berea) and compare results with previous experiments. Core **Al-11** (Short Berea, 5,03 cm) was flooded with SSW and followed by LSW. On Figure 34 you can see oil recovery curve and pH measurements.

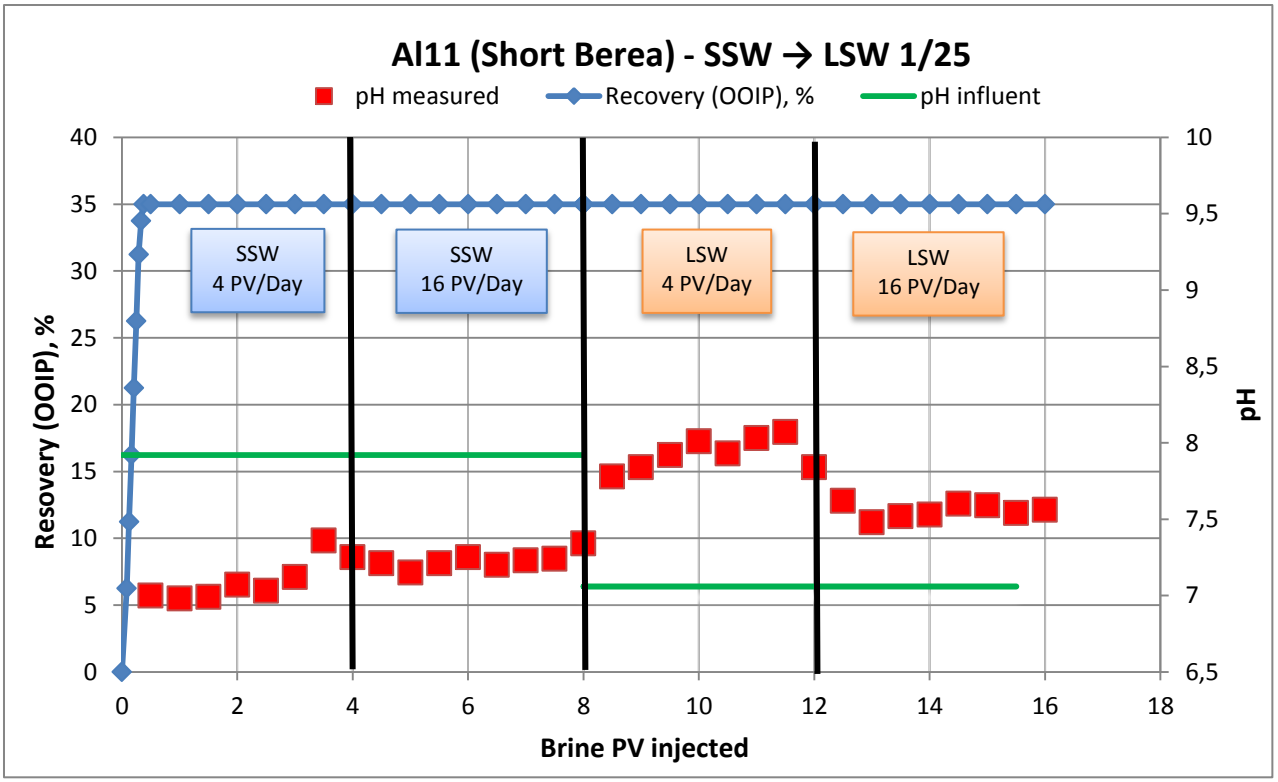

Figure 34 - Oil recovery and pH for influent and effluent during flooding with SSW – LSW for core Al-11

Figure 34 shows that recovery increases linearly and after early water breakthrough (0,3-0,4 PV) very small additional amount of oil was produced. During increasing injection rate to 16 PV/Day or switching injection fluid to LSW no oil recovery increase was observed. This is similar with short Bentheimer core **Al-4** (total recovery about 30%), but total recovery from the Berea core **Al-11** is slightly higher (total recovery about 35%). As we assume the oil recovery can be associated with the amount of rock/brine interactions, so it is reasonable that for other sandstone type we will get different amount of produced oil due to different mineral composition.

It is clear from pressure drop graph (Figure 35) that we have high peak in the beginning: up to 13 mbar versus 9 for short Bentheimer. If we will make parallel between peak height and recovery we will see that cores with higher recovery have higher peak in the beginning. The higher peak is most probably an indication of more flow restrictions. This leads to better sweep efficiency and as result we observe higher recovery.

After pressure drop stabilization we have higher mean value for Berea short core (6,9 mbar) in compare with Bentheimer short core (4,9 mbar). Higher pressure drop values are for both SSW and LSW sections. This phenomenon can be explained by two possible reasons. The main reason is different core heterogeneity and measured absolute permeability for Berea cores is slightly lower (about 0,8 Darcy) than for Bentheimer cores (about 1,05 Darcy). Second possible reason can be higher amount of rock/brine interactions, which can be confirmed by chromatography analysis.

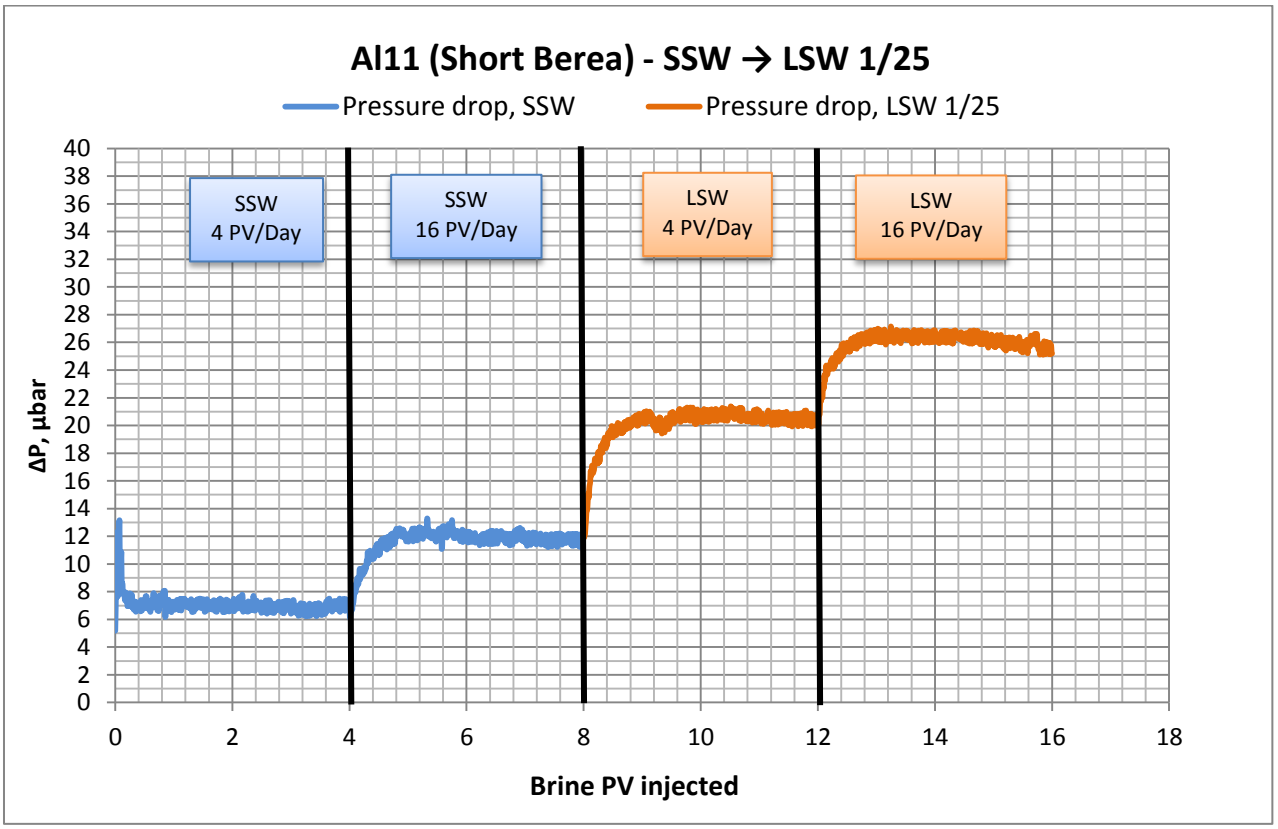

Figure 35 - Pressure drop across the core Al-11 during SSW-LSW flooding

Ion analysis for the SSW - LSW flooding of core Al-11 is presented below on Figure 36. As for previous cores we cannot see any significant changes in ion analysis during SSW flooding. For LSW flooding like in previous cases we can observe excess concentration for potassium and calcium ions. Actual potassium excess level for Berea sandstone (2,3 – 2,4) is slightly higher than for Bentheimer cores (2,2 – 2,3) and concentrations are stabilizing after mixing zone (after 10th PV) on the higher values (up to 3,62 for Berea versus 2,61 for Bentheimer).

This fact together with higher pressure drop can indicate higher amount of clay dissolution. pH measurements of effluent are lower than initial level for SSW and higher for LSW. For LSW flooding pH values are slightly higher in compare with Bentheimer: 7,9 versus 7,7, with trend to decreasing after 12th PV. This can also confirm idea about higher rock/brine interactions for Berea sandstone.

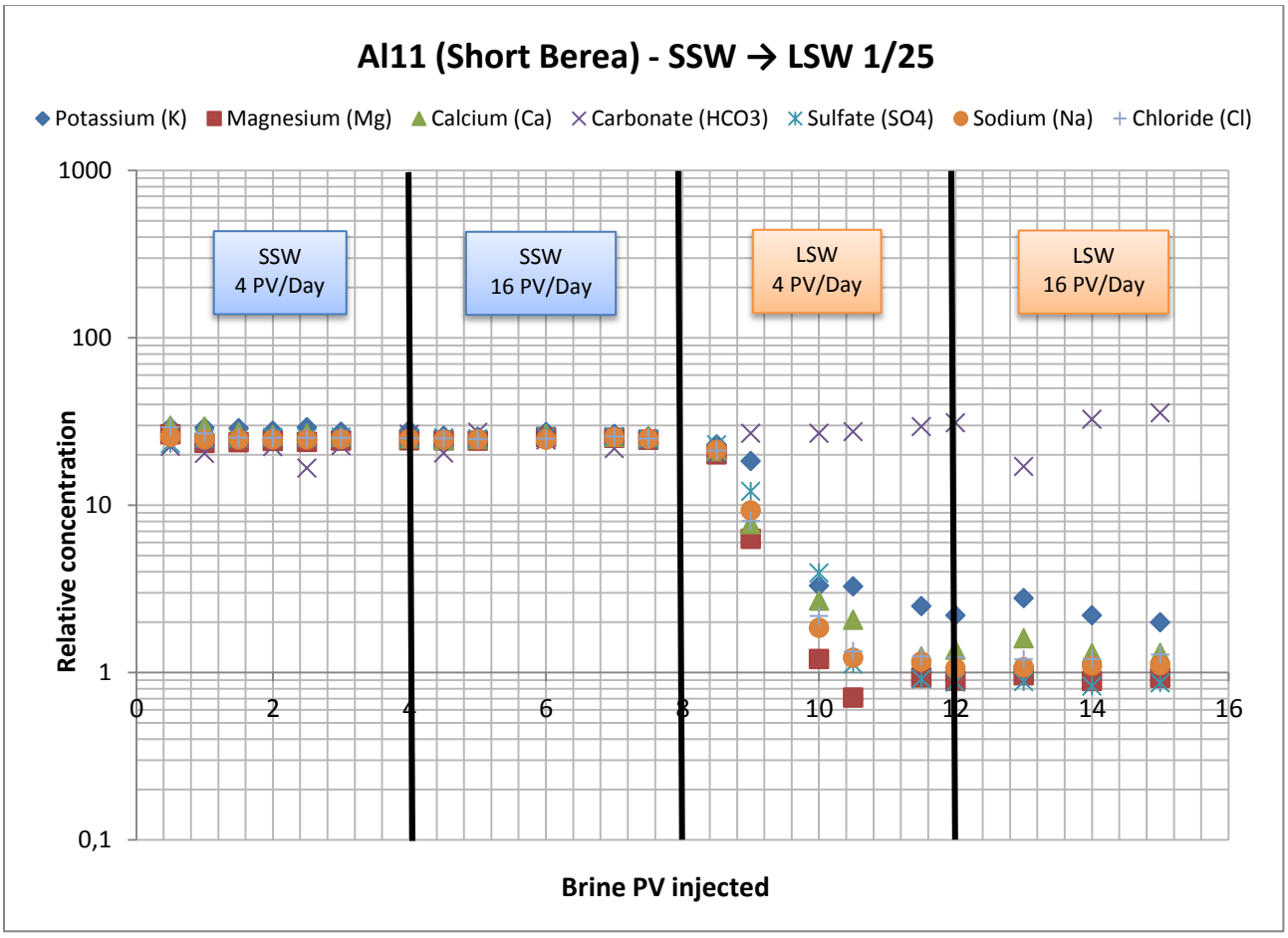

Figure 36 - Ions concentrations for effluent samples taken from the SSW - LSW flooding of core Al-11

Despite of assumptions about higher interactions in Berea than in Bentheimer sandstone, LSW implementation as an EOR did not show any oil increment. Berea sandstone has higher potential for improving oil recovery by LSW, but amount of clay material is still low for observing any positive results.

4.5 Core Al-8 Long Berea, SSW-LSW

As for Bentheimer sandstone, different length was studied for Berea sandstone. Core **Al-8** (Long Berea, 9 cm) was flooded with SSW and followed by LSW. Figure 37 shows oil recovery curve and pH measurement.

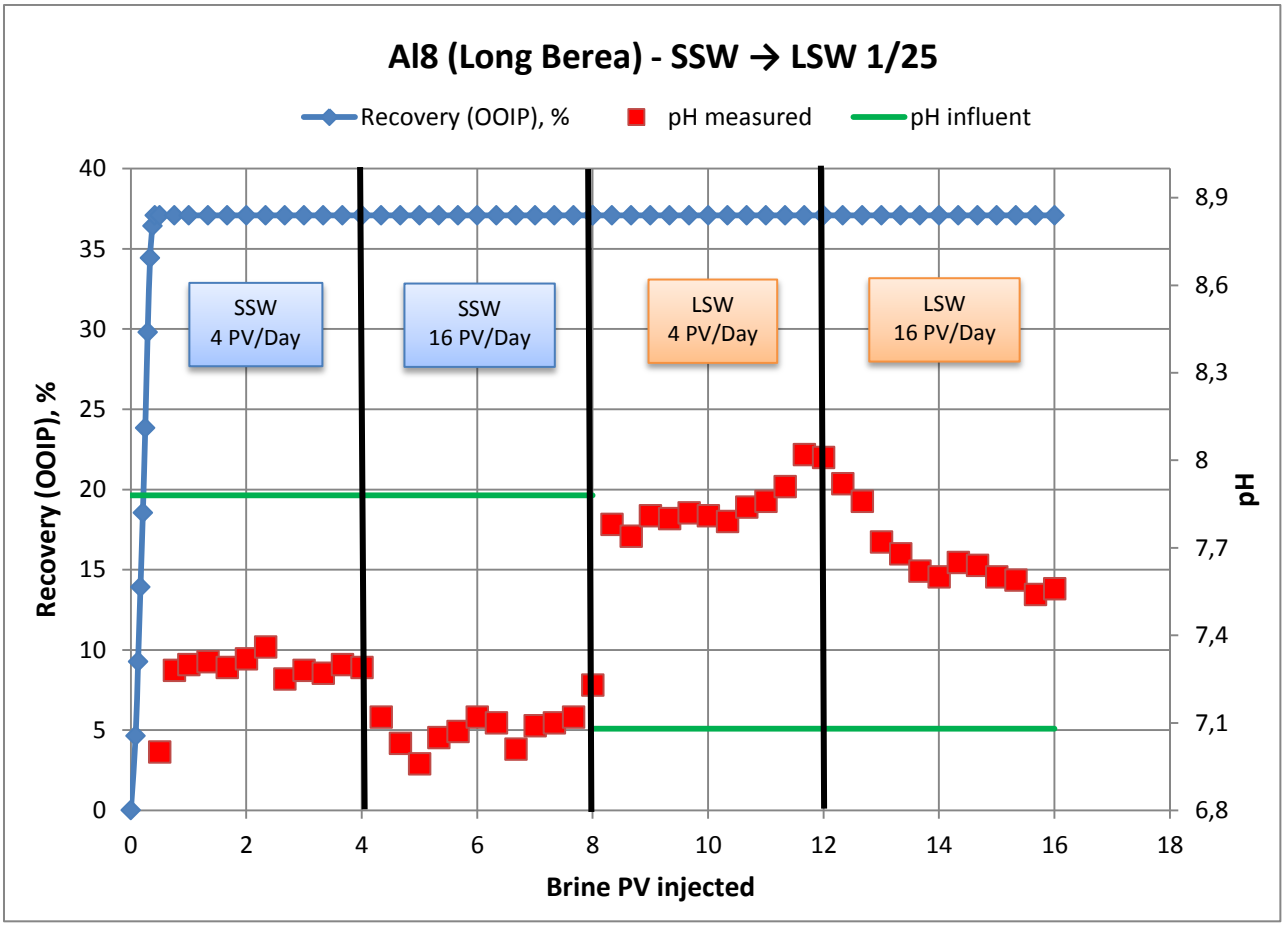

Figure 37 - Oil recovery and pH for influent and effluent during flooding with SSW – LSW for core Al-8

As we can see from Figure 37 total oil recovery for this core is about 37%. In this case we get maximal value for recovery. It is slightly higher than for short Berea core (35%) and for long Bentheimer core (33%). Maximal recovery may be an indication of maximal amount of rock/brine interactions which can be confirmed by going through the other obtained data. Changing injection fluid to LSW and increasing injection rate did not show any oil increment as in previous cases.

Ion chromatography analysis is presented on Figure 38 below. For SSW flooding part we don't have any high deviations from SSW level like for previous cores. Then after switching to LSW ions concentration is decreasing within two PV. Mixing zone is slightly wider than for short Berea core and concentration decreasing rate is slower. After concentration stabilization (10^{th} PV) amount of K^+ and Ca^{2+} is keeping on higher level. In this case maximal concentration of potassium is in 3,4 times higher than for initial LSW level. This value is the highest which was obtained for potassium concentration among experiments with LSW as a secondary injection fluid. It can be indication of maximal amount of rock/brine interactions which can be confirmed by the highest pressure drop curve for this experiment (Figure 39).

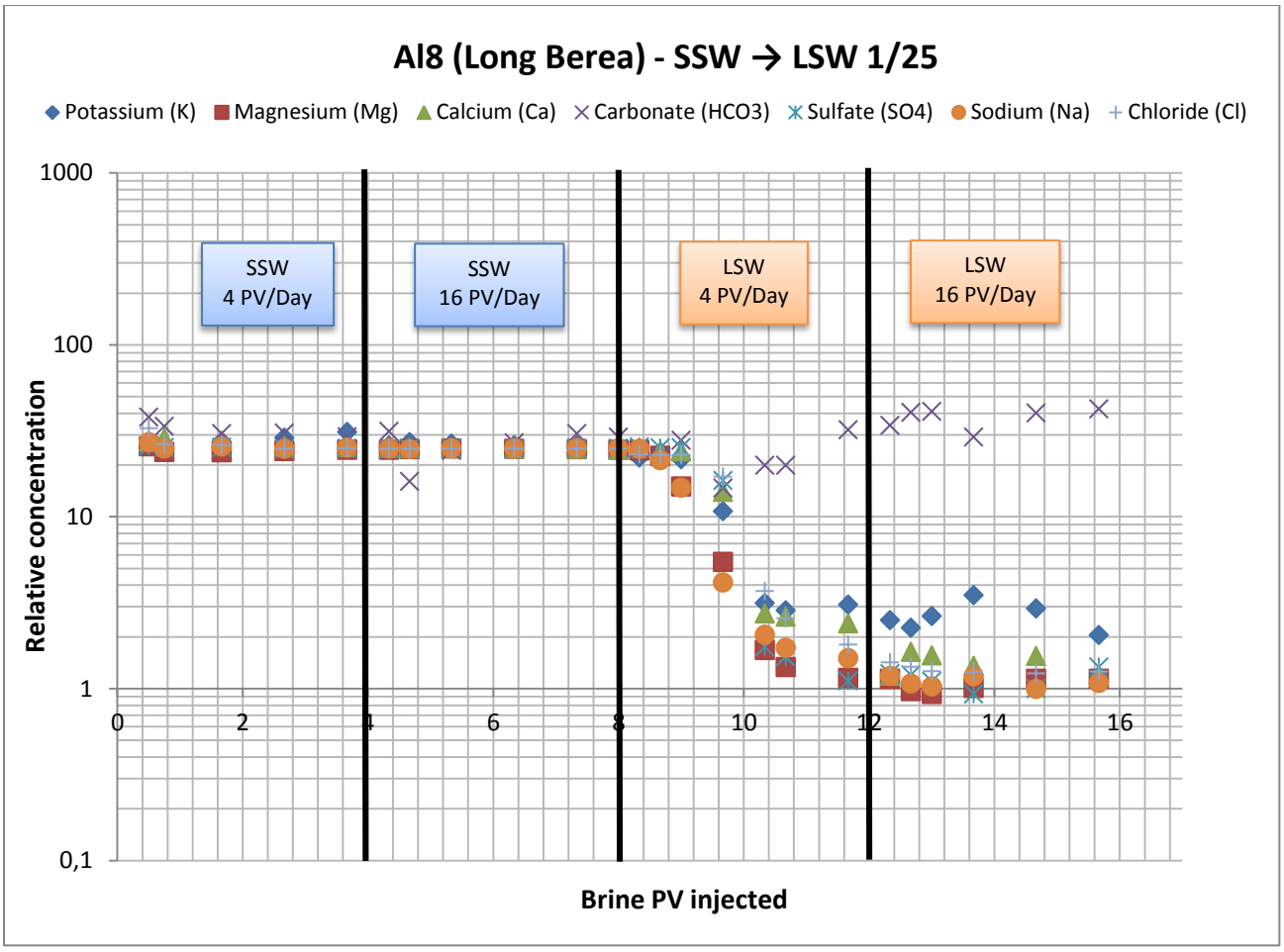

Figure 38 - Ions concentrations for effluent samples taken from the SSW - LSW flooding of core Al-8

On Figure 39 below are presented pressure drop measurements across the core Al-8 for SSW – LSW flooding. Figure shows high peak in the beginning as in previous cores and pressure drop stabilization after 0,33 PV. Trend for ΔP increasing step by step during all flooding is the same with other samples, but actual level is slightly higher (22-23 mbar versus 20-21 mbar for Long Bentheimer and 19-20 mbar for Short Berea with LSW flooding on 4 PV/Day).

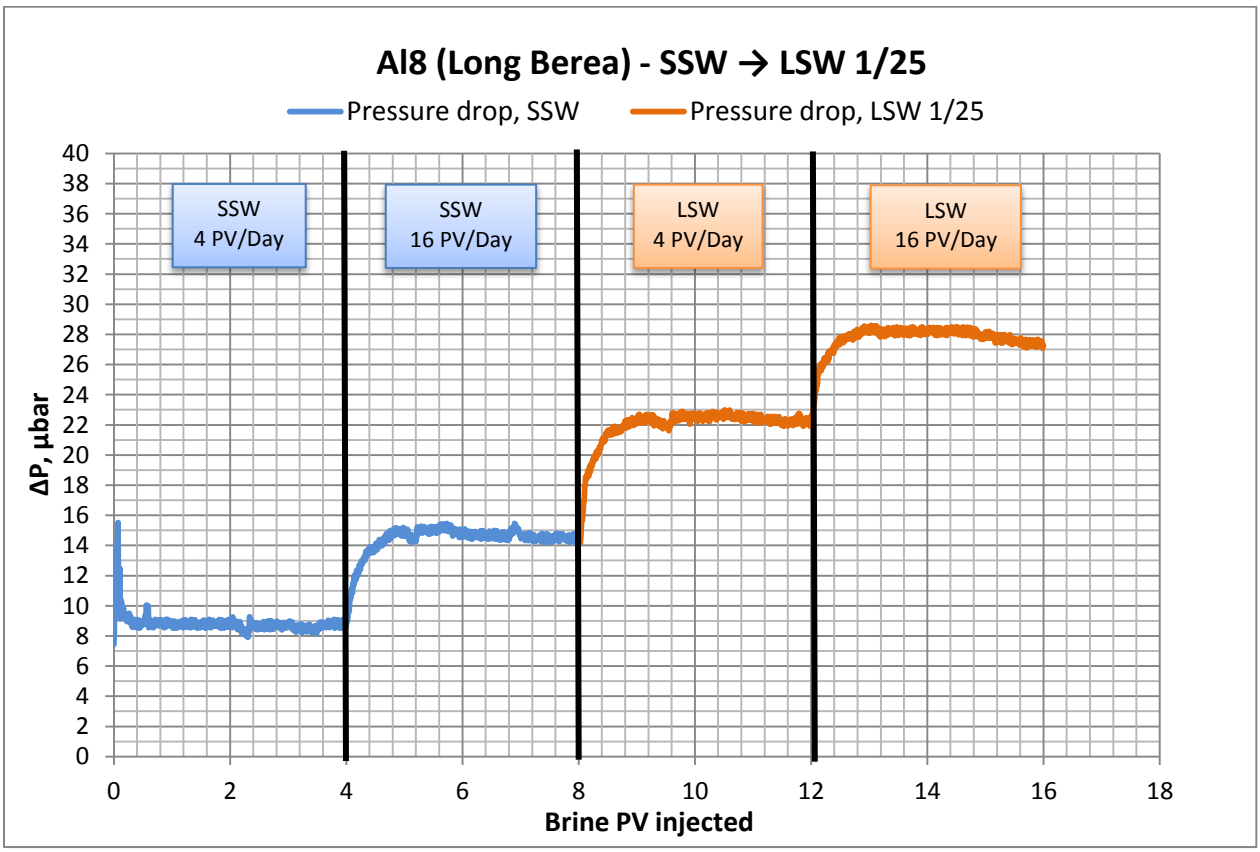

Figure 39 - Pressure drop across the core Al-8 during SSW-LSW flooding

Difference between influent and effluent pH level for SSW flooding is higher for Berea (0,6) than for Bentheimer sandstone (0,3). This can be explained by the amount of brine/rock interactions where for Berea sandstone it should be higher. Mean value of pH for long Berea core is almost the same with short Berea core, but trends are different (slightly increasing after 4th PV for short core and decreasing for long core). It can be due to complexity of pH system. More research work should be done for complete understanding of this process.

4.6 Core Al-6 Short Bentheimer, LSW

Besides of studying LSW as a secondary injection fluid experiments with only LSW flooding (primary injection fluid) were performed. Flooding scenario was the same as for previous cores: first 4 pore volumes were flooded at injection rate 4 PV/Day, then injection rate was switched to 16 PV/Day and another 4 pore volumes were flooded. Experiments were made for two Bentheimer (short and long) and two Berea cores (short and long) for studying connections between core type/length and LSW flooding results.

Let's look at obtained data in the same sequence as for SSW – LSW experiments. Core **Al-6** Short Bentheimer (5,09 cm) was flooded with LSW (25 times diluted SSW). On Figure 40 below you can see recovery calculations and measurements of influent/effluent pH.

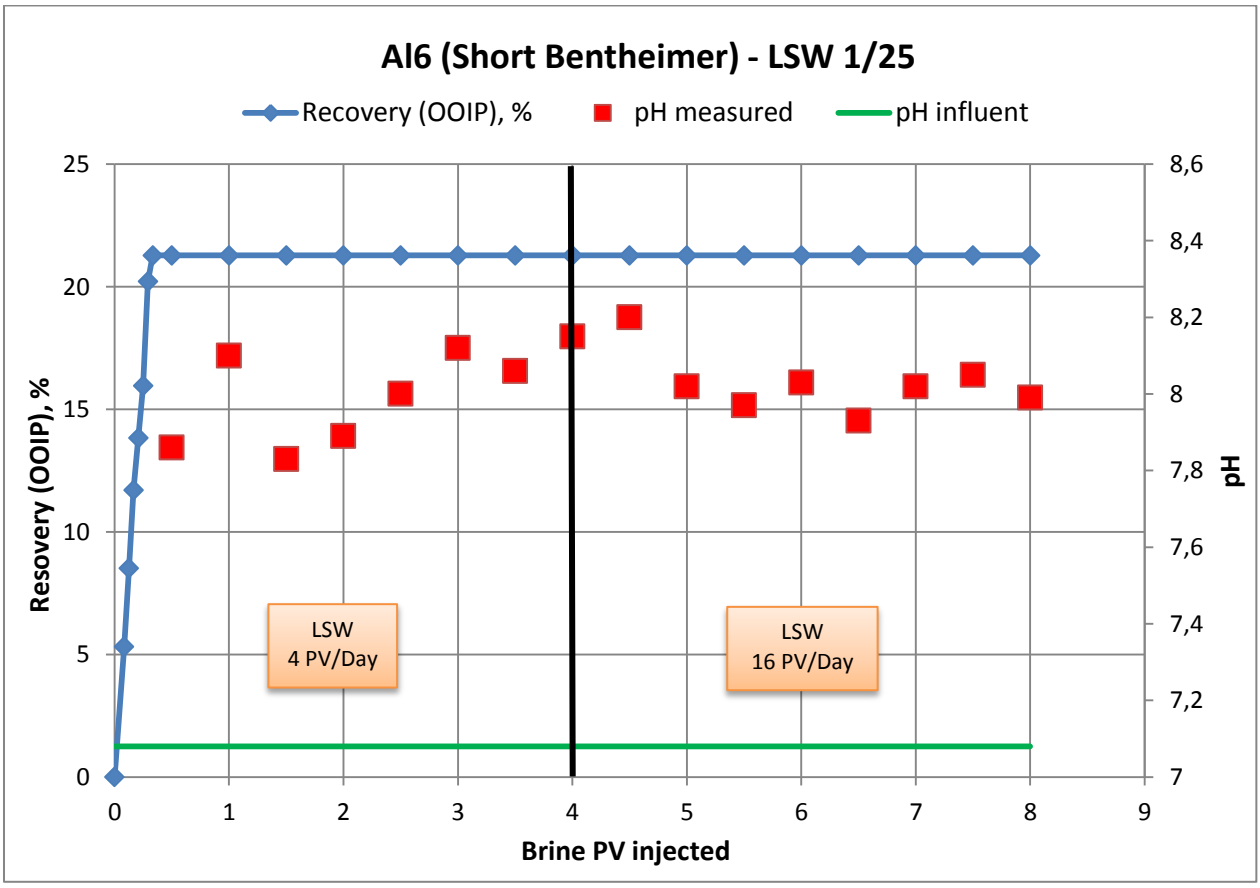

Figure 40 - Oil recovery and pH for influent and effluent during flooding with LSW for core Al-6

Oil recovery measurements showed early water breakthrough (0,28-0,29 PV) and then very small additional oil (≈0,1 ml). Total oil recovery from core is 21,28 % which is almost 9 % lower than for SSW-LSW flooding with the same core (30 % oil recovery for short Bentheimer core Al4). Increasing injection rate also did not show any oil increment. For understanding reason of much lower oil recovery for LSW flooding we need to analyze other obtained data.

Figure 41 shows pressure drop measurements across the core.

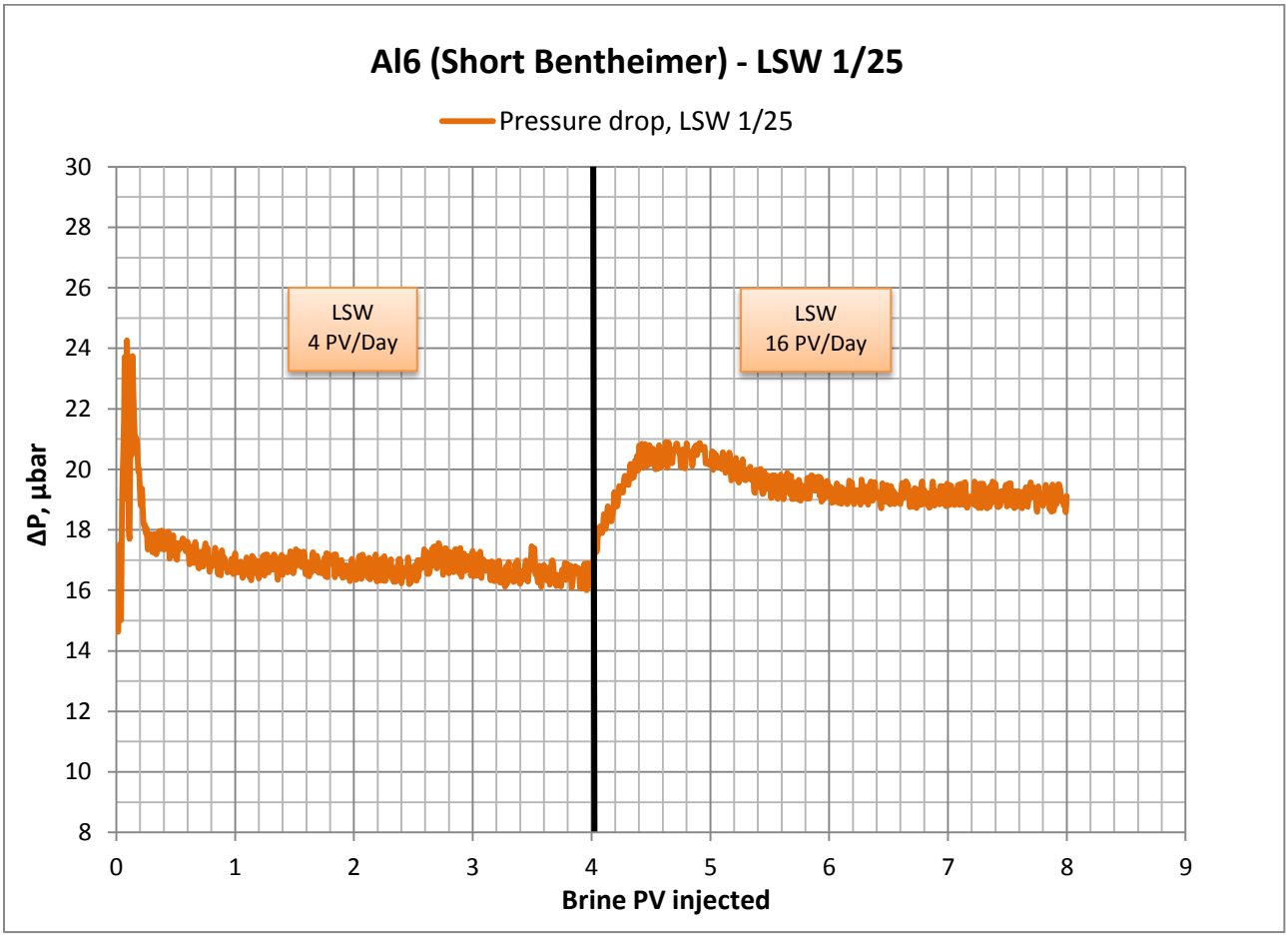

Figure 41 – Pressure drop across the core Al-6 during LSW flooding

As for previous samples we can see high peak in the beginning and then pressure stabilization. Actual pressure drop level for LSW flooding (16,77 mbar at the rate 4 PV/Day) is higher than for SSW flooding of the same core (5-6 mbar at the rate 4 PV/Day for short Bentheimer core Al4). Higher pressure drop level can be an indication of continuous brine/rock interactions during all LSW flooding process.

On Figure 42 below is presented ion analysis and we can see that during first two pore volumes ion concentrations were higher than actual influent LSW level. This is reasonable because first effluent water samples are mix between SSW in the core after aging and influent LSW. After stabilization of ion concentrations (2^{nd} PV) we can see excess values for potassium (2,5-3 times higher than LSW level) and calcium (1,5-2 time higher than LSW level) ions. As for previous cores possible explanation of this can be clay and cementing material dissolution during flooding. Confirmation of dissolution can be effluent pH values which is much higher than influent level (7,08) and keeping stably on level 8,2-8,6. Slight decrease in pH after switching injection rate to 16 PV/Day was observed for other experiments as well and can be explained by less dissolution of cementing material in the end of flooding process.

As for previous experiments concentration level of HCO_3 is continuously keeping on SSW level (25). Overpredicted result is indication of complexity of bicarbonate system due to interactions with air and dependence on pH level.

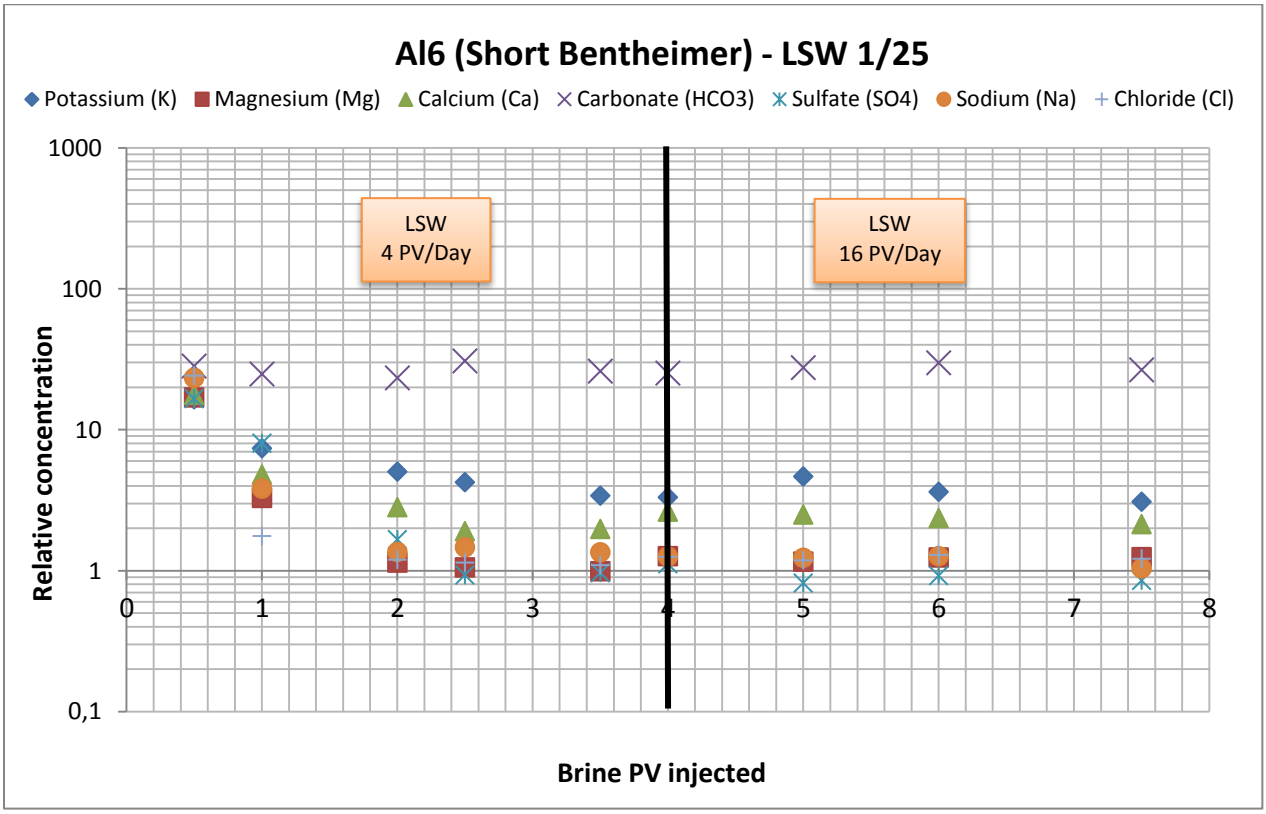

Figure 42 – Ions concentrations for effluent samples taken from the LSW flooding of core Al-6

Contrary to expectations to get higher recovery for LSW flooding as a primary injection mode we got lower values. First of all amount of brine/rock interactions is not enough to increase sweep efficiency. Besides the viscosity of LSW brine is lower than SSW brine. These leads to higher amount of capillary trapped oil and respectively lower recovery.

4.7 Core Al-12 Long Bentheimer, LSW

LSW effects were studied for long Bentheimer core as well. Core **Al-12** Long Bentheimer (8,95 cm) was flooded with LSW. All obtained data and comparison with other experiments are presented below.

Figure 43 shows recovery curve and measurements of influent/effluent pH. As we can see total oil recovery from core Al-12 is about 23,3% without increment during increasing injection rate to 16 PV/Day. This value is slightly higher than for short Bentheimer core (22%), but still lower than recovery values for SSW flooding (about 33% for Long Bentheimer core Al-7, flooded with SSW-LSW). This confirms results for short Bentheimer core Al-6 where we got lower recovery for LSW flooding in compare with SSW.

pH measurements of effluent samples for long Bentheimer core keep on level 7,7-7,8 with trend to slight decrease after switching to 16 PV/Day. These values are much higher than initial pH for LSW (7,03) which can be explained by brine/rock interactions and confirmed by other data.

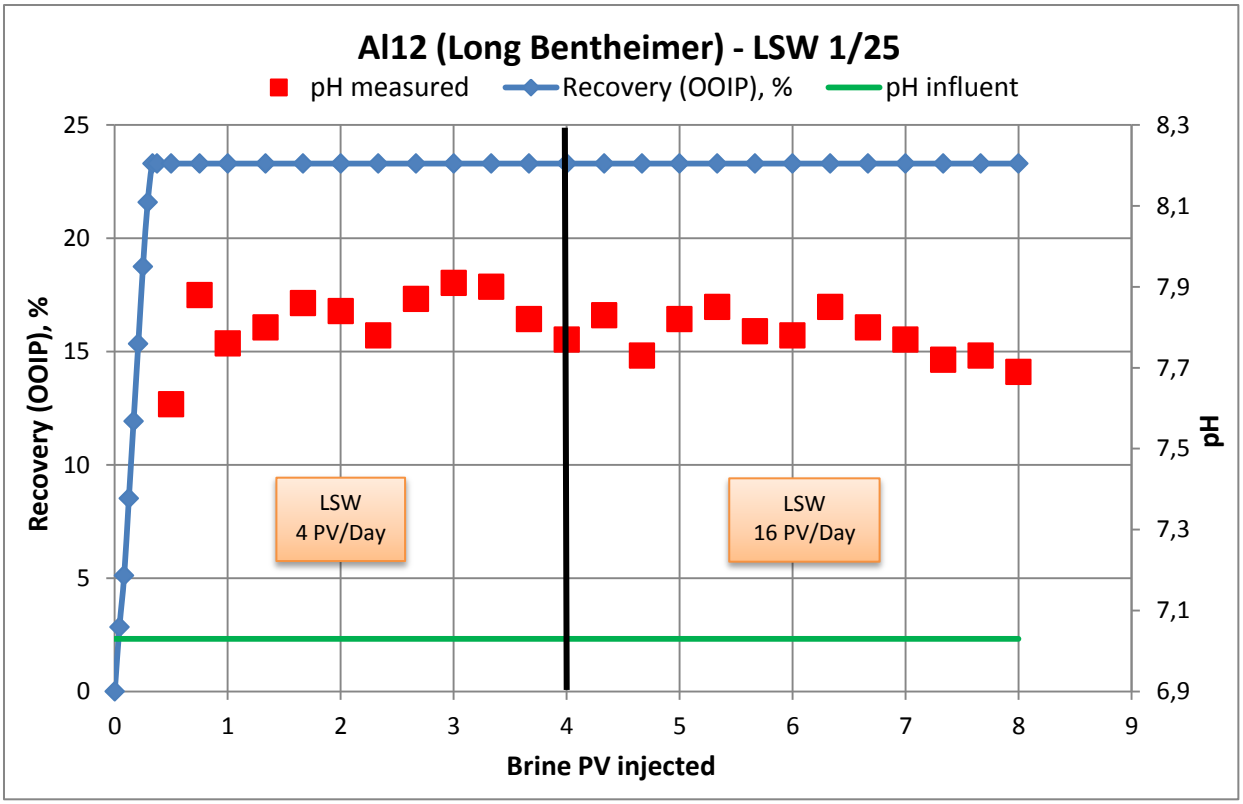

Figure 43 - Oil recovery and pH for influent and effluent during flooding with LSW for core Al-12

Pressure drop curve is presented below on Figure 44. Similarly with previous cores we can see high peak in the beginning and then pressure drop stabilization. In compare with short Bentheimer LSW flooding for long core stabilization rate is lower and actual values are higher (19 mbar for long and 17 mbar for short Bentheimer cores with during flooding with rate 4 PV/Day). Faster pressure drop stabilization is reasonable for short cores due to length. Higher mean values for long cores can be explained by higher amount of interactions, fine migration and flow restriction.

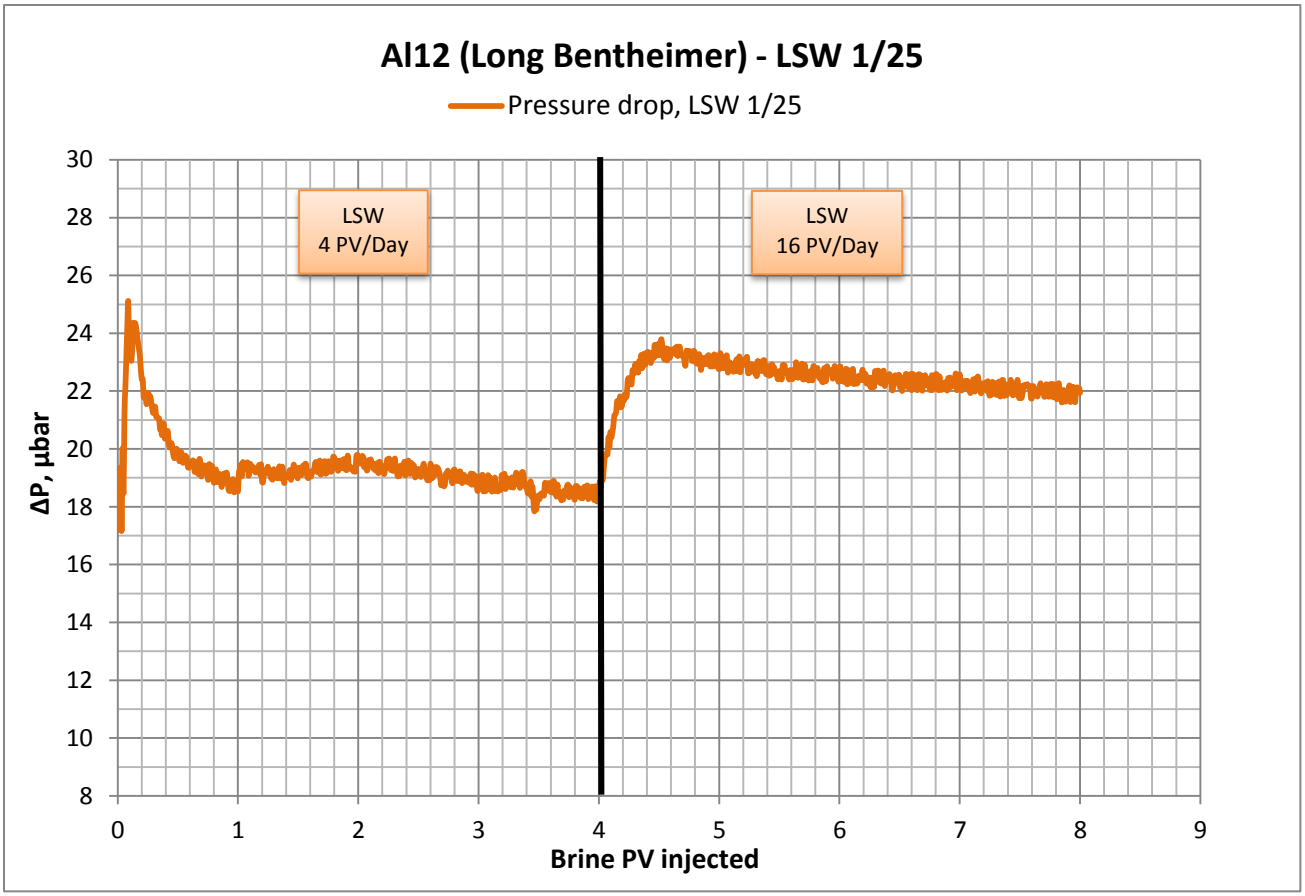

Figure 44 – Pressure drop across the core Al-12 during LSW flooding

Ion chromatography analysis is showed on Figure 45. After stabilization of ions concentration (2nd PV) we can see increased amount of potassium (around 4 times higher than LSW level) and calcium (2,5 times higher than LSW level). Increased concentration can be an indication of dissolution clay/cementing material. Slight decrease of potassium concentration after 5th pore volume may be due to limited amount of clay material in core and decreasing of dissolution in the end of flooding.

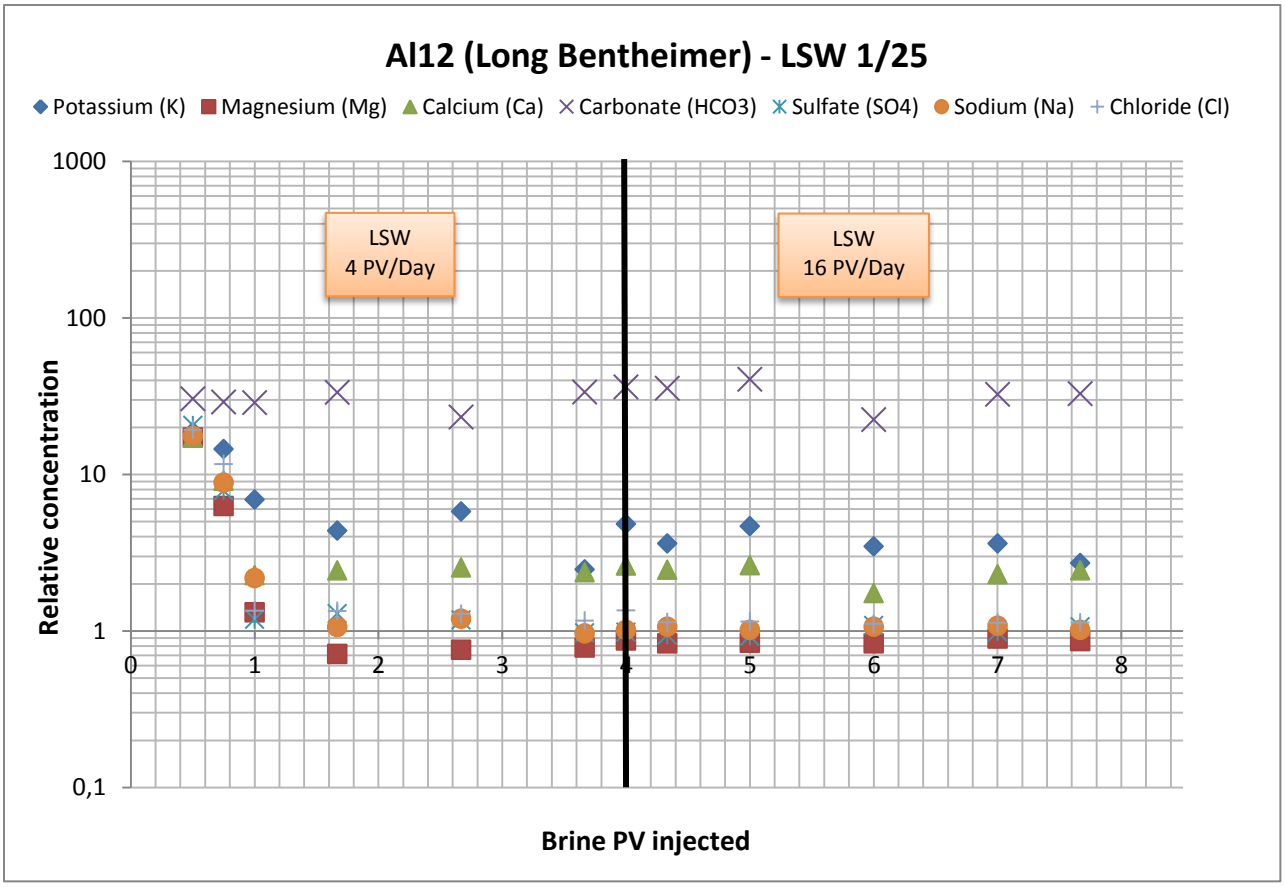

Figure 45 – Ions concentrations for effluent samples taken from the SSW - LSW flooding of core Al-12

LSW flooding for long Bentheimer core confirmed that oil recovery from SSW flooding is higher than for LSW. Moreover dependence of oil recovery on core length was proved. Interpretation of all data shows possible continuous brine/rock interaction during LSW flooding, but still it is not enough for increasing sweep efficiency and improving oil recovery.

4.8 Core Al-10 Short Berea, LSW

Similar experiments with LSW flooding were made for Berea sandstone and the results will be discussed below. First was flooded Short Berea Core **Al-10** (4,96 cm). Oil recovery and influent/effluent pH values are shown on Figure 46.

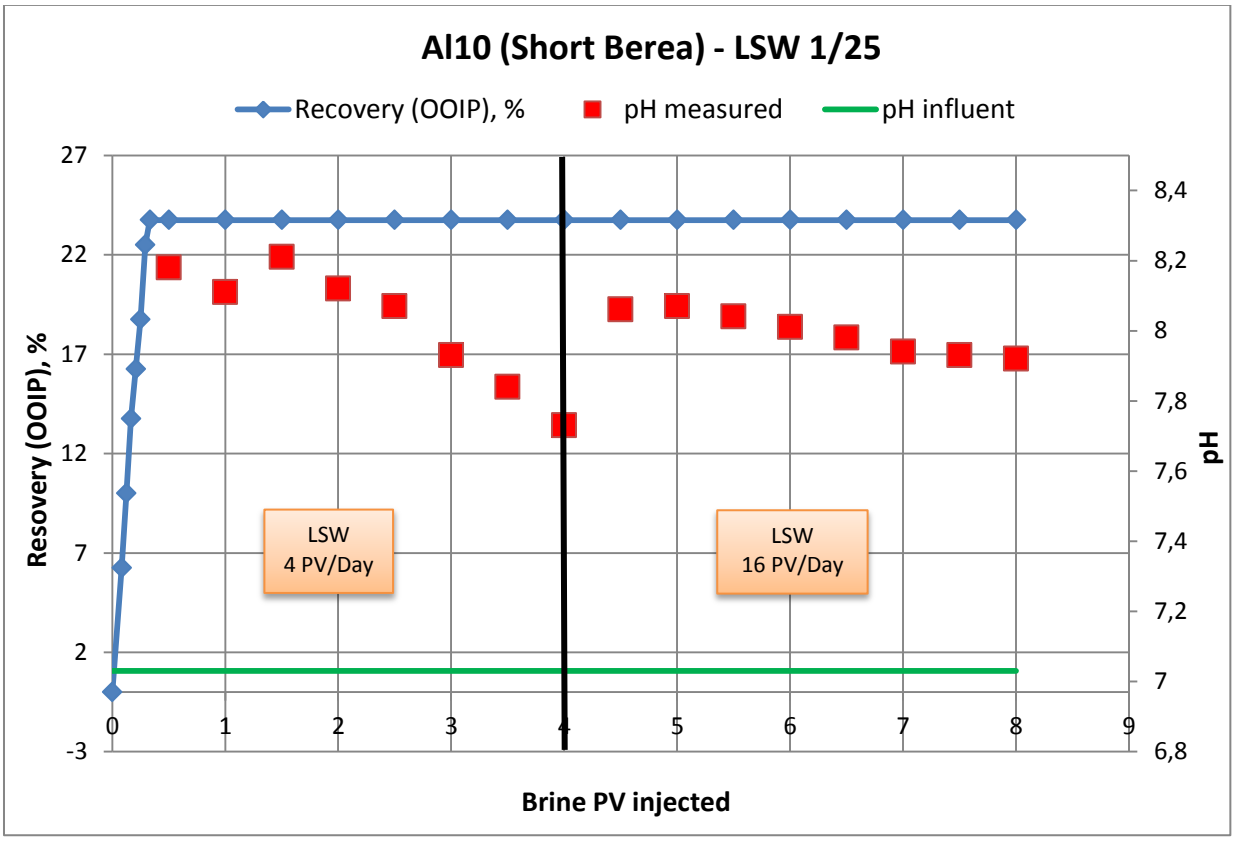

Figure 46 - Oil recovery and pH for influent and effluent during flooding with LSW for core Al-10

Oil recovery curve shape is the same with other experiments. After fast water breakthrough (0,3-0,4 PV) very small amount of oil was produced and increasing the injection rate did not show any oil increment. Total recovery from the core is 23,8%. This value is slightly higher in compare with results for short Bentheimer core Al6 (21,3%). SSW flooding results showed conformity with LSW flooding results. In both cases oil recovery from Berea sandstone was higher than for Bentheimer sandstone. It can be due to different mineralogy and cohesion of sandstone minerals to core surface,

which can be confirmed by difference in absolute permeability and amount of brine/rock interactions.

pH measurements again showed difference (almost 1) between influent and effluent values. Effluent pH values itself (around 8) have trend to slight decreasing from 2nd to 4th PV and from 5th to 8th. pH decrease can be due to less dissolution of cementing material.

Figure 47 shows ion chromatography analysis for this experiment. Concentration of bicarbonate is keeping on the same level like in previous cases. Concentration of other ions is stabilizing after 2nd pore volume. Concentration of potassium ion exceeds initial LSW level 2,9-3 times with decreasing trend after 5th pore volume. Calcium concentration is also keeping on higher level (1,8-2) with some fluctuations and decreasing in the end of flooding.

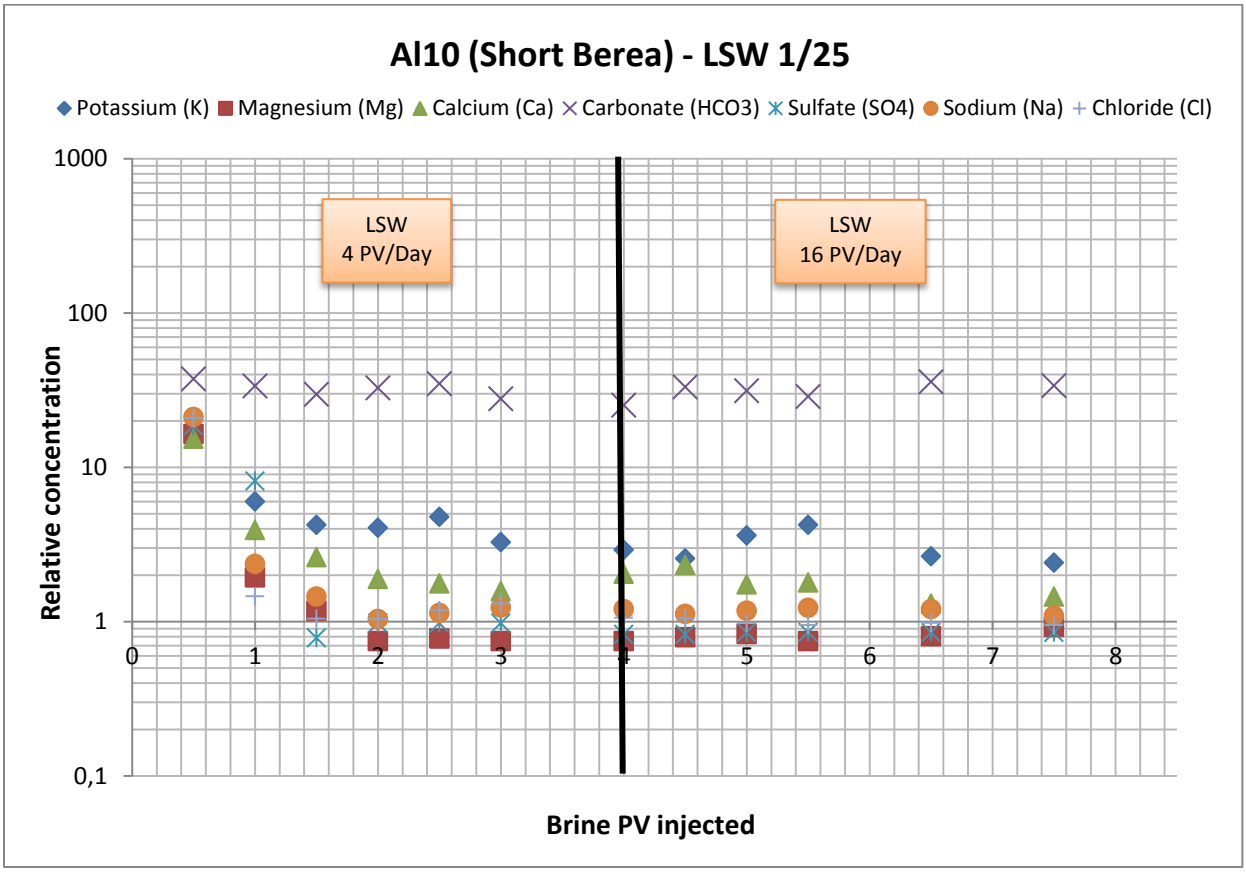

Figure 47 – Ions concentrations for effluent samples taken from the LSW flooding of core Al-10

Pressure drop values are presented on Figure 48 below. After peak in the beginning pressure is stabilizing on level around 21 mbar with trend to decrease after 2nd pore volume. Stabilization level is slightly higher than for short Bentheimer core (17-18 mbar) which is expectable due to lower absolute permeability of Berea sandstone.

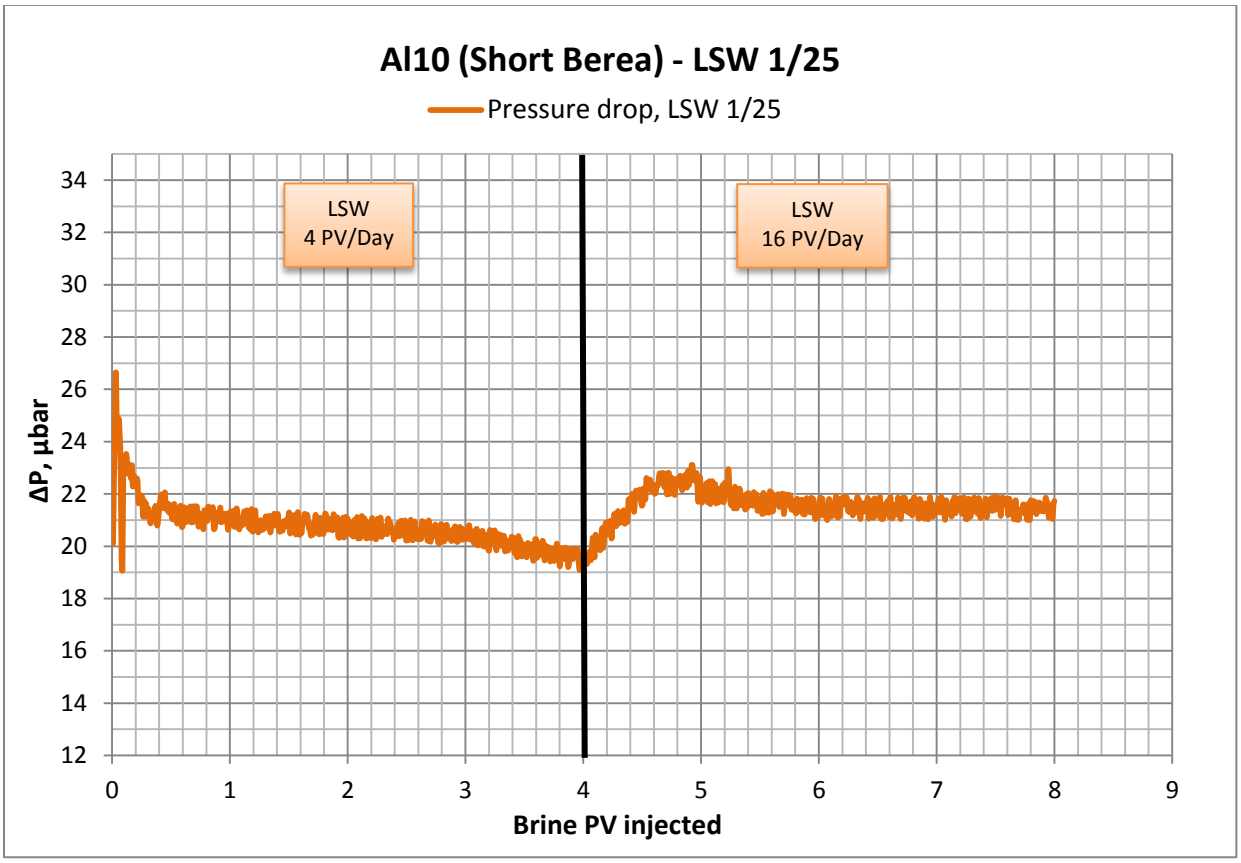

Figure 48 - Pressure drop across the core Al-10 during LSW flooding

LSW flooding of short Berea core Al-10 shows expectable results of recovery, ions concentrations and pressure drop. Despite of slightly higher oil recovery (23,8%) in compare with LSW flooding of short Bentheimer core (21,3%) it is still less than for SSW flooding.

4.9 Core Al-9 Long Berea, LSW

The last LSW flooding experiment was made for long Berea core for comparison with short Berea core and Bentheimer cores. Core **Al-9** Long Berea (9 cm) was flooded with LSW and results will be discussed below. Figure 49 shows oil recovery curve and pH of influent/effluent water samples.

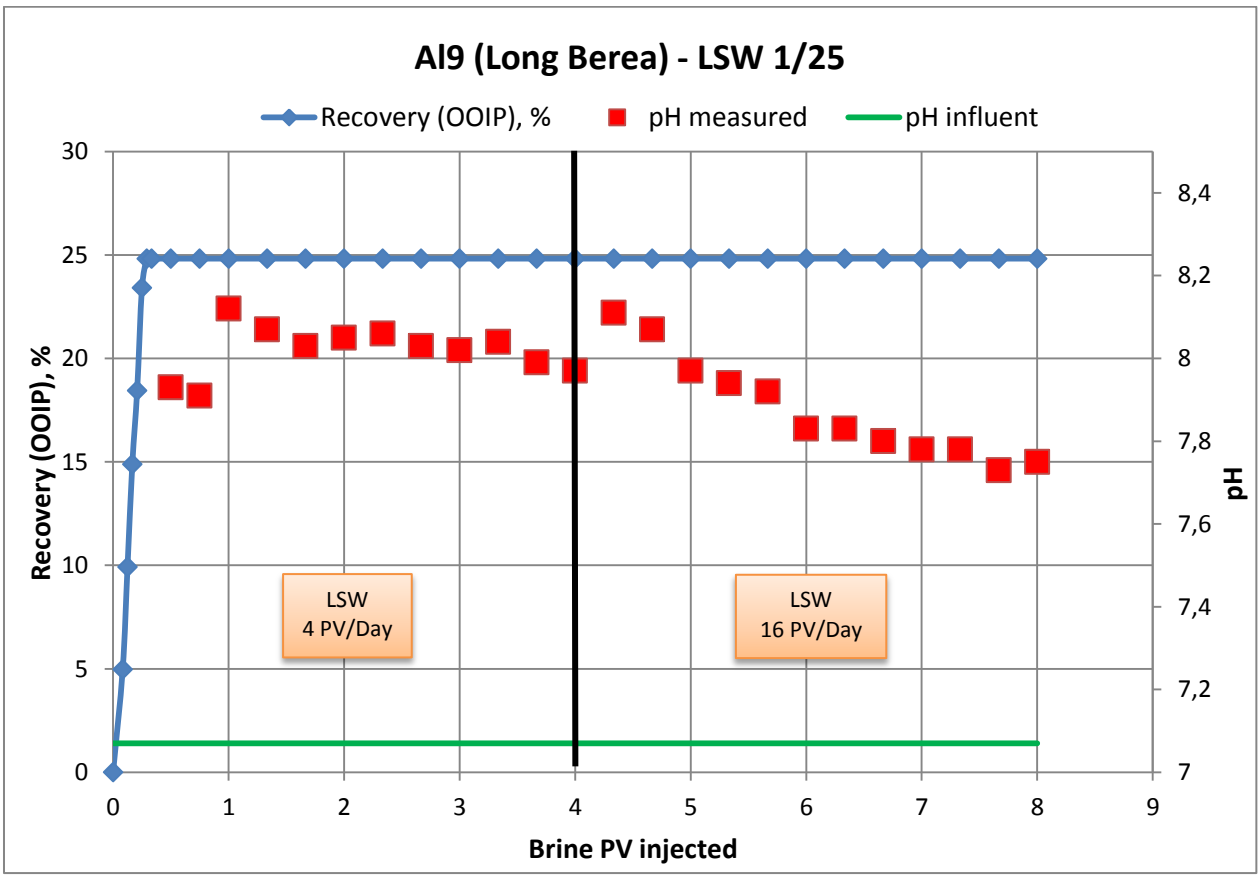

Figure 49 - Oil recovery and pH for influent and effluent during flooding with LSW for core Al-9

Total oil recovery from the long Berea core is about 25% which is higher than for short Berea core (23,75%) and for long Bentheimer core (23%). This can be an indication that Berea sandstone type has higher potential for using LSW as EOR method. Confirmation of this assumption can be found in other data.

Figure 50 shows ion chromatography analysis for LSW flooding of core Al-9. In this case we got very high excess level of potassium (3,5-3,6 times higher than for initial LSW) and high level of calcium (around 2 times higher than for initial LSW). This can be because of continuous dissolution of clay material and cementing material. Also amount of dissoluted potassium in long Berea (3,5-3,6) core is slightly higher than for short Berea (3,0-3,3). Similar results were obtained for Bentheimer sandstone. So it confirms idea about higher amount of interactions in longer cores. pH measurements show the same trend with short Berea core and keep on mean level 8 with slightly decreasing in the end of flooding (after 5th PV).

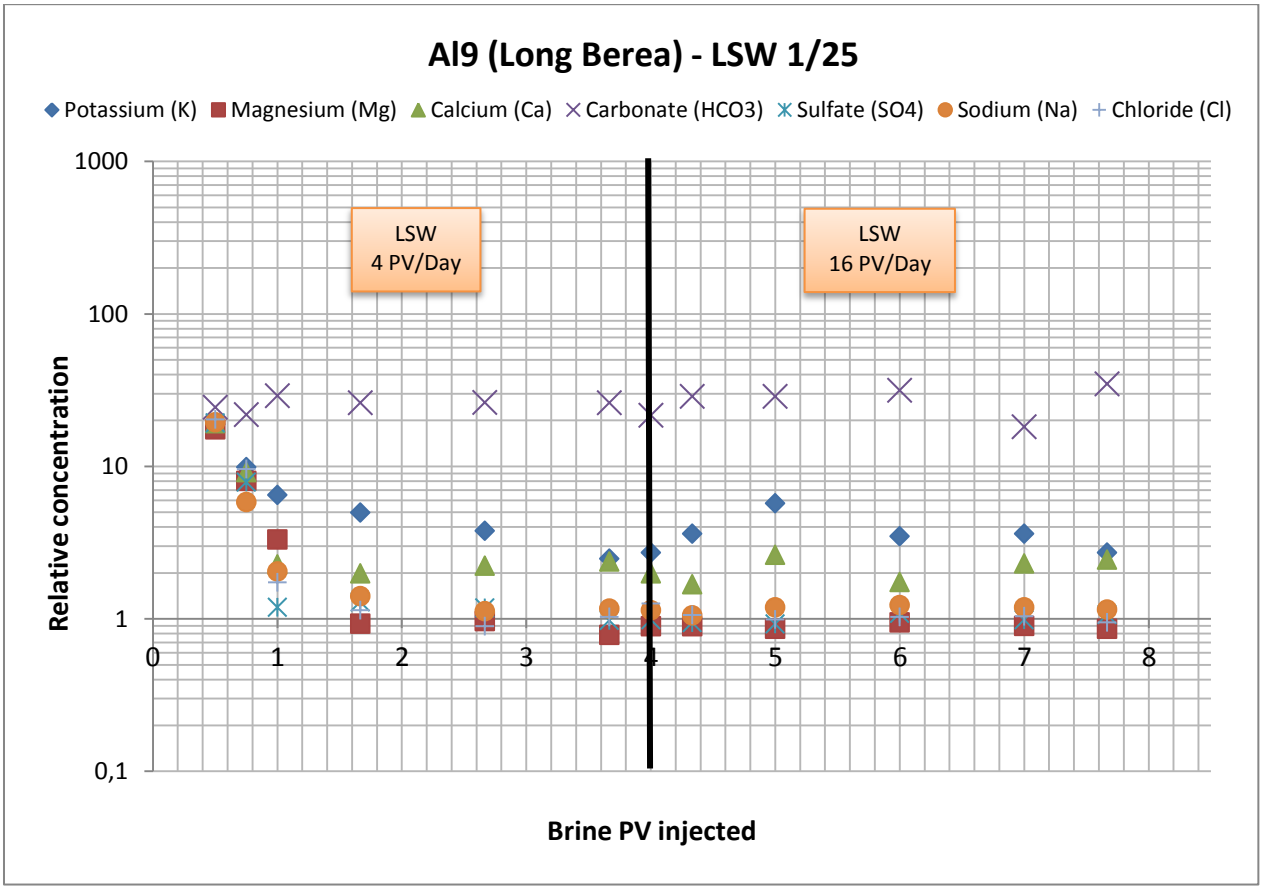

Figure 50 – Ions concentrations for effluent samples taken from the LSW flooding of core Al-9

Pressure drop curve across the core Al-9 is shown on Figure 51. After pressure drop stabilization the values are keeping on 21-21,5 mbar which is higher than for Bentheimer long core (19-20 mbar for long Bentheimer core Al-12). This is reasonable results which can be confirmed by similar comparison between short Bentheimer and Berea cores in previous paragraph.

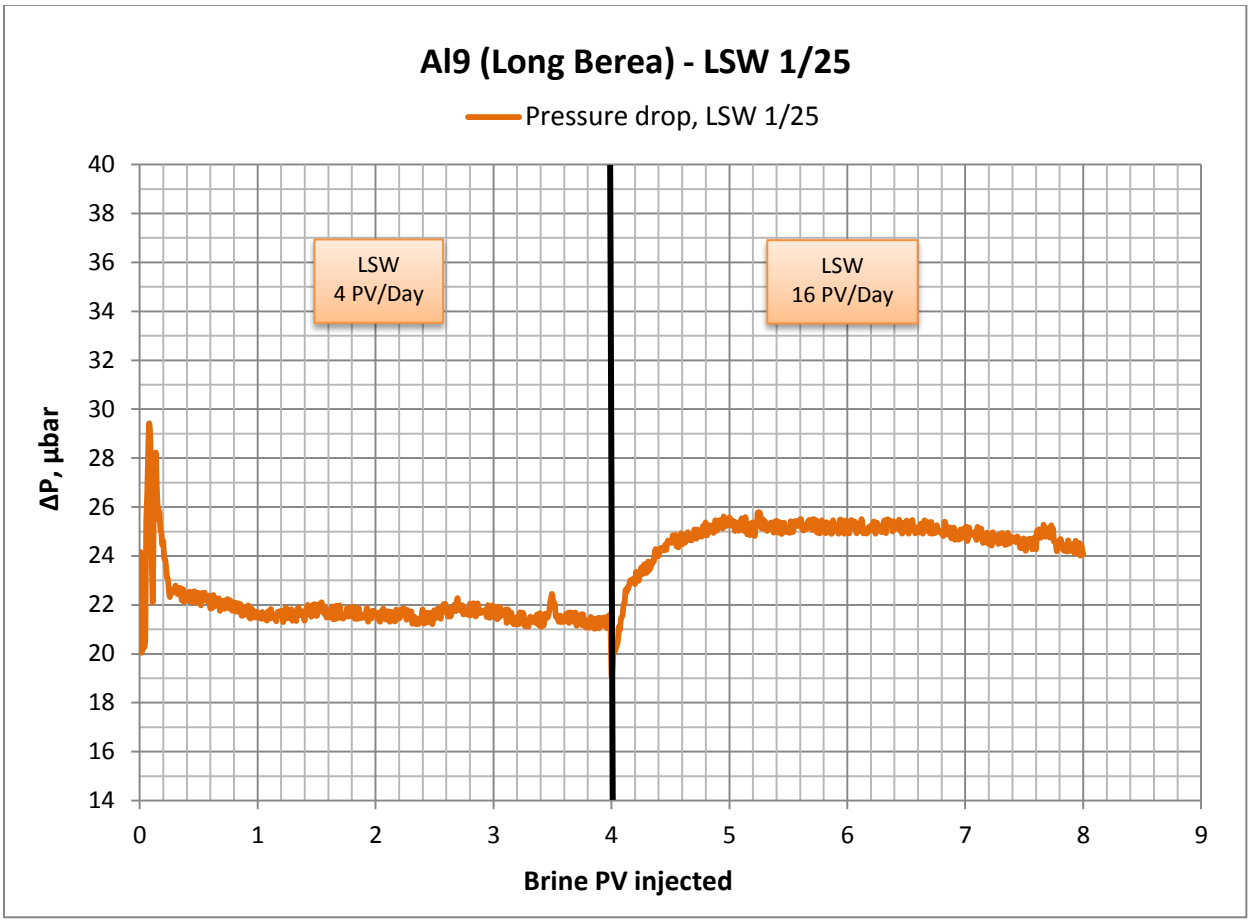

Figure 51 - Pressure drop across the core Al-9 during LSW flooding

LSW flooding for long Berea core showed maximal oil recovery between experiments with LSW as a primary injection fluid. This can be an indication of the highest amount of brine/rock interactions and high potential of Berea sandstone to improve oil recovery by LSW.

4.10 Simulation part

Data obtained from flooding experiments were used for performing calculation of the relative permeabilities in Sendra simulator (version 2013.1). Sendra is a two-phase 1D black-oil simulation model used for analyzing core flooding experiments. It is tailor made for revealing relative permeability and capillary pressure from two-phase and multi-phase flow (Sendra user guide, 2013).

The main aim of these simulations is to get relative permeability curves for water and oil, which we need to understand relative movement of these two phases in core. Relative movement of water/oil phases will affect sweep efficiency and as a result oil recovery.

To generate the relative permeability curves we used Corey correlation. It is an often used approximation of relative permeability. This correlation represents power law in the water saturation S_w. If S_{wi} is the irreducible (minimal) water saturation, and S_{or} is the residual (minimal) oil saturation after water flooding, we can define a normalized (or scaled) water saturation value (Wikipedia, Relative permeability):

$$S_{wn} = \frac{S_w - S_{wi}}{1 - S_{wi} - S_{or}}, \quad (27)$$

where, S_{wi} irreducible water saturation,

S_{or} residual oil saturation.

Then the Corey correlations of the relative permeability of oil and water are (Wikipedia, Relative permeability):

$$K_{ro} = (1 - S_{wn})^{N_o}, \quad (28)$$

$$K_{rw} = K_{rw}^{o} \cdot {S_{wn}}^{N_w}, \quad (29)$$

where, K_{ro} relative permeability for oil,

K_{rw} relative permeability for water,

K_{rw}^{o} the end point of the water relative permeability.

The empirical parameters N_o and N_w can be obtained from measured data either by optimizing to analytical interpretation of measured data, or by optimizing using a core flow numerical simulator to match the experiment (often called history matching) (Wikipedia, Relative permeability). As the basis for simulation following data were used: absolute permeability of the core, length, diameter, porosity, density/viscosity of water and oil, initial water saturation. History matching was made for the experimental data: observed recovery during flooding and pressure drop across the core. Example of history matching is presented below on Figure 52. Horizontal line is time in hours from the beginning of production. Two vertical lines are pressure drop in mbar and oil production in milliliters.

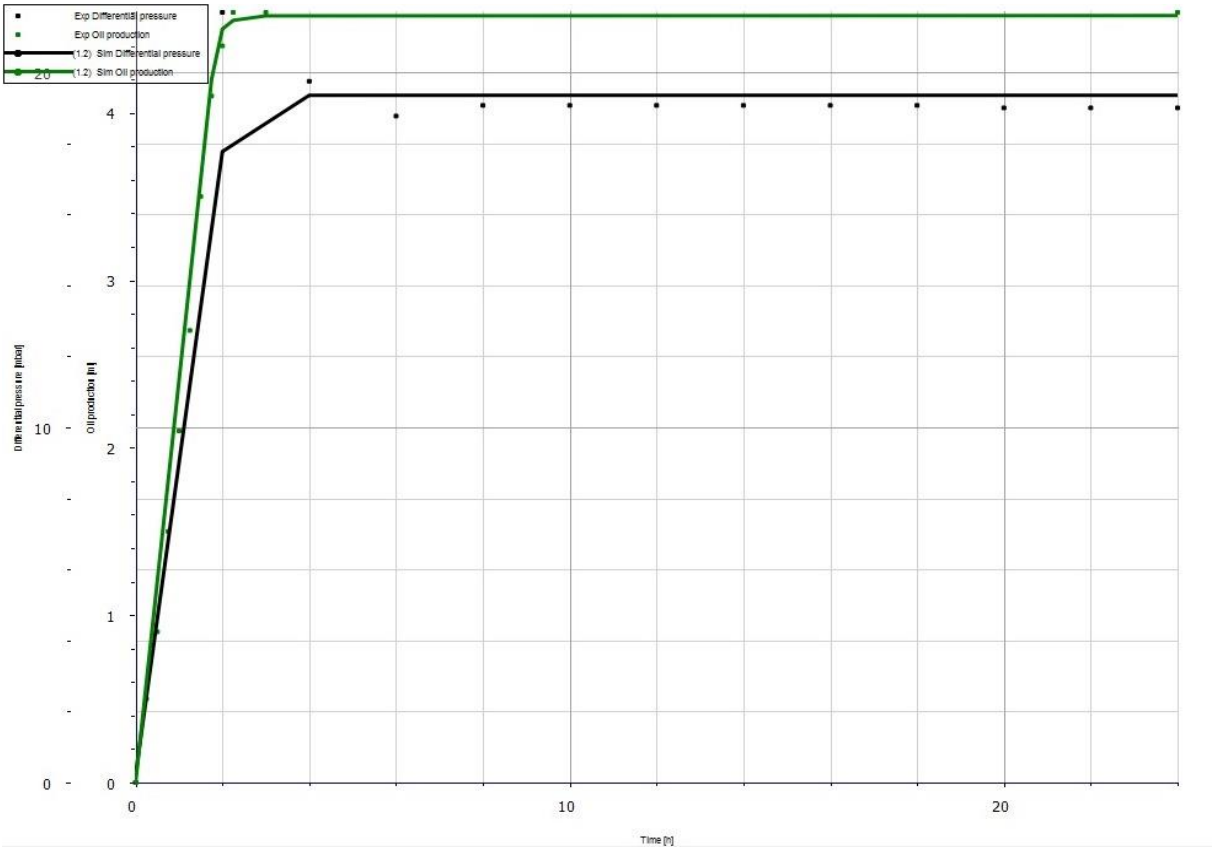

Figure 52 – Example of history matching in Sendra for core Al-12

On Figure 52 are showed experimental data for oil recovery (green dots) and pressure drop (black dots) for core Al-12. Simulated data for oil recovery and pressure drop are presented by green and black line respectively. Well enough matching between experimental and simulated data should lead to presentability of the relative permeability curves. Below we will discuss relative permeabilities for short cores flooded with LSW and SSW as a primary injection fluid for both Berea and Bentheimer sandstone type. Simulation was made only for first part of flooding (4 PV/Day) because Sendra does not take into account possible rock/brine interactions. If we will make one simulation for two different flow rates and salinities we will get incomparable results.

Relative permeability curves for short Bentheimer core Al-4, SSW are presented on Figure 53. Vertical axis show values for relative oil/water permeabilities; horizontal axis shows water saturation values (fractional).

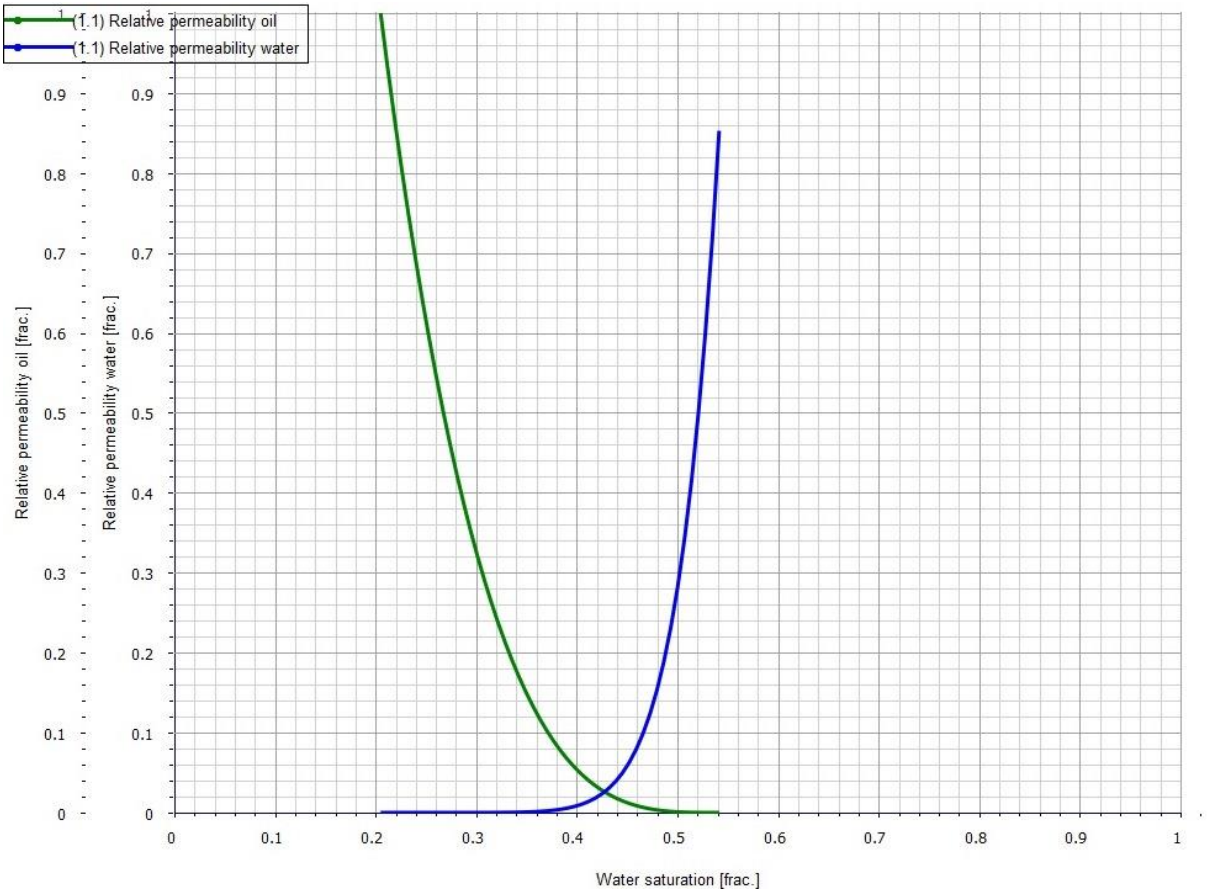

Figure 53 - Simulated relative permeability curves for short Bentheimer core Al-4, SSW flooding

On Figure 53 solid green line is relative permeability for oil (non-wetting phase) and blue line for water (wetting phase). Before starting flooding process we have residual water saturation (around 0,2). Other pore space is filled by oil. Presence of water has small effect on oil movement in the beginning of flooding process, so initial relative permeabilities for oil and water 1 and 0 respectively.

Water injection into the core will lead to water distribution in pore space and reducing oil saturation. Corresponding to this process oil relative permeability decreases and water relative permeability increases due to increase of water saturation. After water breakthrough we have trapped oil in pore space (relative permeability for oil is zero).Water relative permeability reaches a maximum value which is less than absolute permeability due to presence of trapped oil.

Oil trapping happens due to capillary and interfacial tension effects (detailed description of these parameters was given in theoretical part). Low oil recovery can be a result of the oil ganglia being retained in the large pores as a result of capillary forces (Adrian C Todd, 2005).

Figure 54 illustrates the pore doublet model illustrating how oil can be trapped in a large pore. The forces to displace this droplet have to overcome capillary forces and are too great to use pressure through pumping. The force required can be reduced by reducing the interfacial tension which is the basis for many enhanced oil recovery methods; for example, surfactant and miscible flooding (Adrian C Todd, 2005).

Important parameter in oil displacement process is *mobility ratio*. It relates the mobility of the displacing fluid (water in our case) relative to that of the displaced fluid (oil). Equation for mobility ratio is given below (Adrian C Todd, 2005):

$$M = mobility\ ratio = \frac{k'_{rw}/\mu_w}{k'_{ro}/\mu_o},$$

where k'_{rw} - relative permeability at residual oil saturation,

k'_{ro} - relative permeability at the irreducible water saturation.

Cross point for relative permeabilities curves means that relative permeability for oil is equal to relative permeability of water and mobility ratio will be equal approximately 1 (due to comparable viscosities of water and oil: 0,41 cP for n-Decane against 0,405 cP for LSW). For SSW case where viscosity is 0,44 cP the cross point will mean that the mobility ratio is slightly lower than 1.

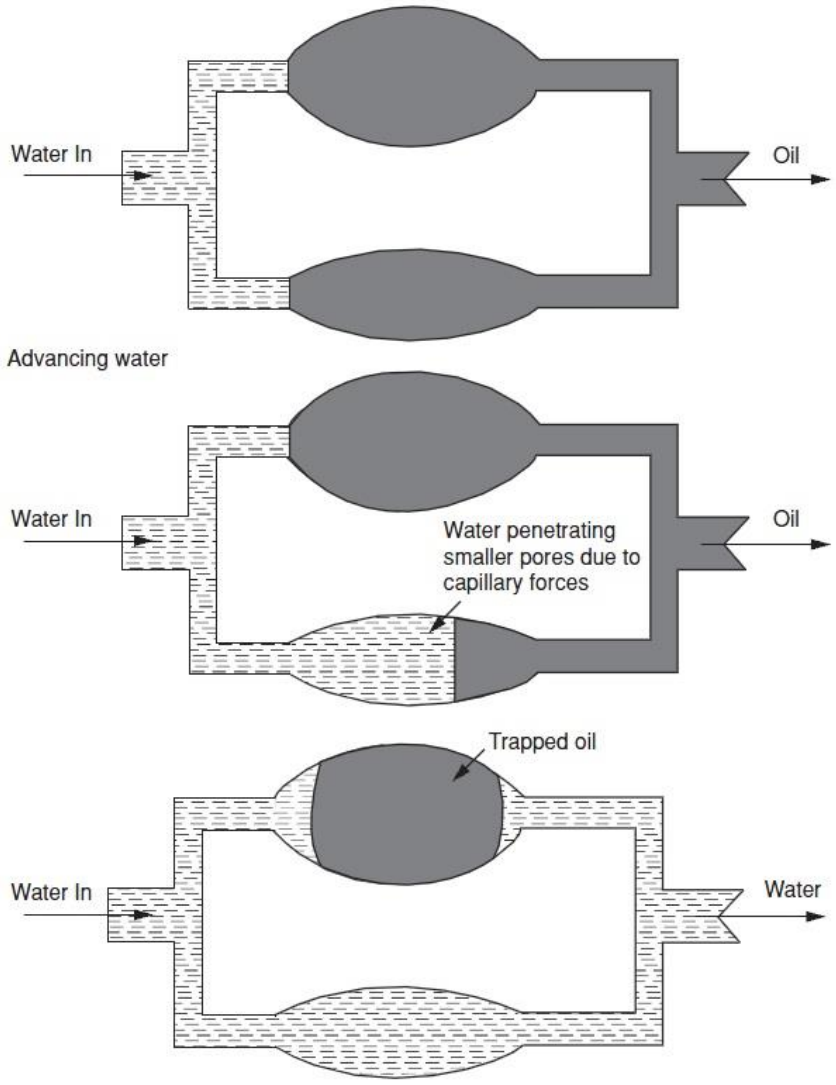

Figure 54 - Pore Doublet Model (Adrian C Todd, 2005)

Returning to the core Al-4 flooding graph we can see that cross point is corresponding to water saturation value 0,422. This number we will use for comparison with other samples. Zone which is before crossing point (mobility ratio less than 1) indicates effective oil displacement. Values of cross point which are higher than 0,421 can indicate later water breakthrough and respectively higher recovery.

Figure 55 shows relative permeability curves for short Berea core. Cross point value in this case is 0,481 which is slightly higher than for short Bentheimer core (0,422). This can indicate slightly later water breakthrough for Berea core and respectable more effectively displaced oil. It is corresponding with oil recovery observations where for Berea sandstone we got slightly higher results (35% for short Berea core versus 30% for short Bentheimer). The shape of the curves is similar.

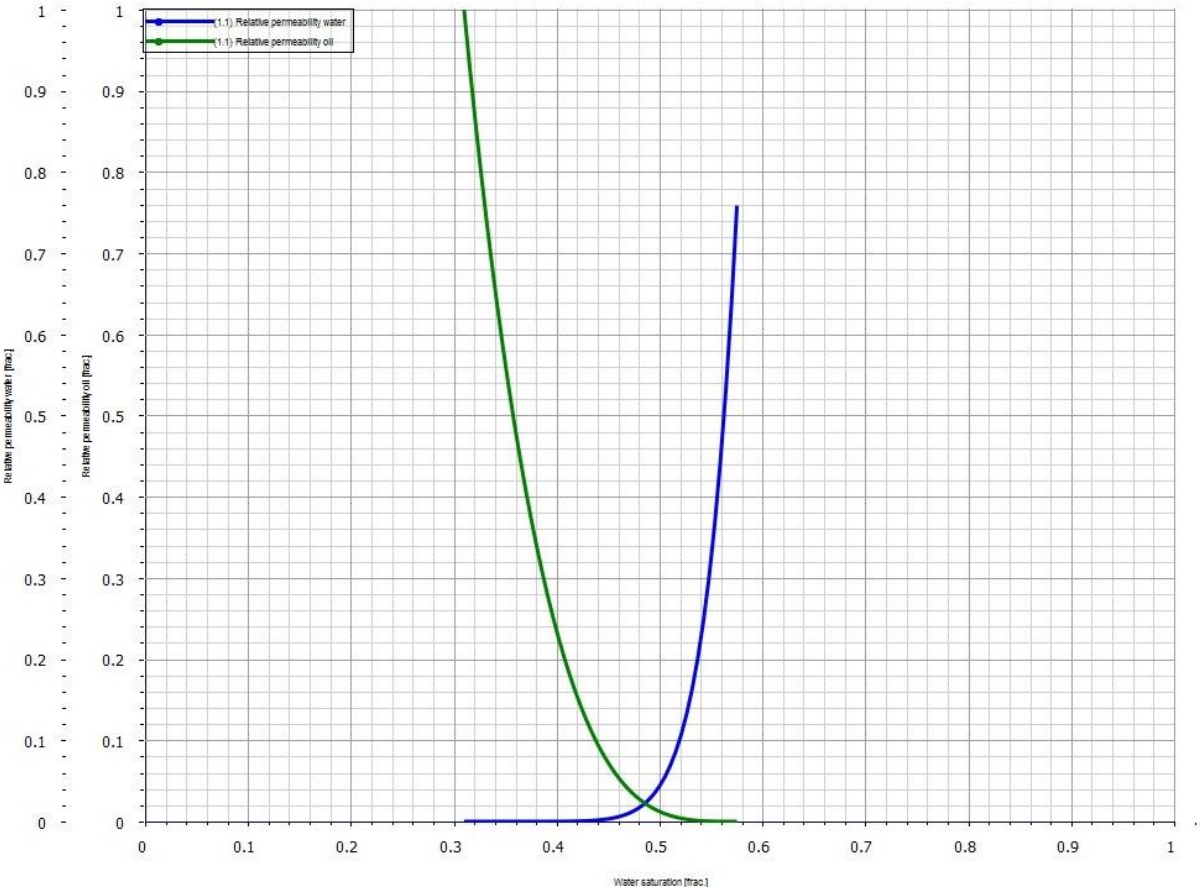

Figure 55 - Simulated relative permeability curves for short Berea core Al-11, SSW flooding

Relative permeabilities simulation results for short Bentheimer LSW flooding are presented on Figure 56 below. Cross point in this experiment is 0,38 which is lower than values for SSW flooding. This can indicate earlier water breakthrough and respectively lower oil recovery in this case. Moreover, shape for water relative permeability is different in compare with SSW flooding. In LSW case it is increasing faster which can indicate worse sweep efficiency. The reason for this is the lower viscosity of LSW in compare with SSW.

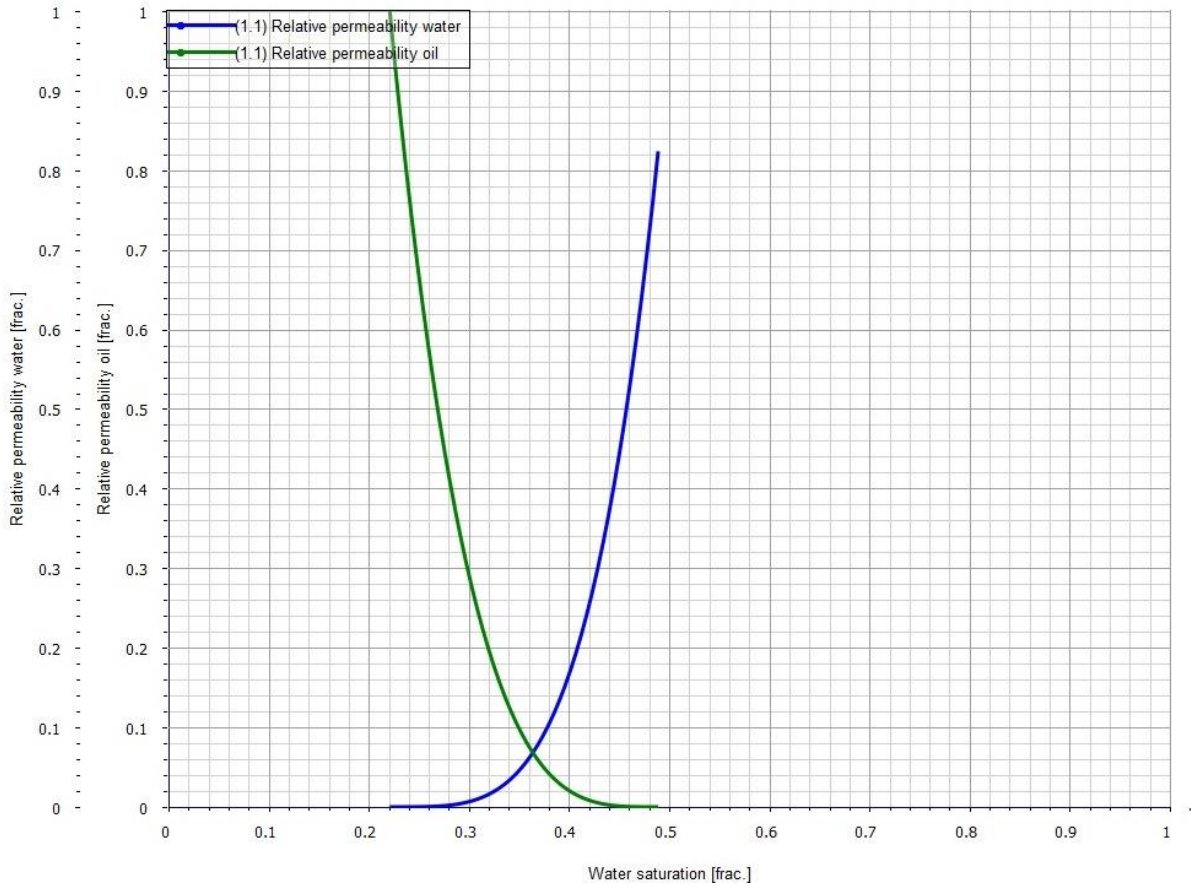

Figure 56 - Simulated relative permeability curves for short Bentheimer core Al-6, LSW flooding

The last relative permeability Figure 57 shows LSW flooding case for short Berea core Al-10. Cross point value in this case is 0,408 which is still lower than for SSW case but slightly higher than for Bentheimer LSW flooding. This is corresponding with oil recovery data (23,75% for Berea which is higher than for

Bentheimer 21,28%). Water relative permeability curve for Bentheimer has more concave shape than for Berea which can indicate higher sweep efficiency.

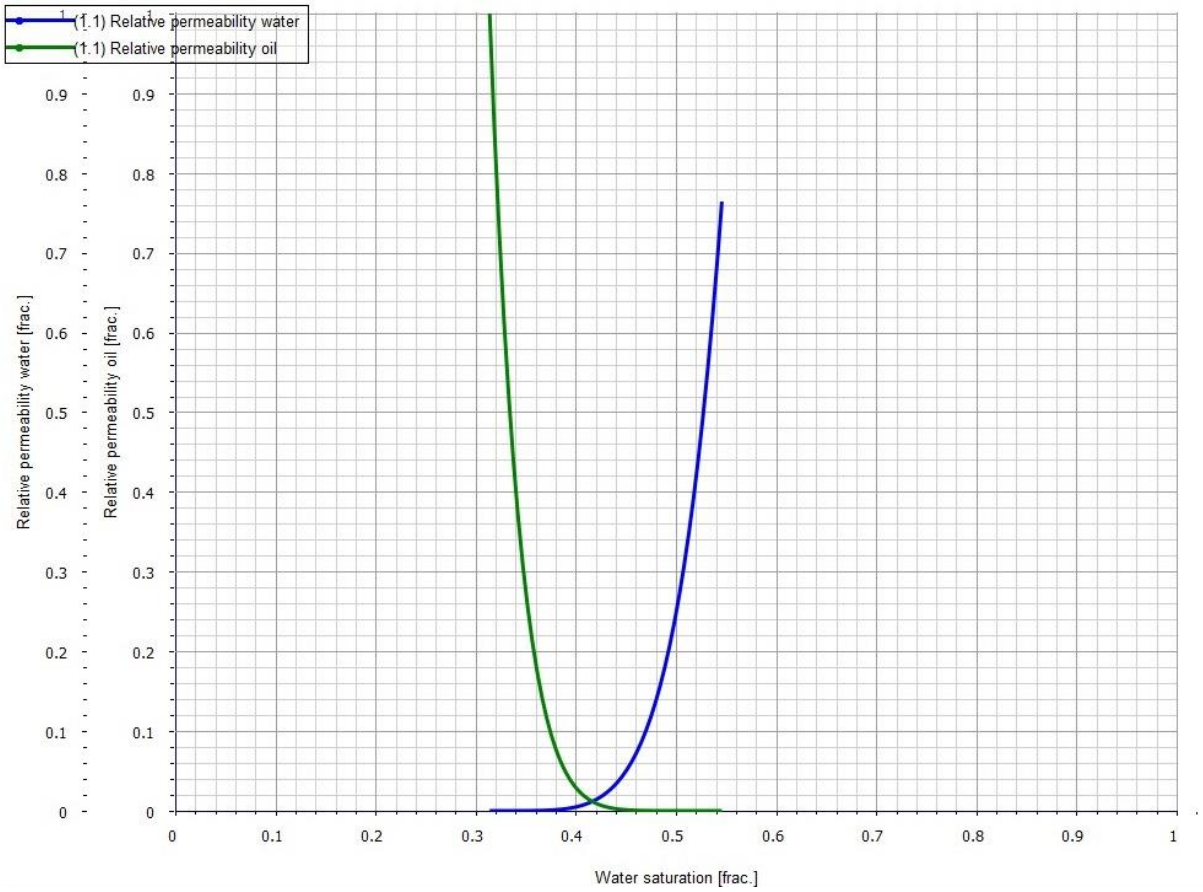

Figure 57 - Simulated relative permeability curves for short Berea core Al-10, LSW flooding

Simulation of water/oil relative permeabilities for our experiments showed results corresponding to other obtained data. For SSW flooding the cross point values are higher than for LSW which can indicate later water breakthrough and higher recovery. Same tendency is for Berea sandstone versus Bentheimer.

4.11 Analysis of aluminum (Al) and silicon (Si)

Additionally to ion chromatography, the analysis of Al and Si content in the effluent samples was made. The main purpose of this analysis is to confirm assumption about sandstone mineral dissolution process during flooding. Very few studies focused on the dissolution of sandstone can be found in literature to date.

Qingjie Gong et al. (2012) studied dissolution of sandstone powders in deionized water over the range 50–350℃. The work done by these researchers is based on quartz, feldspar, calcite and kaolinite dissolution in aqueous brines. The sandstone powders were flooded with deionized water in the pressure vessel reactor at different temperatures. In temperature range of 50-100℃ it was noticed that the dissolution of feldspar and calcite is going on faster than the dissolution of kaolinite and quartz. They made the graph for the amount of Si and Al concentrations in the effluent samples depending on the temperature of the flooding (Figure 58). On Figure 58 vertical axis is concentration in μmol/L and horizontal axis is temperature in ℃.

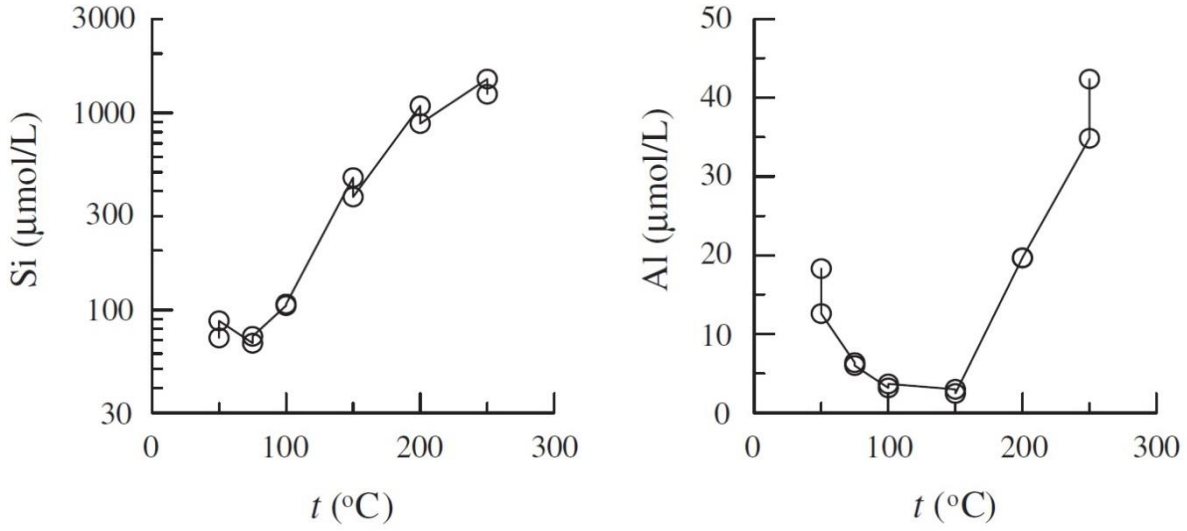

Figure 58 - Relationship between element contents and temperatures (Qingjie Gong et al., 2012)

As we can see very low concentration of aluminum was found in the effluent samples and concentration is decreasing with increasing temperature. Concentration of silicon is much higher and increasing with increasing temperature. This is corresponding to our results in some extent. Core samples which we used in our experiments have a porous matrix and a much smaller reactive area than for sandstone powder described in paper. Moreover, different mineral composition of our sandstone in compare with used in paper will also affect results.

Estimation of possible error

It was noticed that the concentration of Si can show high results due to contamination from glass bottles for storing of water samples. Furthermore this process is time dependent. Based on analysis of reference samples it was found approximate correlation between the time of storing water samples in glass bottles and contamination. Mean contamination value is equal 0,13 mg/L per month and is subtracted from raw data, but still presented values can contain some amount of uncertainties. Table 8 shows dependence of Si amount in the effluent on time. More investigations should be performed for deeper understanding of contamination process and more precise correcting of obtained data.

Table 8 - Dependence of Si concentration in the effluent water on time

Sample	Type	Flooding sequence	Date of flooding	Contamination factor	Date of analysis
Al7	Long Bentheimer	SSW-LSW	01.04.2014	0,26	16.05.2014
Al11	Short Berea	SSW-LSW	03.04.2014	0,26	12.06.2014
Al12	Long Bentheimer	LSW	07.04.2014	0,26	16.05.2014
Al8	Long Berea	SSW-LSW	12.03.2014	0,39	16.05.2014
Al9	Long Berea	LSW	15.03.2014	0,39	16.05.2014
Al6	Short Bentheimer	LSW	25.03.2014	0,39	12.06.2014
Al4	Short Bentheimer	SSW-LSW	18.02.2014	0,52	12.06.2014
Al10	Short Berea	LSW	20.02.2014	0,52	12.06.2014

Figure 59, Figure 60, Figure 61 and Figure 62 show an analysis for Si concentrations in effluent water samples during SSW-LSW and LSW flooding for Bentheimer and Berea cores. If we will compare the analysis of our data with those gotten by Qingjie Gong et al. (2012), we will see that the numbers correspond. In our case maximal concentration for Si reaches about 500 μmol/L, which is 5 times higher than data from the paper. It can mean that our values are overestimated. However, the conditions of experiments in our case were slightly different:

1. Confining pressure is more than 3 times lower.
2. The flooding was done with the core instead of powder.
3. Amount of minerals themselves is different.
4. Water salinity is different.

Despite the complexity of determination of certain numbers we still can compare results for one sandstone type with another. From the graphs we can see that the concentration of silicon during flooding is much higher for Berea sandstone than for Bentheimer. Also after switching injection fluid to LSW we can observe slight increase of Si concentration. This can indicate dissolution of sandstone minerals containing Si. Possible sources can be quartz and K-Feldspar which are containing in our cores.

It was noticed by Qingjie Gong et al. (2012) that dissolution of feldspar is going faster than quartz dissolution in temperature range 50-100℃. This can mean that the main source of dissoluted Si is K-Feldspar according to (26). Moreover, excess concentration of potassium ions was detected during analysis of effluent samples. This is corresponding to idea about brine/rock interactions during flooding.

Analysis for Al did not show any excess concentrations in effluent water. Despite of this we can’t say that there are no aluminum ions in the effluent at all. It was noticed by Qingjie Gong et al. (2012) that the amount of Al is much lower than Si and is decreasing with increasing temperature. So the same can also be applied to our analysis. Together with the dilution of the samples it can make the amount of aluminum to be too low for detection.

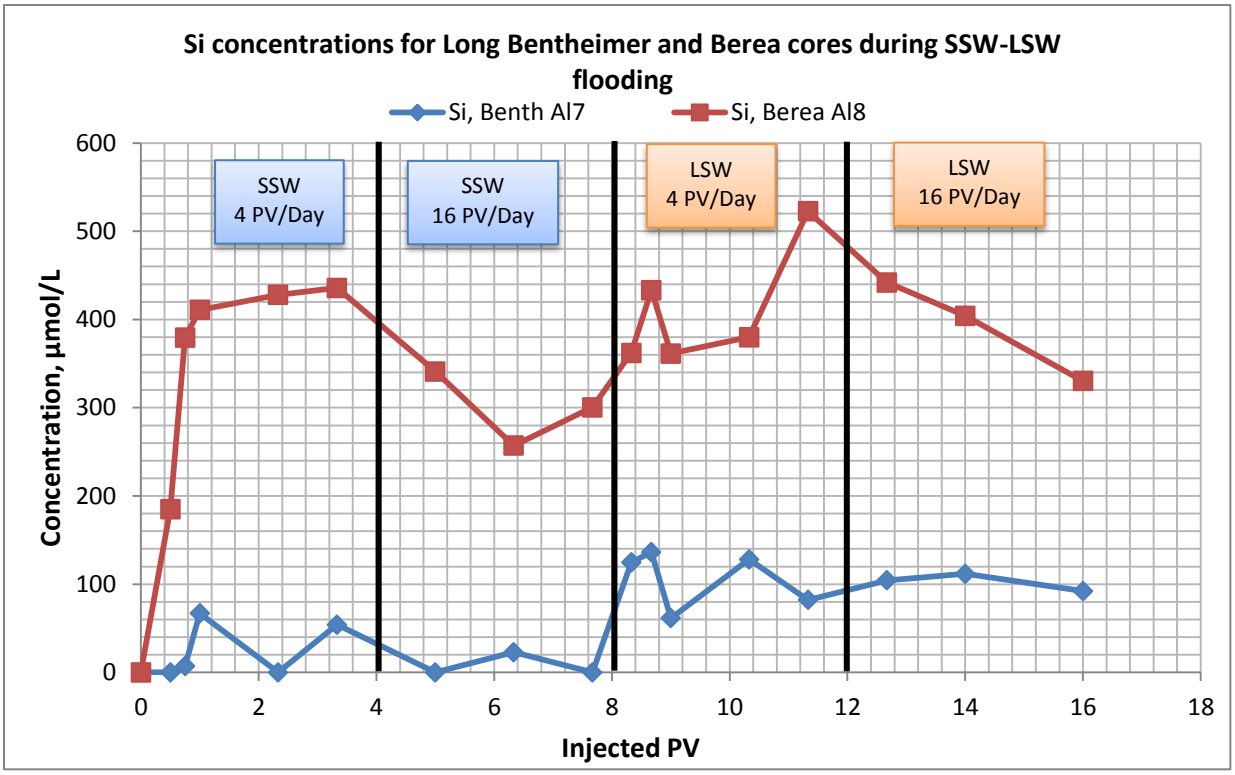

Figure 59 – Concentration of silicon in effluent samples during SSW-LSW flooding for Long Bentheimer and Berea cores

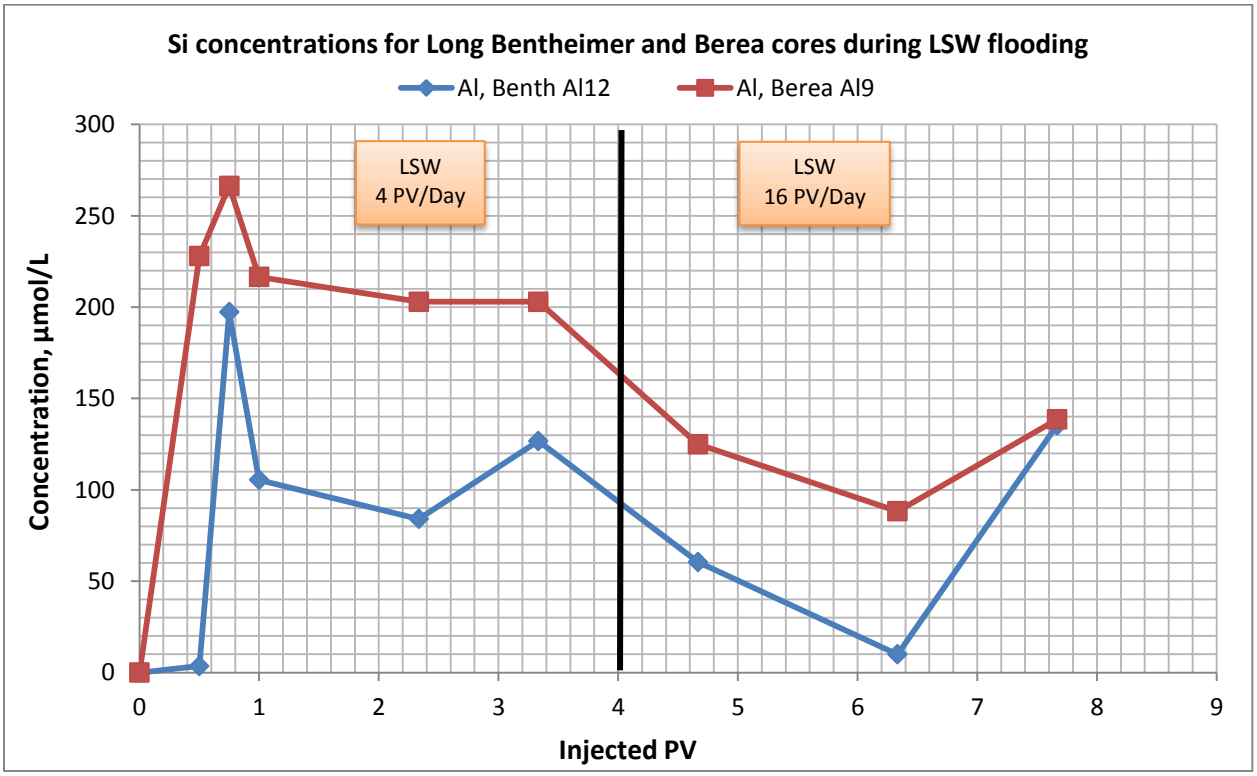

Figure 60 – Concentration of silicon in effluent samples during LSW flooding for Long Bentheimer and Berea cores

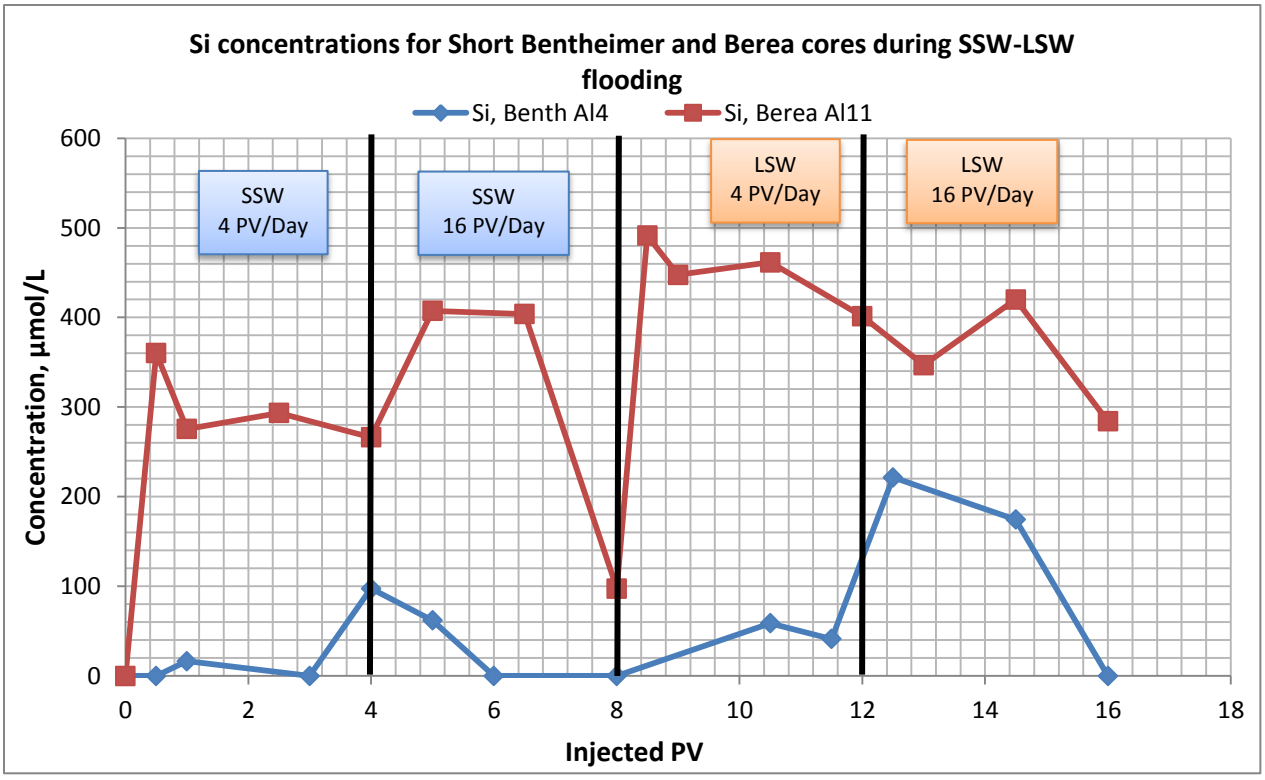

Figure 61 – Concentration of silicon in effluent samples during SSW-LSW flooding for Short Bentheimer and Berea cores

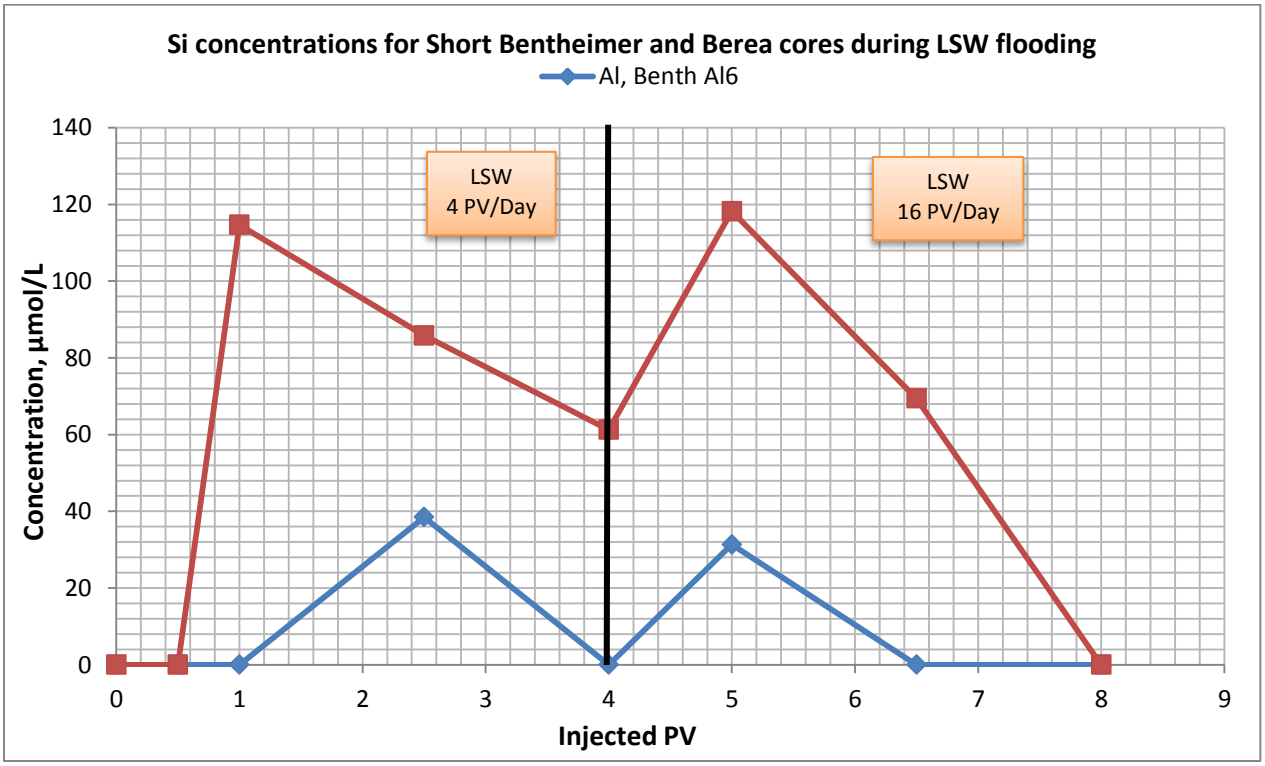

Figure 62 – Concentration of silicon in effluent samples during LSW flooding for Short Bentheimer and Berea cores

4.12 Summary of results

Core flooding results can be divided into two groups for easier comparison. First of all were studied two sandstone types: Bentheimer and Berea, and second was studied different core length. Among obtained results we can find similarities and trends, which can be explained by various assumptions.

On Figure 63 and Figure 64 you can see oil recovery measurements during LSW flooding as a primary injection fluid and LSW as an EOR after SSW (SSW-LSW). In all cases Berea sandstone showed higher total oil recovery in compare with Bentheimer sandstone. It can be due to differences in mineral composition and heterogeneity. Increasing of injection rate (4 PV/Day – 16 PV/Day) and switching from SSW to LSW did not show any oil increment. It means that probably low salinity flooding is not working as a secondary injection mode.

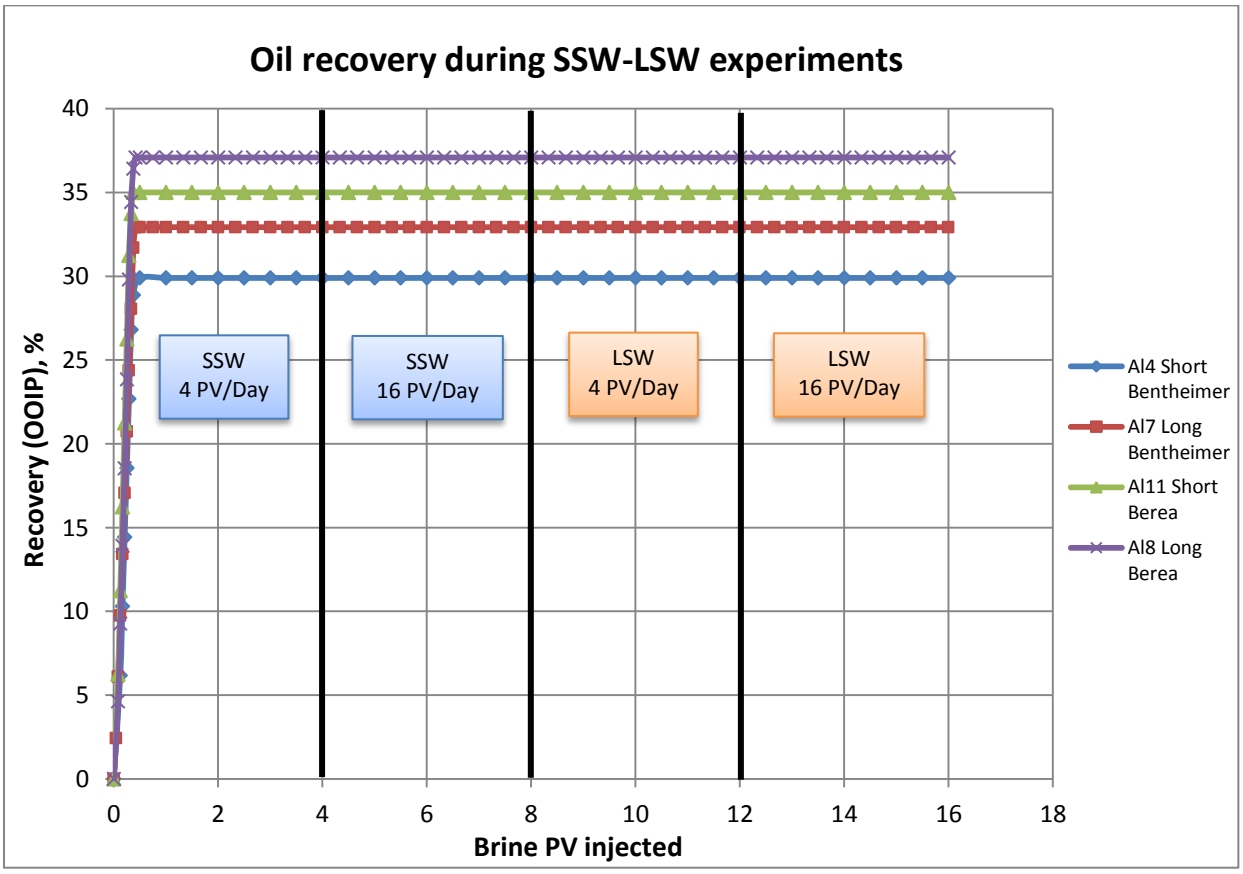

Figure 63 – Oil recovery during SSW-LSW flooding

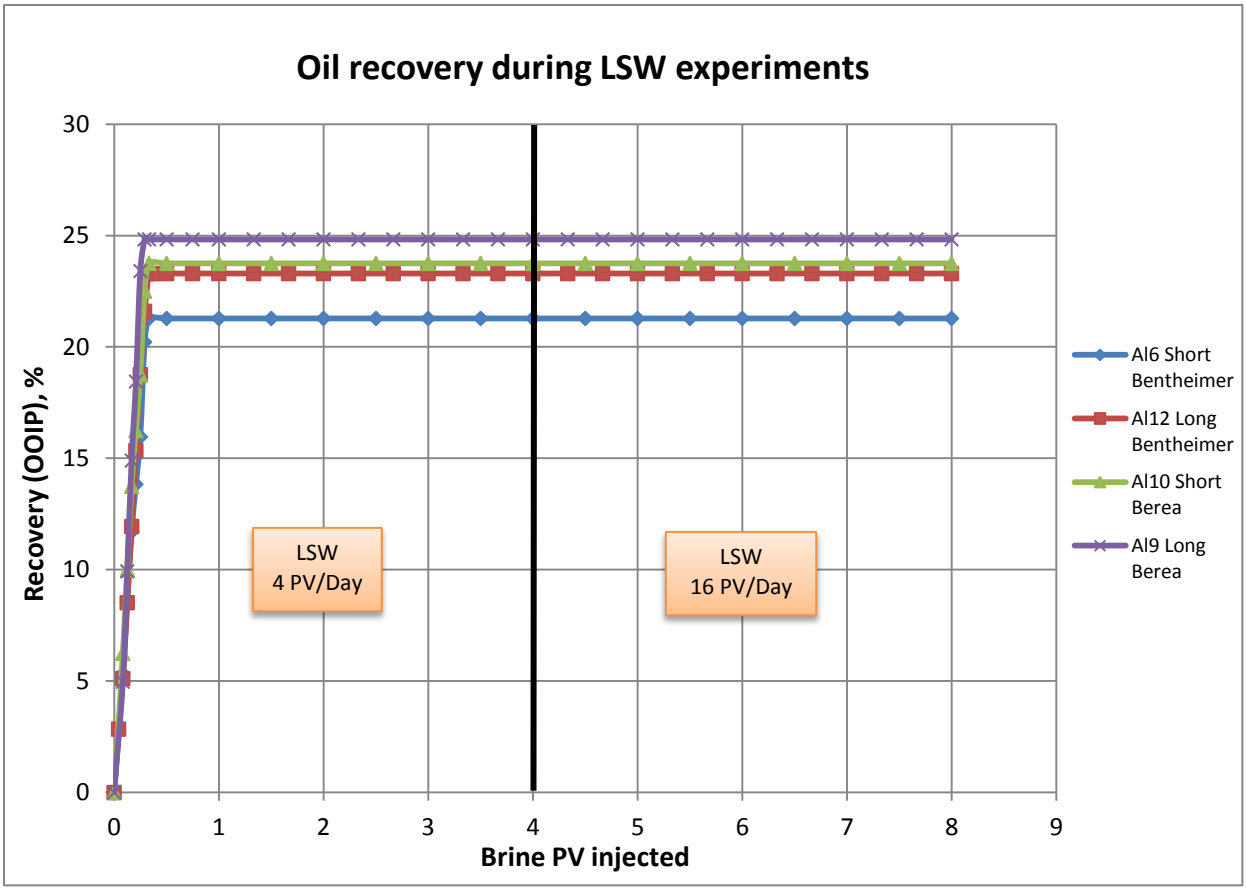

Figure 64 – Oil recovery during LSW flooding

Flooding with LSW as a primary fluid showed lower total oil recovery than for SSW experiments. No additional oil was obtained after switching injection rate to 16 PV/Day. Berea sandstone showed slightly higher recovery values than Bentheimer, but still lower than for SSW flooding. It can indicate that Berea sandstone has higher potential for improving recovery by LSW.

Long cores showed higher recovery in compare with short cores for both SSW and LSW experiments. The reason for this can be higher amount of brine/rock interactions due to higher core length. Brine/rock interactions are represented by dissolution of sandstone minerals and clay/cementing material, which can be confirmed by obtained ions, pressure drop and pH data.

On Figure 65 below are presented measurements of pressure drop across the cores during flooding experiments. In all cases we can observe high peak in the beginning with further stabilization during first 0,5 pore volumes. This phenomenon can be explained by restriction of injecting water flow by synthetic oil in the core after aging. Actual height of the peak can also be influenced by the fine migration due to dissolution of clay material presented in sandstone cores. Level of pressure drop stabilization during flooding with stable injection rate is keeping on the same level with some small peaks and fluctuations. Small peaks can be an indication of fine migrations and fluctuations are the result of low sensitivity of pressure gauge.

Pressure drop across the cores are continuously increasing after switching injection rate to 16 PV/Day during SSW flooding and stabilizing during 1 PV. Switching injection fluid to LSW is leading to pressure drop increasing and keeping on the stably high values. Possible reason of higher pressure drop can be migration of fines due to clay dissolution. The dissolution of clays itself does not lead to increase of pressure, but during this process clay lose its integrity. As a result we have fine migration and some particles block pore throats and the pressure drop across the core increases.

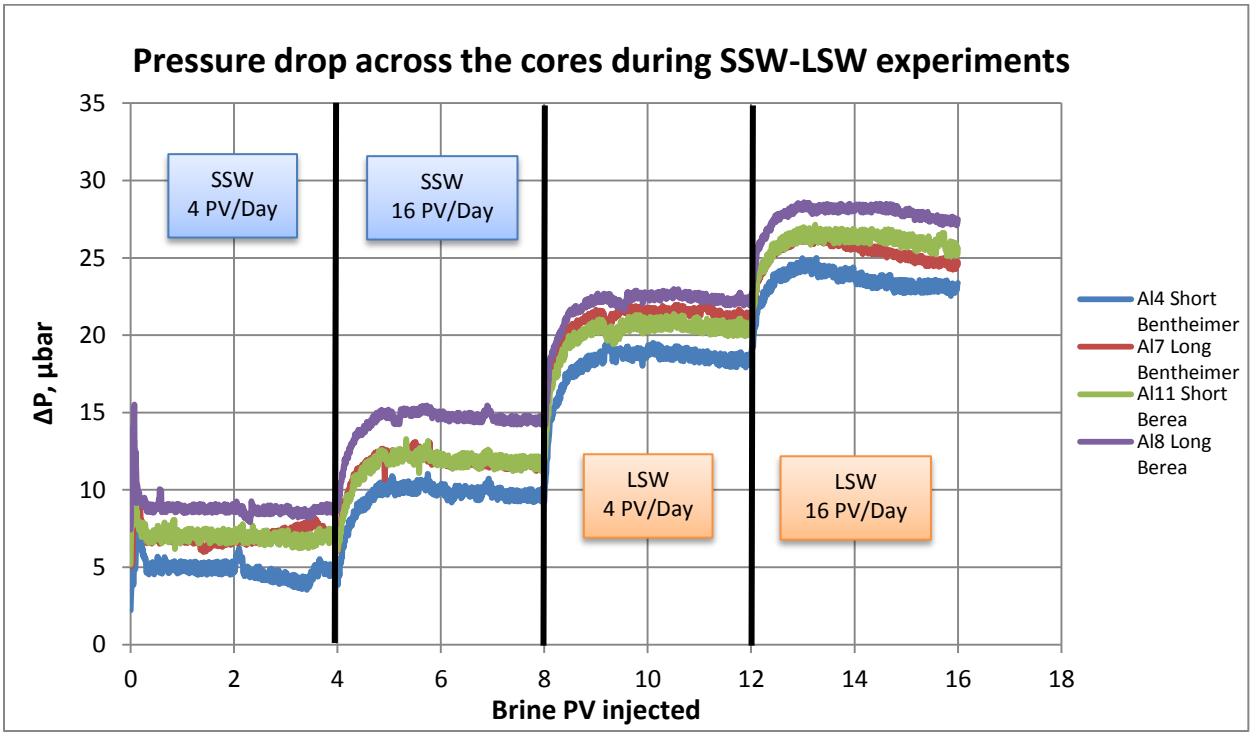

Figure 65 – Pressure drop across the cores during SSW-LSW experiments

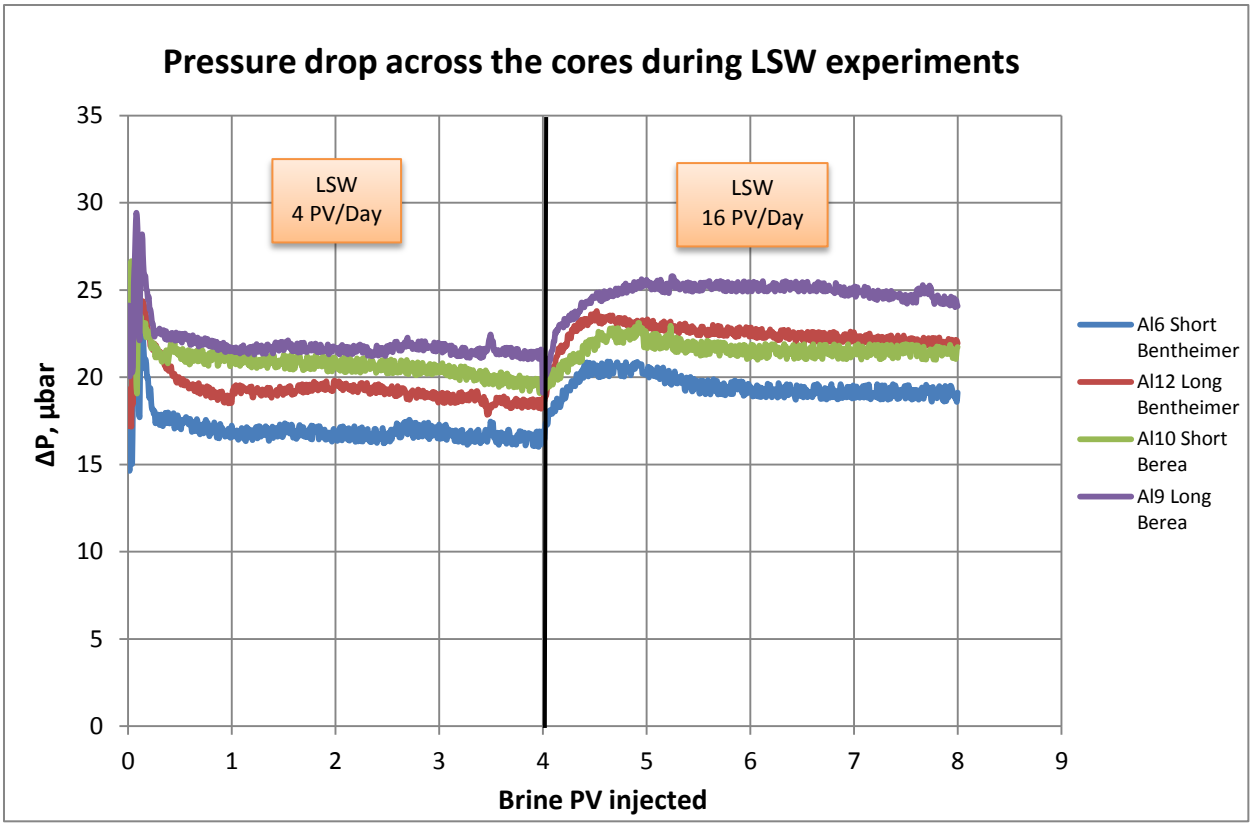

Figure 66 – Pressure drop across the cores during SSW-LSW experiments

Confirmation of fine migration during LSW flooding can be pressure drop measurements for LSW injection as a primary injection fluid. On Figure 66 we can see that after high peak in the beginning pressure drop is stabilizing on higher values in compare with SSW flooding (almost double difference).

For all cases Berea sandstone showed higher pressure drop level than Bentheimer. The main reason of this is the difference in absolute permeability, which is lower for Berea type. Moreover, amount of brine/rock interactions assumed to be higher in Berea, which can be proved by ion chromatography data, pH measurements and analysis of Si content in effluent.

Common trend for pressure drop plots is decreasing in the end of flooding (after 14th PV for SSW-LSW and after 6th for LSW flooding). This can be due to the fact that the amount of clays is small and after continuous flooding the large part of them is already dissolute and we observe less interaction. Possible confirmation can be found in other data, where we also have decreasing trends on the final flooding stage. For longer cores we got higher pressure drop values, which is reasonable.

Figure 67 shows pH measurements of influent and effluent water samples during SSW-LSW flooding experiments. Influent pH values depicted as a solid blue lines and effluent pH as a markers. It is clearly visible the difference between pH of injected fluid and produced fluid. In case with SSW we can observe that effluent pH is lower than initial values. This phenomenon was observed by several researchers and can be related to hydration of magnesium ions (Aly Anis Hamouda and Ole Martin Valderhaug, 2014).

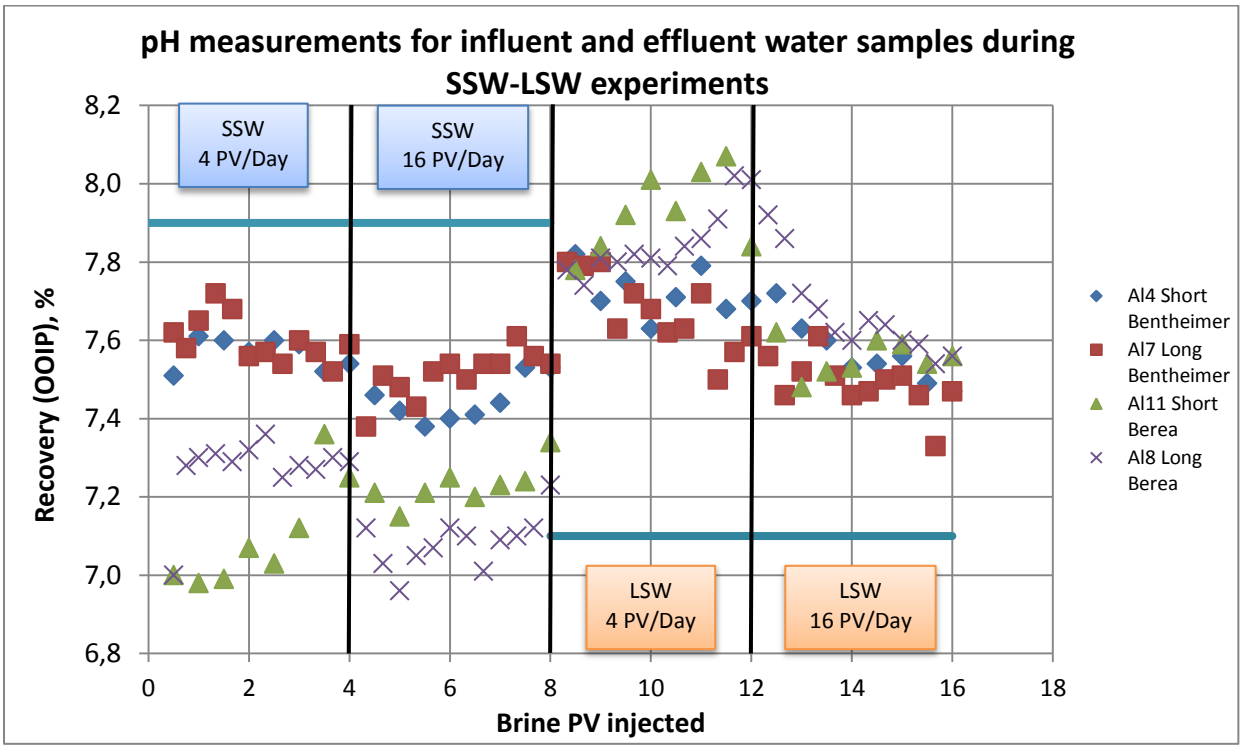

Figure 67 - pH measurements for influent and effluent water samples during SSW-LSW flooding

Conversely, in case with LSW effluent pH is increasing in compare with influent values. This can be an indication of high amount of brine/rock interactions. Possible source of increased pH is sandstone mineral dissolution and in particular K-feldspar. Excess level of potassium in the effluent solution can confirm our assumption. Other possible reason of increased pH can be dissolution of cementing material ($CaCO_3$ – carbonate dissolution). According to this, almost twice higher level of calcium was found in chromatography analysis. Other possible source of higher

amount of Ca^{2+} ion can be desorption of initially adsorbed cations onto the clay as was proposed by Tor Austad et al. (2010).

Influent and effluent pH results for LSW flooding are presented below on Figure 68. During LSW flooding as a primary injection fluid we can see stably increased pH level of effluent samples during all experiment. This can confirm the idea about increased amount of brine/rock interactions. pH level for Berea sandstone is slightly higher than for Bentheimer (during LSW flooding as a primary fluid and EOR). Higher pH can indicate higher mineral dissolution, which will be reflected on ion analysis graphs below.

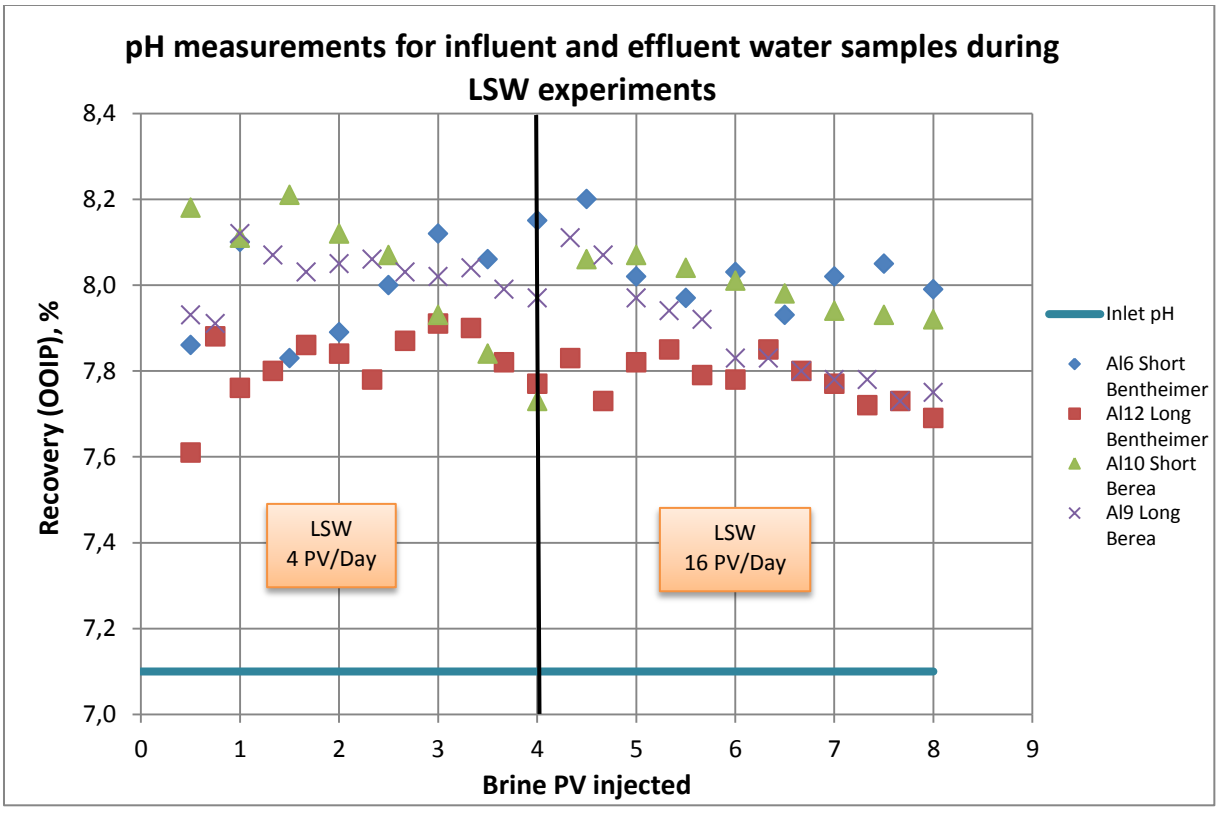

Figure 68 - pH measurements for influent and effluent water samples during LSW flooding

Ion concentration analysis for SSW-LSW and LSW experiments will be presented below. Curves represent ion concentrations in mol/l which is plotted against injected pore volume of brine. Inlet SSW and LSW level is depicted by red dashed lines. Figure 69, Figure 70 show potassium ion concentrations for SSW-LSW and LSW experiments.

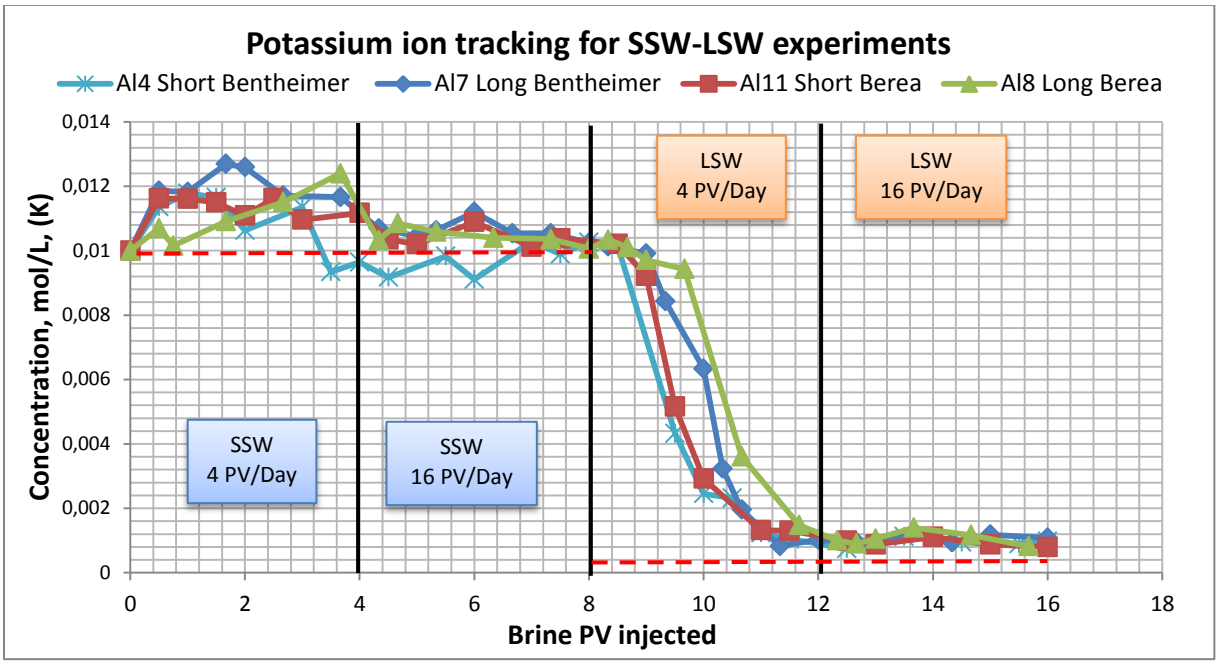

Figure 69 – Ion concentrations for K^+ in effluent water during SSW-LSW flooding

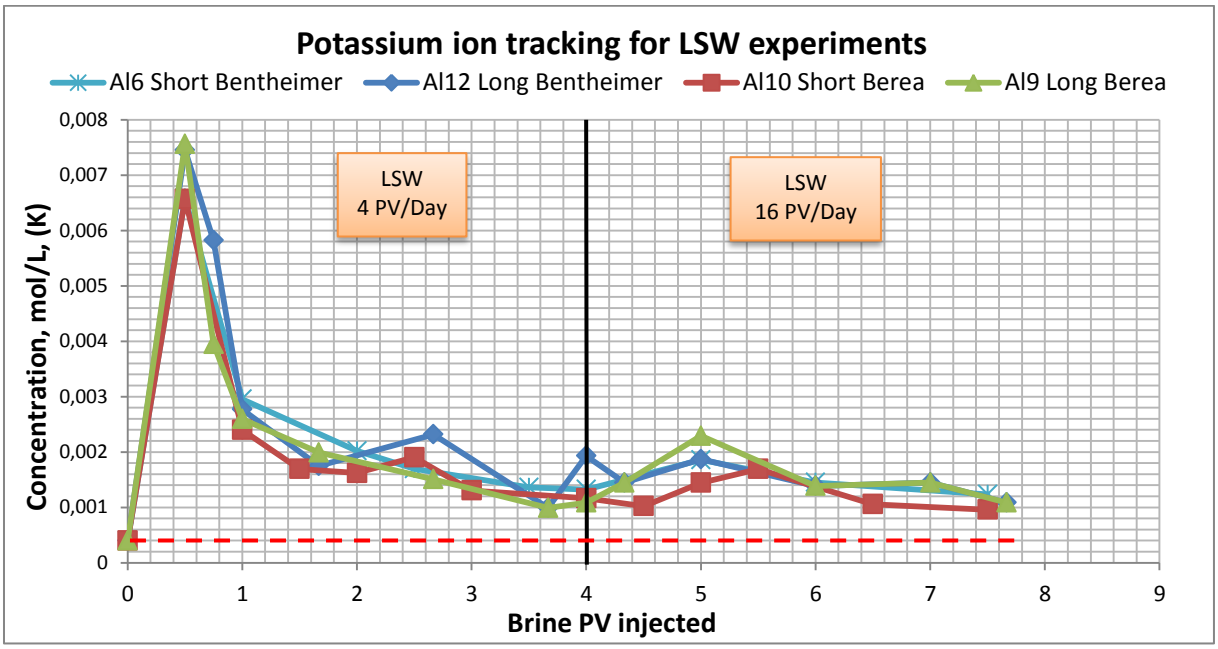

Figure 70 – Ion concentrations for K^+ in effluent water during LSW flooding

Increased values of potassium can be observed on the graphs. On Figure 69 for SSW flooding, increased K^+ concentration reaches maximum value 0,0124 mol/L for long Berea core in compare with initial concentration in SSW 0,01 mol/l. Then after switching injection fluid to LSW we can see decreasing in concentrations, which is going faster for short cores due to smaller length. Concentrations reach stabilization level on 11^{th} – 12^{th} pore volume and keep stable with some fluctuations until the end of flooding. After switching to LSW potassium reaches maximal concentration value 0,0014 mol/l for long Berea core, which is much higher than initial LSW K^+ concentration 0,0004 mol/l. After 14^{th} – 15^{th} PV we can observe concentrations decreasing trend, which can be confirmed by pressure drop results. This may be due to less amount of dissolution in the end of flooding process.

During LSW flooding as a primary injection fluid we also can observe increased potassium level as we can see from Figure 70. High concentration peak in the beginning indicates that we have mixing zone during first pore volume for injected LSW and SSW in the core after aging. After stabilization we have clear excess level for potassium with trend to decreasing after 5^{th} – 6^{th} PV. Potassium reaches maximal concentration value 0,0023 mol/l for long Berea core, which is 5 times higher than initial LSW value. Sandstone mineral dissolution can be the result of increased potassium concentration in effluent water, and respectively increase in pH.

In all cases we got maximal K^+ concentrations values for Berea sandstone, which can indicate higher amount of brine/rock interactions than for Bentheimer type. Moreover, long cores showed slightly higher concentrations in compare with short cores, which can indicate dependence of interactions amount on core length.

Besides potassium, increased amount of calcium ion also was observed in effluent samples. Figure 71 and Figure 72 show Ca^{2+} concentrations for SSW-LSW and LSW flooding experiments.

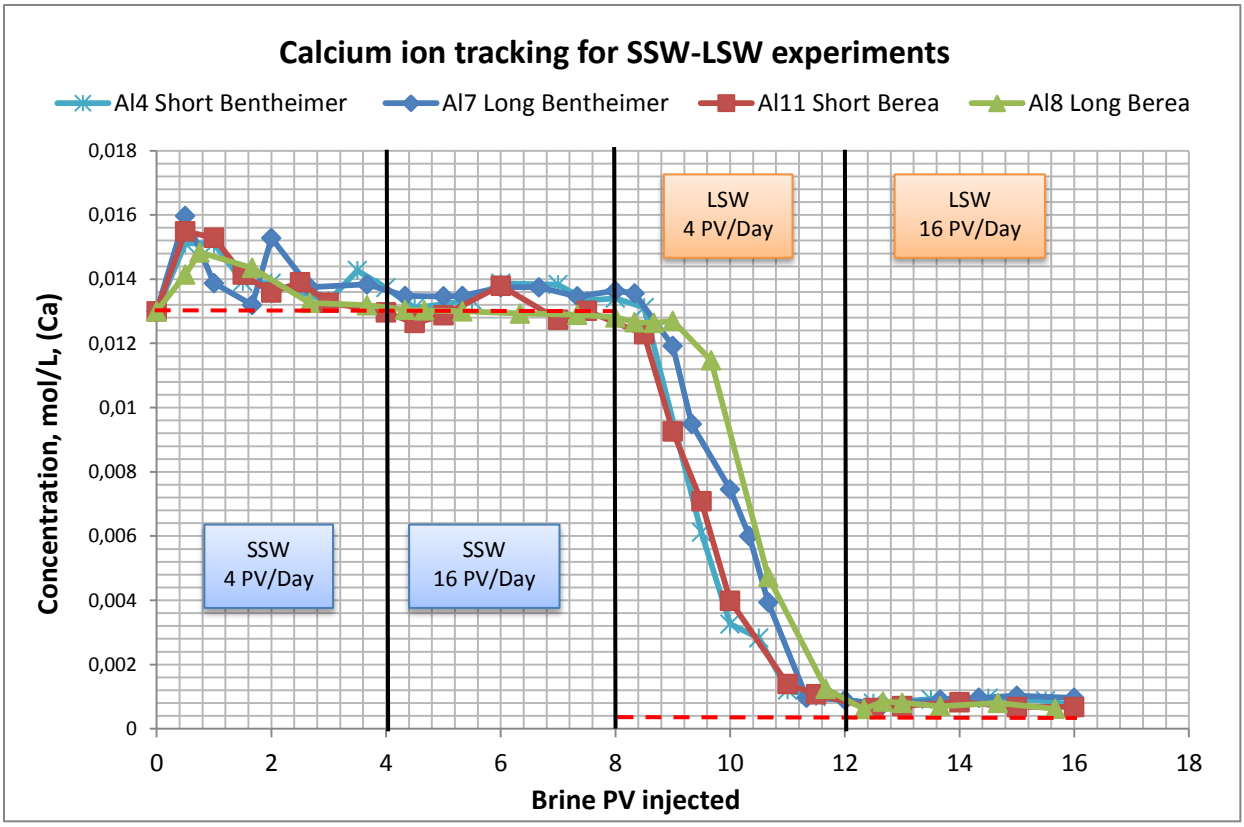

Figure 71 – Ion concentrations for calcium in effluent water during SSW-LSW flooding

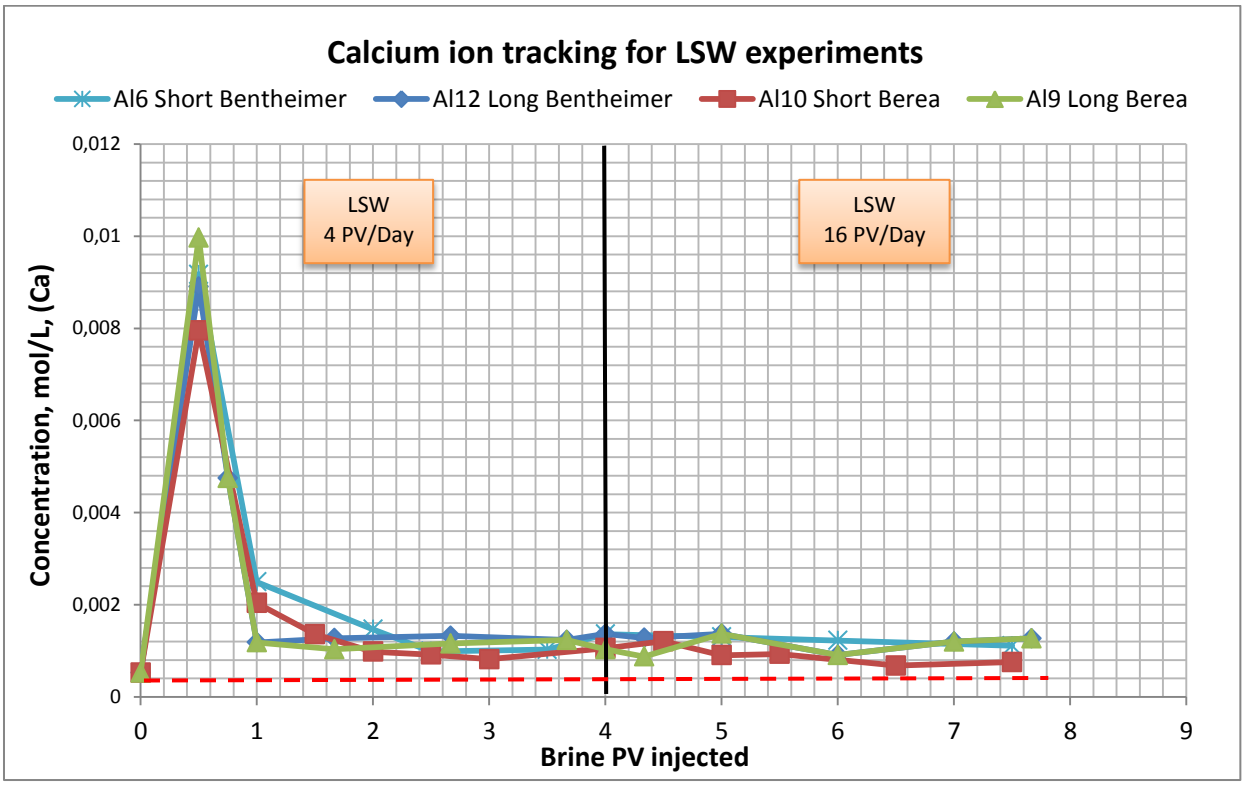

Figure 72 – Ion concentrations for calcium in effluent water during LSW flooding

For SSW flooding increased calcium concentration reaches value 0,016 mol/l for long Bentheimer core versus initial SSW value: 0,013 mol/l. For flooding with LSW calcium concentration reaches the highest value 0,0014 mol/l also for long Bentheimer (influent LSW concentrations is 0,0005 mol/l).

Excess level for calcium concentration is most likely due to dissolution of cementing material in the core. According to Equation (23) we should get increased level of bicarbonate ion (Figure 73), but as was explained in previous parts, bicarbonate HCO_3^- level is keeping high during all flooding procedure. It is system which depends on pH and interactions with air. Notwithstanding the deviations that we get because of the bicarbonate ions represent very complex system, the average amount of HCO_3^- for the LSW flooding is definitely higher than in injection fluid. So it can be taken as an indicator that we have carbonate dissolution.

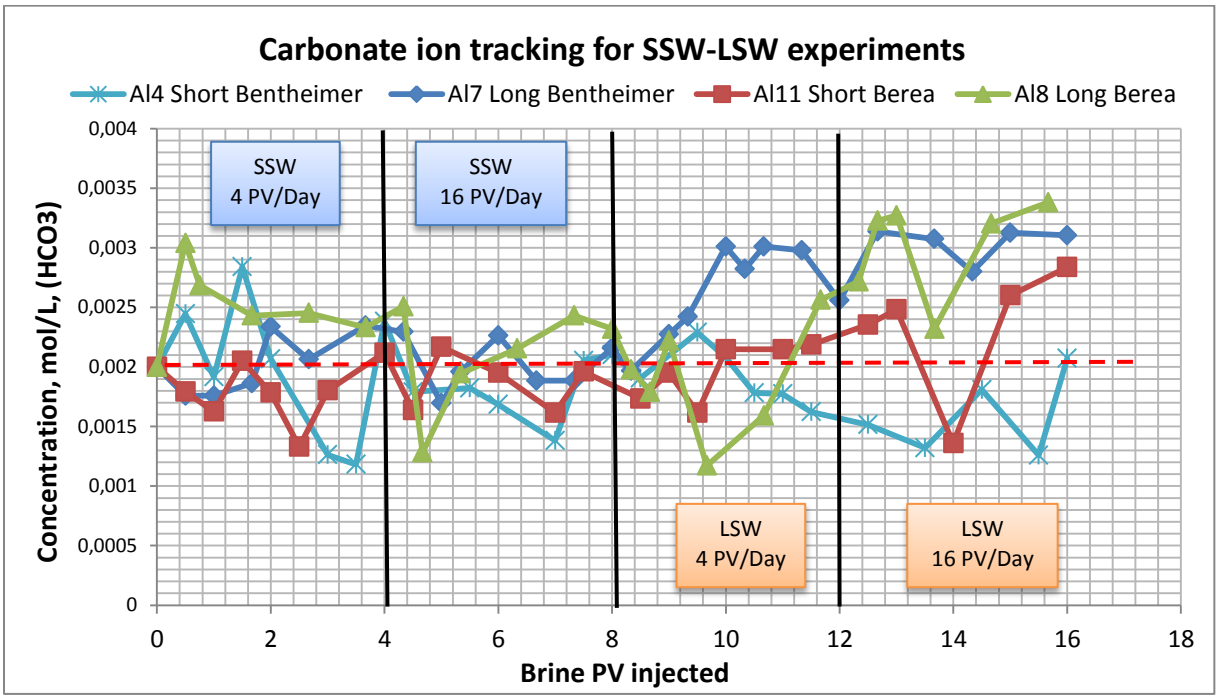

Figure 73 – Ion concentrations for HCO_3^- in effluent water during SSW- LSW flooding

Other ions did not show any significant deviations from initial solution level. Concentrations for magnesium, sodium, sulfate and chloride during SSW-LSW are shown of Figure 74, Figure 75, Figure 76 and Figure 77.

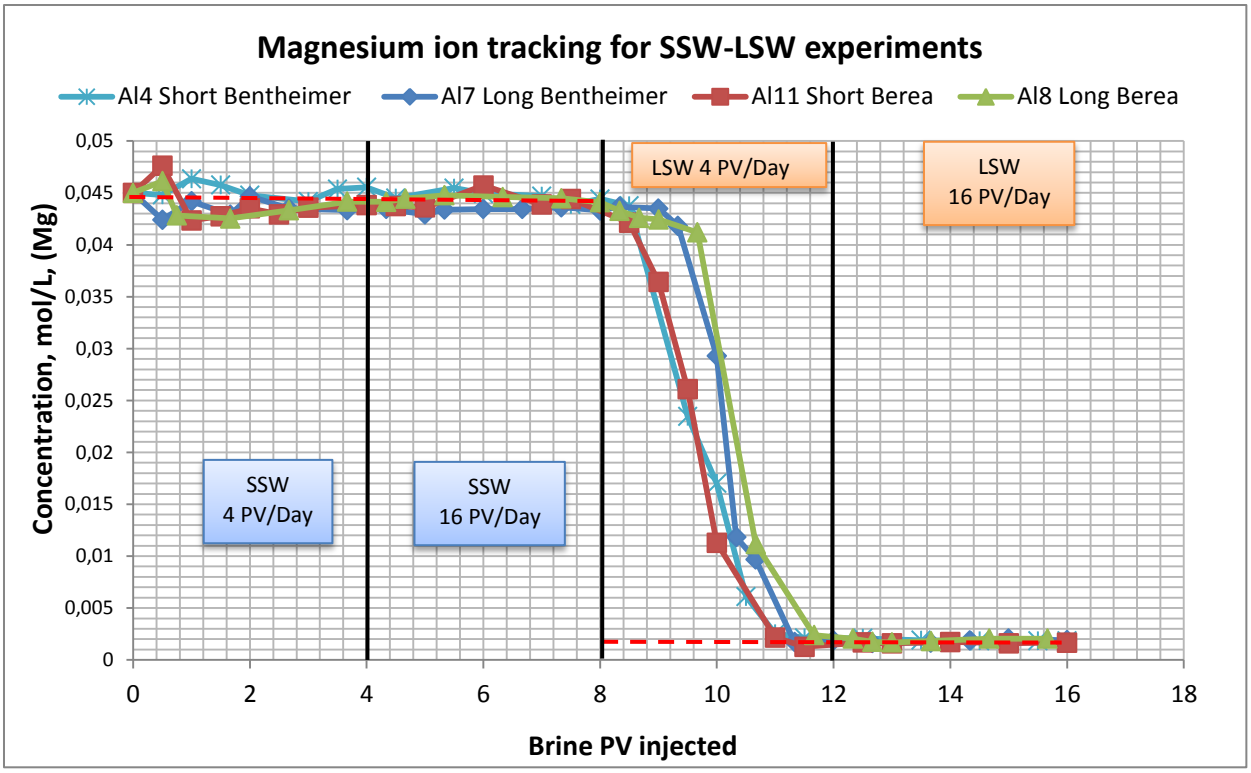

Figure 74 – Ion concentrations for Mg^{2+} in effluent water during SSW- LSW flooding

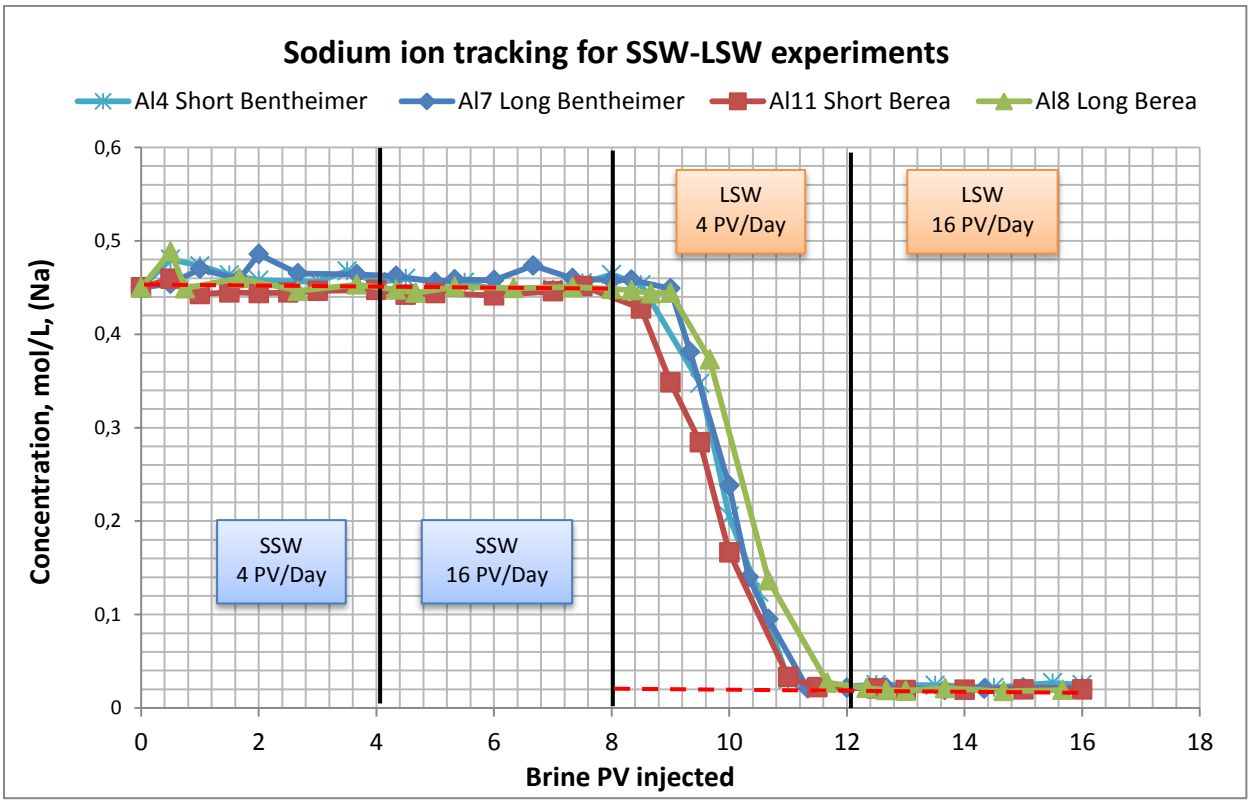

Figure 75 – Ion concentrations for Na^{+} in effluent water during SSW- LSW flooding

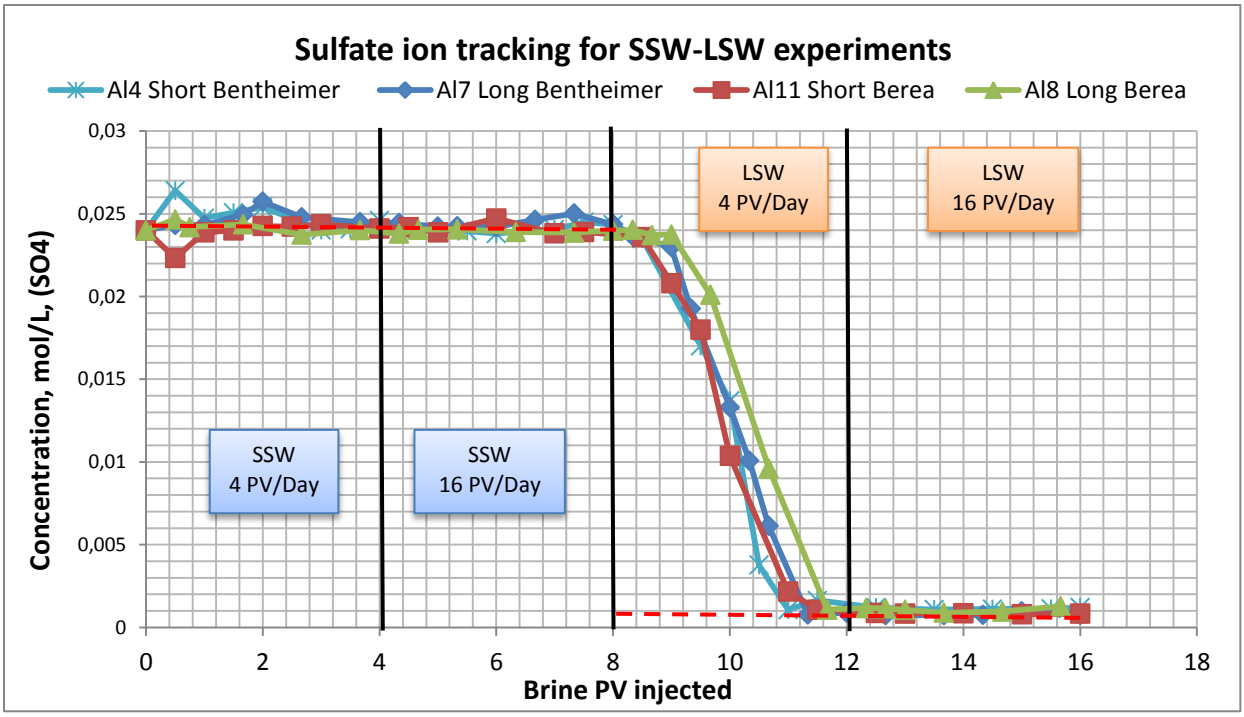

Figure 76 – Ion concentrations for SO_4^{2-} in effluent water during SSW- LSW flooding

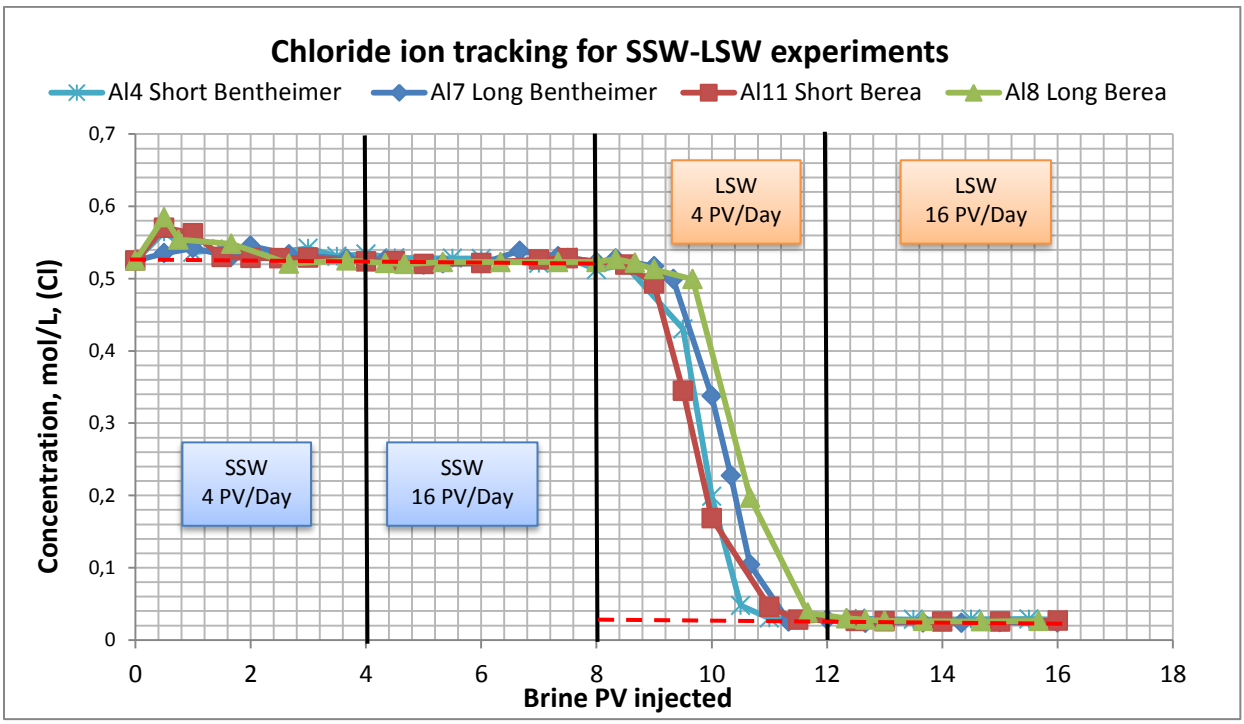

Figure 77 – Ion concentrations for Cl^- in effluent water during SSW- LSW flooding

Obtained results were confirmed by simulation of relative permeability curves for water and oil in Sendra software and by analysis of Al and Si in the effluent water samples.

5 CONCLUSIONS AND PROPOSED MECHANISM

This work was made with the intention of improving the understanding of processes during flooding with low salinity brine. The idea was to study different sandstone types (Bentheimer and Berea) and define relationship between core length and amount of brine/rock interactions.

The main reason for improved oil recovery by using LSW brines can be the wettability changing of the rock surface. There are a lot of proposed mechanisms by which wettability of the rock can be changed. However, obtained results showed that the possible underlying reason for this process is sandstone minerals dissolution. This is indicated by increased amount of potassium in effluent water samples, possibly caused by K-Feldspar dissolution. Excess concentration level for Ca^{2+} and HCO_3^- can be the result of $CaCO_3$ dissolution, which is presented in sandstone cores as a cementing material. pH of effluent water samples showed stably higher values than pH of influent LSW. Minerals dissolution may be the main reason of increasing in pH during LSW flooding.

Possible double layer expansion together with dissolution process could enhance particle detachment, which can be confirmed by increased pressure drop across the cores.

Despite of possible LSW brine interaction with the core the recovery with SSW showed higher results. This can be due to the fact that LSW viscosity is lower and flooding with it leaves more amount of capillary trapped oil. The flooding with LSW in secondary injection mode (EOR) also did not bring any incremental oil. The reason for this can lie in low amount of material for brine/rock interaction.

Based on obtained results, Berea sandstone has higher potential for interactions with LSW brine. Higher amount of K and Si was found in the effluent samples for Berea type in compare with Bentheimer. The observed recovery for Berea sandstone also was higher. Higher amount of brine/rock interaction was detected in long cores, which tell about the dependency of the results on the core length. As a proposition for future work can be advised using of longer Berea cores for studying LSW effects.

REFERENCES

1. Adrian C Todd, 2005, *"Reservoir engineering"*, Manual of Heriot-Watt Institute of Petroleum Engineering, Edinburgh.
2. Ahmad Aladasani, Baojun Bai and Yu-Shu Wu, 2012, *"Investigating Low-Salinity Waterflooding Recovery Mechanisms in Sandstone Reservoirs"*, Paper SPE 152997, Eighteenth SPE Improved Oil Recovery Symposium held in Tulsa, Oklahoma, USA, 14-18 April 2012.
3. Ahmed Tarek, 2001, *"Reservoir engineering handbook. Second edition"*, Houston, Texas, USA, Gulf Professional Publishing is an imprint of Butterworth-Heinemann, ISBN: 0884157709.
4. Aly Anis Hamouda and Ole Martin Valderhaug, 2014, *"Investigating Enhanced Oil Recovery from Sandstone by Low-Salinity Water and Fluid/Rock Interaction"*, American Chemical Society Publications.
5. Archer J.S. and Wall C.G., 1986, *"Petroleum engineering: principles and practice"*, Oxford, Great Britain, Graham and Trotman Ltd., ISBN: 0860l06659.
6. Berg, S., Cense, A.W., Jansen, E. and Bakker, K, 2010, *"Direct Experimental Evidence of Wettability Modification by Low Salinity"*, Society of Petrophysics and Well Log Analysts, International Symposium of the Society of Core Analysts, Noordwijk aan Zee, The Netherlands, September 27-30. 2009.
7. Bruce B. Velde and Alain Meunier, 2008, *"The Origin of Clay Minerals in Soils and Weathered Rocks"*, Springer, ISBN: 3540756347.
8. Buckley, J.S. and Yu Liu, 1997, *"Evolution of Wetting Alteration by Adsorption From Crude Oil"*, Paper SPE 28970, International Symposium on Oilfield Chemistry held in San Antonio, Texas, 14-17 February 1995.
9. Burgot J.-L., 2012, *"Ionic Equilibria in Analytical Chemistry"*, Springer, Science+Business Media, ISBN: 1441983813.
10. Clementz, D.M., 1982, *"Alteration of Rock Properties by Adsorbtion of Petroleum Heavy Ends: Implications of Enhanced Oil Recovery"*, Paper SPE/DOE 10683, Third Joint Symposium on EOR, Tulsa, 4-7 April 1982.

11. Cuong T.Q. Dang, Long .X. Nghiem, Zhangxin Chen, Quoc .P. Nguyen, 2013, *"Modeling Low Salinity Waterflooding: Ion Exchange, Geochemistry and Wettability Alteration"*, SPE Paper 166447, SPE Annual Technical Conference and Exhibition held in New Orleans, Louisiana, USA, 30 September -2 October 2013.
12. Cuong T.Q. Dang, Long X. Nghiem, Zhangxin Chen, Quoc P. Nguyen and Ngoc T.B. Nguyen, 2013, *"State-of-the Art Low Salinity Waterflooding for Enhanced Oil Recovery"*, Paper SPE 165903, Asia Pacific Oil & Gas Conference and Exhibition held in Jakarta, Indonesia, 22-24 October 2013.
13. Dagny Håmsø, 2011, *"Adsorption of quinoline onto illite at high temperature in relation to low salinity water flooding in sandstone reservoirs"*, Master's Thesis, University of Stavanger.
14. Don W. Green and G. Paul Willhite, 1998, *"Enhanced Oil Recovery"*, SPE Textbook, Richardson, Texas, ISBN: 9781555630775.
15. Fabuss, B.M., A. Korosi, and D. F. Othmer, 1969, *"Viscosities of aqueous solutions of several electrolytes present in sea water"*, Chemical Engineering Data 14(2), 192.
16. Gary R. Jerauld, Lin, C.Y., Kevin J. Webb and Jim C. Seccombe, 2008, *"Modeling Low-Salinity Waterflooding"*, Paper SPE 102239, Annual Technical Conference and Exhibition, San Antonio, Texas, 24-27 September 2008.
17. Geology.com, Sandstone picture from: http://geology.com/rocks/pictures/sandstone.jpg
18. Halliburton, 2011, *"Basic Petroleum Geology and Log Analysis"*
19. Lager, A., Webb, K.J. and Black, C.J.J., 2007, *"Impact of Brine Chemistry on Oil Recovery"*, Paper A24, 14 EAGE Symposium on Improved Oil Recovery, Cairo, 22-24 April 2007.
20. Larry W. Lake, 2010, *"Enhanced Oil Recovery"*, SPE Textbook, ISBN: 9781555633059.

21. Ligthelm, D.J., Gronsveld, J., Hofman, J.P., Brussee, N.J., Marcelis, F., and van der Linde, H.A., 2009, "*Novel Waterflooding Strategy by Manipulation of Injection Brine Composition*", Paper SPE 119835, SPE EUROPEC/EAGE Annual Conference and Exhibition, Amsterdam, The Netherlands, 8-11 June 2009.
22. Mysels, K.J., 1967, "*Introduction to Colloid Chemistry*", Interscience Publishers, New York.
23. Nnaemeka Ezekwe, 2011, *"Petroleum Reservoir Engineering Practice"*, Boston, USA, Pearson Education, Inc., ISBN: 0137152833.
24. Ole Martin Valderhaug, 2013, *"Investigating EOR for SS by Low Salinity Water"*, Master's Thesis, University of Stavanger.
25. Qingjie Gong, Jun Deng, Meng Han, Liqiang Yang and Wenquan Wang, 2012, *"Dissolution of sandstone powders in deionised water over the range 50–350℃"*, Applied Geochemistry, Elsevier Ltd.
26. Ramez A. Nasralla and Hisham A. Nasr-El-Din, 2014, "*Double-Layer Expansion: Is It a Primary Mechanism of Improved Oil Recovery by Low-Salinity Waterflooding?",* Paper SPE 154334, Oil Recovery Symposium, Tulsa, April 2012.
27. RezaeiDoust A., 2011, Ph.D. Thesis, University of Stavanger, Stavanger, Norway, September 2011.
28. Robert J. Weimer and Tillman, R.W., 1982, *"Sandstone Reservoirs"*, Paper SPE 10009-MS, International Petroleum Exhibition and Technical Symposium, Beijing, China 17-24 March 1982.
29. Rueslatten, H.G., Hjelmeland, O., and Selle, O.M., 1994, "*Wettability of Reservoir Rocks and the influence of organo-metallic compounds***"**, Paper 22, in Aasen, J.O. et al., eds., North Sea Oil and Gas Reservoirs III: Kluwer Academic Publishers, Dordrecht, 317–324,.
30. Shaw, D.J., 1966, "*Introduction to Colloid and Surface Chemistry*", Butterworths, London.
31. Sheng James J., 2011, *"Modern Chemical Enhanced Oil Recovery: Theory and Practice"*, USA, Gulf Professional Publishing is an imprint of Elsevier, ISBN: 9781856177450.

32. Tang, G.Q. and Morrow, N.R., 1999. "*Influence of brine composition and fines migration on crude oil/brine/rock interactions and oil recovery*", Journal of Petroleum Science and Engineering 24, pp. 99-111.
33. Terence Cosgrove, 2010, *"Colloid Science: Principles, Methods and Applications (2nd Edition)"*, USA, A John Wiley and Sons, Ltd, Publication.
34. Tor Austad, Alireza RezaeiDoust and Tina Puntervold, 2010, *"Chemical Mechanism of Low Salinity Water Flooding in Sandstone Reservoirs"*, Paper SPE 129767, Improved Oil Recovery Symposium held in Tulsa, Oklahoma, USA, 24-28 April 2010.
35. Vladimir Alvarado and Eduardo Manrique, 2010, *"Enhanced Oil Recovery. Field Planning and Development Strategies",* USA, Gulf Professional Publishing is an imprint of Elsevier.
36. Water Density Calculator, 2011 from: http://www.csgnetwork.com/h2odenscalc.html
37. Weatherford Petroleum Consultants AS, 2013, *"Sendra user guide"*
38. Wikipedia, pH from: http://en.wikipedia.org/wiki/PH
39. Wikipedia, Relative permeability from: http://en.wikipedia.org/wiki/Relative_permeability

APPENDIX

Table 9 - Solid analysis of the Bentheimer sandstone (Ole Martin Valderhaug, 2013)

Parameter	Results	Unit	PQL			Uncertainty	
Elements in solids, XRF			Lower	Upper	Method/Standard	Rel	Abs
Aluminum, Al	1.8	wt%	0.1	-	X-021 (XRF)	10%	-
Barium, Ba	<0.1	wt%	0.1	-	X-021 (XRF)	10%	-
Calcium, Ca	0.1	wt%	0.1	-	X-021 (XRF)	10%	-
Chromium, Cr	<0.1	wt%	0.1	-	X-021 (XRF)	10%	-
Copper, Cu	<0.1	wt%	0.1	-	X-021 (XRF)	10%	-
Iron, Fe	0.2	wt%	0.1	-	X-021 (XRF)	10%	-
Potassium, K	0.6	wt%	0.1	-	X-021 (XRF)	10%	-
Magnesium, Mg	<0.1	wt%	0.1	-	X-021 (XRF)	10%	-
Manganese, Mn	<0.1	wt%	0.1	-	X-021 (XRF)	10%	-
Sodium, Na	<0.1	wt%	0.1	-	X-021 (XRF)	10%	-
Nickel, Ni	<0.1	wt%	0.1	-	X-021 (XRF)	10%	-
Phosphorus, P	<0.1	wt%	0.1	-	X-021 (XRF)	10%	-
Lead, Pb	<0.1	wt%	0.1	-	X-021 (XRF)	10%	-
Silicon, Si	44	wt%	0.1	-	X-021 (XRF)	10%	-
Strontium, Sr	<0.1	wt%	0.1	-	X-021 (XRF)	10%	-
Titanium, Ti	<0.1	wt%	0.1	-	X-021 (XRF)	10%	-
Zinc, Zn	<0.1	wt%	0.1	-	X-021 (XRF)	10%	-
Sulphur, S	<0.1	wt%	0.1	-	X-021 (XRF)	10%	-
Chlorine, Cl	0.1	wt%	0.1	-	X-021 (XRF)	10%	-

Table 10 - Mineral analysis of Bentheimer sandstone (Ole Martin Valderhaug, 2013)

Mineral Name	Chemical Formula	Semi Quantitive (%)
Quartz	SiO_2	94
Kaolinite	$Al_2Si_2O_5(OH)_4$	1
Muscovite	$(K,Na)(Al,Mg,Fe)_2$ $(Si_3.Al,O_{10})O_{10}(F,OH)_2$	1
Microline	$KAlSi_3O_8$	1

Table 11 - Concentration of Potassium ion for all SSW-LSW and LSW experiments

Potassium concentration for all SSW-LSW experiments in mol/L							
PV	Al4	PV	Al7	PV	Al11	PV	Al8
0	0,0100	0	0,0100	0	0,0100	0	0,0100
0,5	0,0114	0,5	0,0119	0,5	0,0116	0,5	0,0107
1,0	0,0118	1,0	0,0118	1	0,0116	0,75	0,0102
1,5	0,0117	1,7	0,0127	1,5	0,0115	1,7	0,0109
2,0	0,0106	2,0	0,0126	2	0,0111	2,7	0,0115
3,0	0,0114	2,7	0,0117	2,5	0,0116	3,7	0,0124
3,5	0,0093	3,7	0,0117	3	0,0110	4,3	0,0103
4,0	0,0096	4,3	0,0107	4	0,0112	4,7	0,0109
4,5	0,0092	5,0	0,0105	4,5	0,0104	5,3	0,0106
5,5	0,0098	5,3	0,0106	5	0,0102	6,3	0,0104
6,0	0,0091	6,0	0,0112	6	0,0109	7,3	0,0104
7,0	0,0103	6,7	0,0105	7	0,0101	8,0	0,0101
7,5	0,0099	7,3	0,0105	7,5	0,0104	8,3	0,0103
8,0	0,0103	8,0	0,0102	8,5	0,0102	8,7	0,0101
8,5	0,0102	8,3	0,0101	9	0,0092	9,0	0,0097
9,5	0,0043	9,0	0,0099	9,5	0,0052	9,7	0,0094
10,0	0,0025	9,3	0,0084	10	0,0029	10,7	0,0036
10,5	0,0023	10,0	0,0063	11	0,0013	11,7	0,0015
11,0	0,0012	10,3	0,0032	11,5	0,0013	12,3	0,0010
11,5	0,0010	10,7	0,0020	12,5	0,0010	12,7	0,0009
12,5	0,0007	11,3	0,0008	13	0,0009	13,0	0,0011
13,5	0,0011	12,0	0,0010	14	0,0011	13,7	0,0014
14,5	0,0009	12,7	0,0009	15	0,0009	14,7	0,0012
15,5	0,0009	13,7	0,0012	16	0,0008	15,7	0,0008
16,0	0,0010	14,3	0,0009				
		15,0	0,0012				
		16,0	0,0011				
Potassium concentration for all LSW experiments in mol/L							
PV	Al6	PV	Al12	PV	Al10	PV	Al9
0	0,0004	0	0,0004	0	0,0004	0	0,0004
0,5	0,0066	0,5	0,0075	0,5	0,0066	0,5	0,0076
1	0,0030	0,75	0,0058	1	0,0024	0,75	0,0039
2	0,0020	1	0,0028	1,5	0,0017	1	0,0026
2,5	0,0017	1,7	0,0017	2	0,0016	1,7	0,0020
3,5	0,0014	2,7	0,0023	2,5	0,0019	2,7	0,0015
4	0,0013	3,7	0,0010	3	0,0013	3,7	0,0010
5	0,0019	4,0	0,0019	4	0,0012	4,0	0,0011
6	0,0014	4,3	0,0014	4,5	0,0010	4,3	0,0014
7,5	0,0012	5,0	0,0019	5	0,0014	5,0	0,0023
		6,0	0,0014	5,5	0,0017	6,0	0,0014
		7,0	0,0014	6,5	0,0011	7,0	0,0014
		7,7	0,0011	7,5	0,0010	7,7	0,0011

Table 12 - Concentration of Calcium ion for all SSW-LSW and LSW experiments

Calcium concentration for all SSW-LSW experiments in mol/L							
PV	Al4	PV	Al7	PV	Al11	PV	Al8
0	0,0130	0	0,0130	0	0,0130	0	0,0130
0,5	0,0151	0,5	0,0160	0,5	0,0155	0,5	0,0141
1,0	0,0151	1,0	0,0139	1	0,0153	0,75	0,0148
1,5	0,0139	1,7	0,0132	1,5	0,0141	1,7	0,0144
2,0	0,0139	2,0	0,0153	2	0,0136	2,7	0,0133
3,0	0,0133	2,7	0,0137	2,5	0,0139	3,7	0,0132
3,5	0,0143	3,7	0,0138	3	0,0133	4,3	0,0130
4,0	0,0137	4,3	0,0135	4	0,0130	4,7	0,0130
4,5	0,0131	5,0	0,0135	4,5	0,0126	5,3	0,0130
5,5	0,0133	5,3	0,0135	5	0,0129	6,3	0,0129
6,0	0,0139	6,0	0,0137	6	0,0138	7,3	0,0129
7,0	0,0138	6,7	0,0137	7	0,0127	8,0	0,0128
7,5	0,0133	7,3	0,0135	7,5	0,0130	8,3	0,0127
8,0	0,0134	8,0	0,0136	8,5	0,0123	8,7	0,0126
8,5	0,0131	8,3	0,0136	9	0,0093	9,0	0,0127
9,5	0,0061	9,0	0,0119	9,5	0,0071	9,7	0,0115
10,0	0,0033	9,3	0,0095	10	0,0040	10,7	0,0047
10,5	0,0028	10,0	0,0075	11	0,0014	11,7	0,0012
11,0	0,0012	10,3	0,0060	11,5	0,0011	12,3	0,0006
11,5	0,0010	10,7	0,0039	12,5	0,0006	12,7	0,0009
12,5	0,0008	11,3	0,0010	13	0,0007	13,0	0,0008
13,5	0,0009	12,0	0,0009	14	0,0008	13,7	0,0007
14,5	0,0010	12,7	0,0008	15	0,0007	14,7	0,0008
15,5	0,0009	13,7	0,0009	16	0,0007	15,7	0,0006
16,0	0,0007	14,3	0,0010				
		15,0	0,0010				
		16,0	0,0010				
Calcium concentration for all LSW experiments in mol/L							
PV	Al6	PV	Al12	PV	Al10	PV	Al9
0	0,0005	0	0,0005	0	0,0005	0	0,0005
0,5	0,0092	0,5	0,0089	0,5	0,0080	0,5	0,0100
1	0,0025	0,75	0,0047	1	0,0020	0,75	0,0047
2	0,0015	1	0,0012	1,5	0,0014	1	0,0012
2,5	0,0010	1,7	0,0013	2	0,0010	1,7	0,0010
3,5	0,0010	2,7	0,0013	2,5	0,0009	2,7	0,0012
4	0,0014	3,7	0,0012	3	0,0008	3,7	0,0012
5	0,0013	4,0	0,0014	4	0,0011	4,0	0,0010
6	0,0012	4,3	0,0013	4,5	0,0012	4,3	0,0009
7,5	0,0011	5,0	0,0014	5	0,0009	5,0	0,0014
		6,0	0,0009	5,5	0,0009	6,0	0,0009
		7,0	0,0012	6,5	0,0007	7,0	0,0012
		7,7	0,0013	7,5	0,0008	7,7	0,0013

Table 13 - Concentration of Magnesium ion for all SSW-LSW and LSW experiments

Magnesium concentration for all SSW-LSW experiments in mol/L							
PV	Al4	PV	Al7	PV	Al11	PV	Al8
0	0,0450	0	0,0450	0	0,0450	0	0,0450
0,5	0,0448	0,5	0,0424	0,5	0,0476	0,5	0,0461
1,0	0,0464	1,0	0,0442	1	0,0424	0,75	0,0428
1,5	0,0458	1,7	0,0429	1,5	0,0427	1,7	0,0425
2,0	0,0448	2,0	0,0447	2	0,0435	2,7	0,0433
3,0	0,0442	2,7	0,0435	2,5	0,0429	3,7	0,0442
3,5	0,0454	3,7	0,0433	3	0,0436	4,3	0,0441
4,0	0,0456	4,3	0,0435	4	0,0438	4,7	0,0445
4,5	0,0445	5,0	0,0429	4,5	0,0437	5,3	0,0448
5,5	0,0455	5,3	0,0434	5	0,0436	6,3	0,0446
6,0	0,0449	6,0	0,0435	6	0,0457	7,3	0,0445
7,0	0,0447	6,7	0,0435	7	0,0439	8,0	0,0441
7,5	0,0439	7,3	0,0436	7,5	0,0444	8,3	0,0433
8,0	0,0444	8,0	0,0433	8,5	0,0421	8,7	0,0426
8,5	0,0438	8,3	0,0437	9	0,0364	9,0	0,0425
9,5	0,0235	9,0	0,0435	9,5	0,0261	9,7	0,0412
10,0	0,0170	9,3	0,0418	10	0,0113	10,7	0,0112
10,5	0,0061	10,0	0,0293	11	0,0022	11,7	0,0024
11,0	0,0025	10,3	0,0118	11,5	0,0013	12,3	0,0021
11,5	0,0021	10,7	0,0097	12,5	0,0017	12,7	0,0017
12,5	0,0021	11,3	0,0017	13	0,0016	13,0	0,0017
13,5	0,0019	12,0	0,0019	14	0,0017	13,7	0,0018
14,5	0,0018	12,7	0,0016	15	0,0016	14,7	0,0021
15,5	0,0018	13,7	0,0017	16	0,0017	15,7	0,0021
16,0	0,0018	14,3	0,0019				
		15,0	0,0021				
		16,0	0,0019				
Magnesium concentration for all LSW experiments in mol/L							
PV	Al6	PV	Al12	PV	Al10	PV	Al9
0	0,0018	0	0,0018	0	0,0018	0	0,0018
0,5	0,0305	0,5	0,0310	0,5	0,0295	0,5	0,0314
1	0,0059	0,75	0,0113	1	0,0035	0,75	0,0144
2	0,0020	1	0,0024	1,5	0,0021	1	0,0060
2,5	0,0019	1,7	0,0013	2	0,0013	1,7	0,0017
3,5	0,0018	2,7	0,0014	2,5	0,0014	2,7	0,0017
4	0,0023	3,7	0,0014	3	0,0013	3,7	0,0014
5	0,0021	4,0	0,0016	4	0,0013	4,0	0,0016
6	0,0022	4,3	0,0015	4,5	0,0014	4,3	0,0016
7,5	0,0022	5,0	0,0015	5	0,0015	5,0	0,0015
		6,0	0,0015	5,5	0,0013	6,0	0,0017
		7,0	0,0016	6,5	0,0014	7,0	0,0016
		7,7	0,0015	7,5	0,0017	7,7	0,0015

Table 14 - Concentration of Sodium ion for all SSW-LSW and LSW experiments

Sodium concentration for all SSW-LSW experiments in mol/L							
PV	Al4	PV	Al7	PV	Al11	PV	Al8
0	0,4500	0	0,4500	0	0,4500	0	0,4500
0,5	0,4802	0,5	0,4540	0,5	0,4595	0,5	0,4884
1,0	0,4733	1,0	0,4699	1	0,4429	0,75	0,4491
1,5	0,4635	1,7	0,4589	1,5	0,4447	1,7	0,4600
2,0	0,4578	2,0	0,4856	2	0,4441	2,7	0,4465
3,0	0,4563	2,7	0,4651	2,5	0,4445	3,7	0,4531
3,5	0,4677	3,7	0,4641	3	0,4465	4,3	0,4478
4,0	0,4558	4,3	0,4624	4	0,4472	4,7	0,4443
4,5	0,4596	5,0	0,4561	4,5	0,4423	5,3	0,4507
5,5	0,4555	5,3	0,4586	5	0,4438	6,3	0,4493
6,0	0,4481	6,0	0,4579	6	0,4416	7,3	0,4506
7,0	0,4480	6,7	0,4735	7	0,4460	8,0	0,4485
7,5	0,4548	7,3	0,4599	7,5	0,4516	8,3	0,4472
8,0	0,4640	8,0	0,4578	8,5	0,4277	8,7	0,4438
8,5	0,4529	8,3	0,4582	9	0,3483	9,0	0,4444
9,5	0,3475	9,0	0,4490	9,5	0,2843	9,7	0,3730
10,0	0,2050	9,3	0,3814	10	0,1666	10,7	0,1366
10,5	0,1239	10,0	0,2380	11	0,0333	11,7	0,0270
11,0	0,0303	10,3	0,1402	11,5	0,0220	12,3	0,0213
11,5	0,0221	10,7	0,0952	12,5	0,0208	12,7	0,0192
12,5	0,0248	11,3	0,0206	13	0,0191	13,0	0,0185
13,5	0,0243	12,0	0,0213	14	0,0193	13,7	0,0212
14,5	0,0219	12,7	0,0219	15	0,0197	14,7	0,0179
15,5	0,0269	13,7	0,0192	16	0,0199	15,7	0,0194
16,0	0,0249	14,3	0,0205				
		15,0	0,0219				
		16,0	0,0212				
Sodium concentration for all LSW experiments in mol/L							
PV	Al6	PV	Al12	PV	Al10	PV	Al9
0	0,0180	0	0,0180	0	0,0180	0	0,0180
0,5	0,4192	0,5	0,3169	0,5	0,3802	0,5	0,3494
1	0,0687	0,75	0,1597	1	0,0424	0,75	0,1051
2	0,0244	1	0,0393	1,5	0,0261	1	0,0367
2,5	0,0263	1,7	0,0191	2	0,0187	1,7	0,0253
3,5	0,0242	2,7	0,0216	2,5	0,0204	2,7	0,0202
4	0,0227	3,7	0,0174	3	0,0222	3,7	0,0209
5	0,0222	4,0	0,0183	4	0,0216	4,0	0,0204
6	0,0228	4,3	0,0191	4,5	0,0201	4,3	0,0189
7,5	0,0187	5,0	0,0183	5	0,0211	5,0	0,0214
		6,0	0,0191	5,5	0,0221	6,0	0,0221
		7,0	0,0195	6,5	0,0216	7,0	0,0214
		7,7	0,0183	7,5	0,0196	7,7	0,0207

Table 15 - Concentration of Sulfate ion for all SSW-LSW and LSW experiments

Sulfate concentration for all SSW-LSW experiments in mol/L							
PV	Al4	PV	Al7	PV	Al11	PV	Al8
0	0,0240	0	0,0240	0	0,0240	0	0,0240
0,5	0,0264	0,5	0,0243	0,5	0,0223	0,5	0,0247
1,0	0,0247	1,0	0,0243	1	0,0239	0,75	0,0242
1,5	0,0251	1,7	0,0249	1,5	0,0240	1,7	0,0244
2,0	0,0254	2,0	0,0257	2	0,0243	2,7	0,0237
3,0	0,0240	2,7	0,0248	2,5	0,0242	3,7	0,0240
3,5	0,0241	3,7	0,0245	3	0,0244	4,3	0,0238
4,0	0,0246	4,3	0,0244	4	0,0241	4,7	0,0240
4,5	0,0240	5,0	0,0242	4,5	0,0242	5,3	0,0241
5,5	0,0240	5,3	0,0242	5	0,0239	6,3	0,0239
6,0	0,0238	6,0	0,0242	6	0,0247	7,3	0,0239
7,0	0,0241	6,7	0,0246	7	0,0238	8,0	0,0240
7,5	0,0245	7,3	0,0250	7,5	0,0239	8,3	0,0240
8,0	0,0243	8,0	0,0244	8,5	0,0236	8,7	0,0237
8,5	0,0235	8,3	0,0237	9	0,0208	9,0	0,0237
9,5	0,0170	9,0	0,0230	9,5	0,0180	9,7	0,0201
10,0	0,0137	9,3	0,0193	10	0,0104	10,7	0,0096
10,5	0,0038	10,0	0,0133	11	0,0022	11,7	0,0011
11,0	0,0011	10,3	0,0101	11,5	0,0011	12,3	0,0012
11,5	0,0016	10,7	0,0061	12,5	0,0009	12,7	0,0011
12,5	0,0012	11,3	0,0008	13	0,0008	13,0	0,0011
13,5	0,0011	12,0	0,0009	14	0,0008	13,7	0,0009
14,5	0,0011	12,7	0,0007	15	0,0008	14,7	0,0010
15,5	0,0011	13,7	0,0007	16	0,0008	15,7	0,0013
16,0	0,0012	14,3	0,0008				
		15,0	0,0010				
		16,0	0,0007				
Sulfate concentration for all LSW experiments in mol/L							
PV	Al6	PV	Al12	PV	Al10	PV	Al9
0	0,0010	0	0,0010	0	0,0010	0	0,0010
0,5	0,0159	0,5	0,0197	0,5	0,0178	0,5	0,0185
1	0,0077	0,75	0,0096	1	0,0078	0,75	0,0096
2	0,0016	1	0,0061	1,5	0,0008	1	0,0071
2,5	0,0009	1,7	0,0012	2	0,0009	1,7	0,0012
3,5	0,0009	2,7	0,0011	2,5	0,0009	2,7	0,0011
4	0,0011	3,7	0,0009	3	0,0009	3,7	0,0009
5	0,0008	4,0	0,0009	4	0,0008	4,0	0,0009
6	0,0009	4,3	0,0009	4,5	0,0008	4,3	0,0009
7,5	0,0008	5,0	0,0009	5	0,0008	5,0	0,0009
		6,0	0,0010	5,5	0,0008	6,0	0,0010
		7,0	0,0009	6,5	0,0008	7,0	0,0009
		7,7	0,0010	7,5	0,0008	7,7	0,0010

Table 16 - Concentration of Chloride ion for all SSW-LSW and LSW experiments

Chloride concentration for all SSW-LSW experiments in mol/L							
PV	Al4	PV	Al7	PV	Al11	PV	Al8
0	0,5250	0	0,5250	0	0,5250	0	0,5250
0,5	0,5646	0,5	0,5351	0,5	0,5703	0,5	0,5849
1,0	0,5362	1,0	0,5421	1	0,5627	0,75	0,5539
1,5	0,5408	1,7	0,5304	1,5	0,5300	1,7	0,5482
2,0	0,5314	2,0	0,5453	2	0,5285	2,7	0,5206
3,0	0,5421	2,7	0,5336	2,5	0,5283	3,7	0,5251
3,5	0,5310	3,7	0,5274	3	0,5289	4,3	0,5215
4,0	0,5340	4,3	0,5261	4	0,5238	4,7	0,5201
4,5	0,5287	5,0	0,5191	4,5	0,5240	5,3	0,5228
5,5	0,5279	5,3	0,5210	5	0,5201	6,3	0,5229
6,0	0,5278	6,0	0,5210	6	0,5217	7,3	0,5228
7,0	0,5209	6,7	0,5384	7	0,5264	8,0	0,5228
7,5	0,5293	7,3	0,5308	7,5	0,5283	8,3	0,5269
8,0	0,5124	8,0	0,5228	8,5	0,5194	8,7	0,5217
8,5	0,5190	8,3	0,5277	9	0,4932	9,0	0,5129
9,5	0,4302	9,0	0,5170	9,5	0,3447	9,7	0,4991
10,0	0,1984	9,3	0,4992	10	0,1684	10,7	0,1968
10,5	0,0477	10,0	0,3377	11	0,0456	11,7	0,0377
11,0	0,0301	10,3	0,2276	11,5	0,0280	12,3	0,0299
11,5	0,0286	10,7	0,1042	12,5	0,0261	12,7	0,0281
12,5	0,0297	11,3	0,0255	13	0,0257	13,0	0,0265
13,5	0,0284	12,0	0,0283	14	0,0252	13,7	0,0261
14,5	0,0288	12,7	0,0236	15	0,0252	14,7	0,0257
15,5	0,0290	13,7	0,0241	16	0,0268	15,7	0,0263
16,0	0,0282	14,3	0,0236				
		15,0	0,0243				
		16,0	0,0239				
Chloride concentration for all LSW experiments in mol/L							
PV	Al6	PV	Al12	PV	Al10	PV	Al9
0	0,0210	0	0,0210	0	0,0210	0	0,0210
0,5	0,4278	0,5	0,4042	0,5	0,4365	0,5	0,4264
1	0,0370	0,75	0,2441	1	0,0306	0,75	0,2018
2	0,0250	1	0,0282	1,5	0,0219	1	0,0363
2,5	0,0239	1,7	0,0282	2	0,0217	1,7	0,0238
3,5	0,0229	2,7	0,0270	2,5	0,0247	2,7	0,0188
4	0,0263	3,7	0,0244	3	0,0275	3,7	0,0216
5	0,0249	4,0	0,0285	4	0,0222	4,0	0,0265
6	0,0271	4,3	0,0239	4,5	0,0219	4,3	0,0222
7,5	0,0255	5,0	0,0241	5	0,0206	5,0	0,0208
		6,0	0,0233	5,5	0,0198	6,0	0,0215
		7,0	0,0236	6,5	0,0206	7,0	0,0217
		7,7	0,0238	7,5	0,0199	7,7	0,0199

Table 17 - Concentration of Carbonate ion for all SSW-LSW and LSW experiments

Carbonate concentration for all SSW-LSW experiments in mol/L							
PV	Al4	PV	Al7	PV	Al11	PV	Al8
0	0,0020	0	0,0020	0	0,0020	0	0,0020
0,5	0,0024	0,5	0,0018	0,5	0,0018	0,5	0,0030
1,0	0,0019	1,0	0,0018	1	0,0016	0,75	0,0027
1,5	0,0028	1,7	0,0019	1,5	0,0020	1,7	0,0024
2,0	0,0021	2,0	0,0023	2	0,0018	2,7	0,0025
3,0	0,0013	2,7	0,0021	2,5	0,0013	3,7	0,0023
3,5	0,0012	3,7	0,0023	3	0,0018	4,3	0,0025
4,0	0,0024	4,3	0,0023	4	0,0021	4,7	0,0013
4,5	0,0018	5,0	0,0017	4,5	0,0016	5,3	0,0019
5,5	0,0018	5,3	0,0020	5	0,0022	6,3	0,0022
6,0	0,0017	6,0	0,0023	6	0,0020	7,3	0,0024
7,0	0,0014	6,7	0,0019	7	0,0016	8,0	0,0023
7,5	0,0021	7,3	0,0019	7,5	0,0020	8,3	0,0020
8,0	0,0021	8,0	0,0022	8,5	0,0017	8,7	0,0018
8,5	0,0019	8,3	0,0020	9	0,0020	9,0	0,0022
9,5	0,0023	9,0	0,0023	9,5	0,0016	9,7	0,0012
10,0	0,0021	9,3	0,0024	10	0,0021	10,7	0,0016
10,5	0,0018	10,0	0,0030	11	0,0021	11,7	0,0026
11,0	0,0018	10,3	0,0028	11,5	0,0022	12,3	0,0027
11,5	0,0016	10,7	0,0030	12,5	0,0024	12,7	0,0032
12,5	0,0015	11,3	0,0030	13	0,0025	13,0	0,0033
13,5	0,0013	12,0	0,0026	14	0,0014	13,7	0,0023
14,5	0,0018	12,7	0,0031	15	0,0026	14,7	0,0032
15,5	0,0013	13,7	0,0031	16	0,0028	15,7	0,0034
16,0	0,0021	14,3	0,0028				
		15,0	0,0031				
		16,0	0,0031				
Carbonate concentration for all LSW experiments in mol/L							
PV	Al6	PV	Al12	PV	Al10	PV	Al9
0	0,0001	0	0,0001	0	0,0001	0	0,0001
0,5	0,0023	0,5	0,0024	0,5	0,0030	0,5	0,0019
1	0,0020	0,75	0,0023	1	0,0027	0,75	0,0017
2	0,0019	1	0,0023	1,5	0,0024	1	0,0023
2,5	0,0025	1,7	0,0027	2	0,0026	1,7	0,0021
3,5	0,0021	2,7	0,0019	2,5	0,0028	2,7	0,0021
4	0,0020	3,7	0,0027	3	0,0022	3,7	0,0021
5	0,0022	4,0	0,0029	4	0,0020	4,0	0,0017
6	0,0024	4,3	0,0028	4,5	0,0026	4,3	0,0023
7,5	0,0021	5,0	0,0032	5	0,0025	5,0	0,0023
		6,0	0,0018	5,5	0,0023	6,0	0,0025
		7,0	0,0026	6,5	0,0029	7,0	0,0015
		7,7	0,0026	7,5	0,0027	7,7	0,0028